Space Science Reviews manuscript No.
(will be inserted by the editor)

Jupiter Science Enabled by ESA's Jupiter Icy Moons Explorer

Leigh N. Fletcher · Thibault Cavalié · Davide Grassi · Ricardo Hueso · Luisa M. Lara · Yohai Kaspi · Eli Galanti · Thomas K. Greathouse · Philippa M. Molyneux · Marina Galand · Claire Vallat · Olivier Witasse · Rosario Lorente · Paul Hartogh · François Poulet · Yves Langevin · Pasquale Palumbo · G. Randall Gladstone · Kurt D. Retherford · Michele K. Dougherty · Jan-Erik Wahlund · Stas Barabash · Luciano Iess · Lorenzo Bruzonne · Hauke Hussmann · Leonid I. Gurvits · Ondřej Santolik · Ivana Kolmasova · Georg Fischer · Ingo Müller-Wodarg · Giuseppe Piccioni · Thierry Fouchet · Jean-Claude Gérard · Agustin Sánchez-Lavega · Patrick G. J. Irwin · Denis Grodent · Francesca Altieri · Alessandro Mura · Pierre Drossart · Josh Kammer · Rohini Giles · Stéphanie Cazaux · Geraint Jones · Maria Smirnova · Emmanuel Lellouch · Alexander S. Medvedev · Raphael Moreno · Ladislav Rezac · Athena Coustenis · Marc Costa

Received: date / Accepted: date

Leigh N. Fletcher
School of Physics and Astronomy, University of Leicester, University Road, Leicester, LE1 7RH, UK
E-mail: leigh.fletcher@leicester.ac.uk

Thibault Cavalié
Laboratoire d'Astrophysique de Bordeaux, Univ. Bordeaux, CNRS, B18N, allée Geoffroy Saint-Hilaire, 33615 Pessac, France

Davide Grassi, Pasquale Palumbo, Giuseppe Piccioni, Francesca Altieri, Alessandro Mura
Istituto di Astrofisica e Planetologia Spaziali - Istituto Nazionale di Astrofisica, Via del Fosso del Cavaliere, I-00133, Roma, Italy

Ricardo Hueso, Agustin Sánchez-Lavega
Física Aplicada, Escuela de Ingeniería de Bilbao Universidad del País Vasco UPV/EHU, Plaza Ingeniero Torres Quevedo, 1, 48013 Bilbao, Spain

Luisa M. Lara
Instituto de Astrofísica de Andalucía-CSIC, c/Glorieta de la Astronomía 3, 18008 Granada, Spain

Yohai Kaspi, Eli Galanti, Maria Smirnova
Dept. of Earth and Planetray Science, Weizmann Institute of Science, Rehovot, Israel, 76100

Thomas K. Greathouse, Philippa Molyneux, G. Randall Gladstone, Kurt D. Retherford, Josh Kammer, Rohini Giles
Southwest Research Institute, San Antonio, TX 78228, United States

Marina Galand
Department of Physics, Imperial College London, Prince Consort Road, London SW7 2AZ, UK

Claire Vallat, Rosario Lorente
European Space Agency (ESA) - ESAC Camino Bajo del Castillo s/n Villafranca del Castillo, 28692, Villanueva de la Cañada (Madrid), Spain

Olivier Witasse
European Space Agency (ESA), European Space Research and Technology Centre (ESTEC), Noordwijk, Netherlands

Marc Costa
Rhea Group, for European Space Agency, ESAC, Madrid, Spain

Paul Hartogh, Alexander S. Medvedev, Ladislav Rezac
Max-Planck-Institut für Sonnensystemforschung, 37077 Göttingen, Germany

François Poulet, Yves Langevin
Institut d'Astrophysique Spatiale, CNRS/Université Paris-Sud, 91405 Orsay Cedex, France

Michele K. Dougherty, Ingo Müller-Wodarg
Blackett Laboratory, Imperial College London, London, UK

Jan-Erik Wahlund
Swedish Institute of Space Physics (IRF), Uppsala, Sweden

Stas Barabash
Swedish Institute of Space Physics (IRF), Kiruna, Sweden

Luciano Iess
Dipartimento di ingegneria meccanica e aerospaziale, Universit á La Sapienza, Roma, Italy

Lorenzo Bruzzone
University of Trento, Department of Information Engineering and Computer Science, Remote Sensing Laboratory, Via Sommarive 14, Trento, I-38123, Italy

Hauke Hussmann
Deutsches Zentrum für Luft- und Raumfahrt (DLR), Berlin, Germany

Leonid I. Gurvits
Joint Institute for VLBI ERIC, Oude Hoogeveensedijk 4, 7991 PD Dwingeloo, The Netherlands

Leonid I. Gurvits
Aerospace Faculty, Delft University of Technology, Kluyverweg 1, 2629 HS Delft, The Netherlands

O. Santolik, I. Komalsova
Department of Space Physics, Institute of Atmospheric Physics of the Czech Academy of Sciences, Prague, Czechia; Faculty of Mathematics and Physics, Charles University, Prague, Czechia

Georg Fischer
Space Research Institute, Austrian Academy of Sciences, Graz, Austria

Thibault Cavalié, Thierry Fouchet, Pierre Drossart, Emmanuel Lellouch, Raphael Moreno, Athena Coustenis
LESIA, Observatoire de Paris, Université PSL, Sorbonne Université, Université Paris Cité, CNRS, 5 place Jules Janssen, 92195 Meudon, France

Jean-claude Gérard, Denis Grodent
LPAP, STAR Institute, Université de Liège, Belgium

Contents

Abstract ESA's Jupiter Icy Moons Explorer (JUICE) will provide a detailed investigation of the Jovian system in the 2030s, combining a suite of state-of-the-art instruments with an orbital tour tailored to maximise observing opportunities. We review the Jupiter science enabled by the JUICE mission, building on the legacy of discoveries from the Galileo, Cassini, and Juno missions, alongside ground- and space-based observatories. We focus on remote sensing of the climate, meteorology, and chemistry of the atmosphere and auroras from the cloud-forming weather layer, through the upper troposphere, into the stratosphere and ionosphere. The Jupiter orbital tour provides a wealth of opportunities for atmospheric and auroral science: global perspectives with its near-equatorial and inclined phases, sampling all phase angles from dayside to nightside, and investigating phenomena evolving on timescales from minutes to months. The remote sensing payload spans far-UV spectroscopy (50-210 nm), visible imaging (340-1080 nm), visible/near-infrared spectroscopy (0.49-5.56 μm), and sub-millimetre sounding (near 530-625 GHz and 1067-1275 GHz). This is coupled to radio, stellar, and solar occultation opportunities to explore the atmosphere at high vertical resolution; and radio and plasma wave measurements of electric discharges in the Jovian atmosphere and auroras. Cross-disciplinary scientific investigations enable JUICE to explore coupling processes in giant planet atmospheres, to show how the atmosphere is connected to (i) the deep circulation and composition of the hydrogen-dominated interior; and (ii) to the currents and charged particle environments of the external magnetosphere. JUICE will provide a comprehensive characterisation of the atmosphere and auroras of this archetypal giant planet.

Keywords JUICE · Jupiter · Atmospheres · Auroras · Dynamics · Chemistry

Patrick G. J. Irwin
Atmospheric, Oceanic and Planetary Physics, Department of Physics, University of Oxford, Parks Rd, Oxford OX1 3PU

Stéphanie Cazaux
Faculty of Aerospace Engineering, Delft University of Technology, Delft, The Netherlands

Geraint Jones
UCL Mullard Space Science Laboratory, Hombury St. Mary, Dorking RH5 6NT, UK and The Centre for Planetary Sciences at UCL/Birkbeck, London WC1E 6BT, UK

G. Randall Gladstone, Kurt D. Retherford
University of Texas at San Antonio, San Antonio, TX, United States

Pierre Drossart
Institut d'Astrophysique de Paris, CNRS, Sorbonne Université, 98bis Boulevard Arago, 75014 Paris

1 Introduction

Jupiter is our closest and best example of a hydrogen-dominated gas giant planet, representing a class of objects $\sim 10\times$ the size of Earth that may be commonplace across our galaxy. The formation and migration of such a large planet (317.8 Earth masses, approximately 0.1% of the mass of the Sun) shaped the architecture of our Solar System, such that the origin of Jupiter is an essential piece of the puzzle of planetary system evolution, providing a window on the epoch of planet formation. Jupiter provides a perfect planetary-scale laboratory for the exploration of atmospheric physics and chemistry (e.g., climate, meteorology, and convective processes on a rapidly-rotating hydrogen-rich world), without the complicating influences of terrestrial topography or large seasonal changes[1]. Jupiter also provides a means to explore how the layers within a giant planet are coupled, from the interior to the external plasma environment, and vice versa. For example, the interaction between the upper atmosphere and the plasma environment of the magnetosphere creates an auroral lightshow that is unrivalled in the Solar System. The influence of solar ultraviolet light on the chemicals in Jupiter's stratosphere generates a rich atmospheric chemistry. And motions within the interior, from the metallic hydrogen to the deep atmosphere, influence the ever-shifting clouds and colours in the visible atmosphere.

For all these reasons and more, a comprehensive investigation of Jupiter as the archetypal giant planet is one of the two primary goals of ESA's Jupiter Icy Moons Explorer (JUICE), Europe's first mission to the Jupiter system (Witasse et al. in prep.). The emergence of habitable worlds within Gas Giant systems is explored by Tobie et al. (in prep.) and Tosi et al. (in prep.), focussing on Ganymede, Europa and Callisto. The wider Jovian system, and the magnetosphere, are covered by Masters et al. (in prep.), Schmidt et al. (in prep.) and Denk et al. (in prep.), here we focus on the Jupiter scientific investigations enabled by the JUICE orbital tour and its suite of state-of-the-art instruments. Jupiter science, particularly atmospheric, magnetospheric, and auroral science and how they connect to the wider system of potentially-habitable satellites, formed a key component of ESA's Jupiter mission from the outset, when it was first formulated as the multi-spacecraft Laplace mission in 2007 (Blanc et al. 2009) for ESA's Cosmic Vision. The science case evolved as it became the Jupiter Ganymede Orbiter (JGO, Blanc and Greeley 2010), ESA's contribution to the Europa-Jupiter System Mission (EJSM) between 2008 and 2011. Finally, Jupiter exploration was a cornerstone in the science case for JUICE (Grasset et al. 2013), which was selected (2012) and adopted (2014) as ESA's first 'L-class' mission, and which launched on April 14th, 2023.

The science case presented by Grasset et al. (2013) built on the discoveries of the Galileo orbiter (1995-2003) and *in situ* probe (1995); the Voyager 1 and 2 (1979), Cassini (2000) and New Horizons (2007) flybys; and the wealth of remote sensing investigations from ground-based and earth-orbiting observatories. These previous missions had provided snapshots of Jupiter at specific times, often lacking adequate sampling of Jovian variability over minutes (e.g., auroras, lightning), days (e.g., storm

[1] Jupiter's axial tilt is 3° and its orbital eccentricity introduces a 14% maximum change in insolation at Equator (Levine et al. 1977), providing limited seasonal forcing during its 11.9-year orbit

plumes, impacts), months (belt/zone changes), and years (vortices) to determine the mean atmospheric state and the drivers of variability. It was hoped that JUICE would provide a continuity of data coverage over long temporal baselines to address the shortcomings of the previous snapshots, particularly the challenging Galileo observations due to the failed deployment of its high-gain antenna. JUICE would also use broad and quasi-simultaneous spectral coverage from the UV to the sub-millimetre to probe different atmospheric layers. At the time of mission adoption, the Jupiter science case (Grasset et al. 2013) aimed to provide *'the first four-dimensional climate database for the study of Jovian meteorology and chemistry,'* creating a global picture of the processes shaping the Jovian atmosphere *'from the thermosphere down to the lower troposphere.'* This led to three science objectives to characterise atmospheric (a) dynamics and circulation; (b) composition and chemistry; and (c) vertical structure and clouds. It also determined a series of mission requirements that would contribute to the design of the JUICE orbital tour, sampling both low- and high-latitude domains over a long span of time.

Since the JUICE Jupiter science case was developed, both the orbital tour (Boutonnet et al. in prep.) and the payload capabilities have been fully specified. Furthermore, NASA's Juno mission has been providing new discoveries and insights into the planet's interior, atmosphere, and magnetosphere since its arrival at Jupiter in 2016 (e.g., Bolton et al. 2017). Juno's elliptical polar orbit brought the spacecraft close to Jupiter every $\sim$ 53 days (reducing to $\sim$ 40 days during the extended mission) to provide high-resolution regional views, whereas JUICE will have a near-equatorial orbit that provides opportunities for longer-term monitoring and global views. The tour strategies for Juno and JUICE are therefore different and complementary. Furthermore, Juno's exploration of the deep interior via gravity sounding and microwave remote sensing complements the JUICE observations at lower pressures. Given the wealth of new discoveries from Juno and supporting Earth-based observations since the original JUICE objectives were developed, and new insights gained from the culmination of the Cassini mission at Saturn between 2004-2017, this paper revisits and significantly updates the JUICE Jupiter science case.

This paper is organised as follows. Section 2 provides a brief review of the Jupiter science case for JUICE, in light of the latest discoveries, and focusing on key questions and objectives that must be addressed by the tour and payload. Requirements for the tour, and the observation opportunities needed to address the science objectives, are discussed in Section 3. Details of the payload relevant to Jupiter science, and how the instruments will operate both independently and synergistically to achieve the science goals, are provided in Sections 4-5. We place the JUICE science case into broader context of other missions and astronomical facilities operating in the 2030s in Section 6, and emphasise the need for Earth-based support from amateur and professional observers. Finally, Section 7 confirms how the instruments and tour achieves closure of the science requirements.

2 Jupiter Scientific Objectives

Jupiter's atmosphere, and its connections to both the deep interior and external plasma environment, are to be explored via a carefully-designed remote sensing investigation (Section 4) across a $\sim 4-year$ orbital tour that samples a range of illumination conditions, geometries, and orbital inclinations (see Section 3). The original JUICE Jupiter science case was subdivided into three scientific objectives that sought to 'characterise atmospheric (a) dynamics and circulation; (b) composition and chemistry; and (c) vertical structure and clouds.' This led to a traceability matrix with 11 specific science investigations (Table 1, and summarised in Figure 1), and 12 level-one science requirements (based on Science Requirements Document JUI-EST-SGS-RS-001). These requirements on the spacecraft capabilities and tour are emphasised in **boldface font** and discussed in detail in this Section, but first we briefly introduce the payload elements that will be crucial to achieving the JUICE Jupiter-science objectives: an ultraviolet spectrograph (UVS, Gladstone et al. in prep., and Section 4.1); visible-light camera (JANUS, Palumbo et al. in prep., and Section 4.4); near-infrared mapping spectrometer (MAJIS, Poulet et al. in prep., and Section 4.2); sub-millimetre wave instrument (SWI, Hartogh et al. in prep., and Section 4.3); a radio science experiment for atmospheric occultations (3GM, Iess et al. in prep. and Section 4.5; PRIDE, Gurvits et al. in prep.); and a radio and plasma wave instrument (RPWI, Wahlund et al. in prep., and Section 4.6). These studies, conducted synergistically by six onboard instruments and an Earth-based experiment (PRIDE), will be used to achieve the scientific goals described in the following sections.

JA	**Characterise the atmospheric dynamics and circulation**
JA.1	Investigate the dynamics and variability of Jupiter's weather layer.
JA.2	Determine the thermodynamics of atmospheric meteorology.
JA.3	Quantify the roles of wave propagation and atmospheric coupling on energy and material transport.
JA.4	Investigate auroral structure and energy transport mechanisms at high latitudes.
JA.5	Understand the interrelationships between the ionosphere and thermosphere.
JB	**Characterise the atmospheric composition and chemistry**
JB.1	Determine Jupiter's bulk elemental composition to constrain formation and evolution.
JB.2	Investigate upper atmospheric chemistry and exogenic inputs from the stratosphere to the thermosphere.
JB.3	Study spatial variation in composition associated with discrete phenomena and polar vortices.
JB.4	Determine the importance of moist convection in meteorology, cloud formation, and chemistry.
JC	**Characterise the atmospheric vertical structure and clouds**
JC.1	Determine the three-dimensional temperature, cloud and aerosols structure from Jupiter's upper troposphere to the lower thermosphere.
JC.2	Study coupling by waves, eddy mixing and global circulation across atmospheric layers.

Table 1 JUICE Jupiter Scientific Objectives

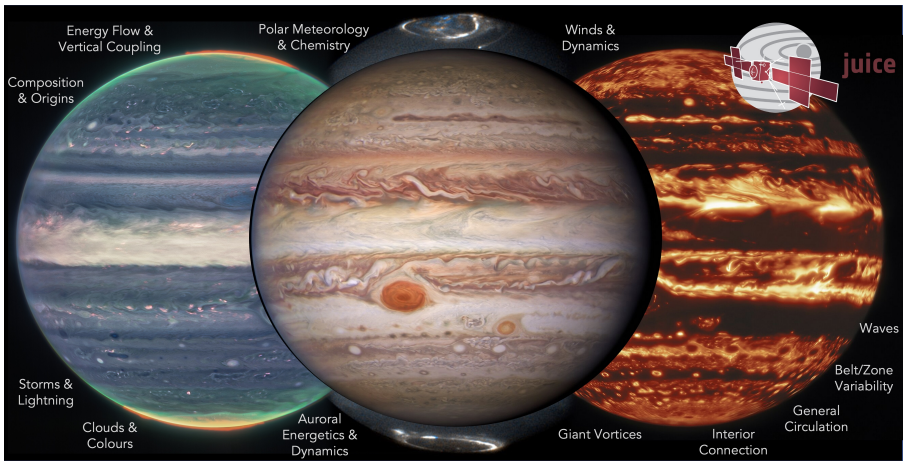

Fig. 1 Summary of the Jupiter science enabled by the JUICE mission. Images show Jupiter in visible light from Hubble (centre, Credit: NASA, ESA, NOIRLab, NSF, AURA, M.H. Wong and I. de Pater *et al.*), near-infrared from JWST (left, credit: NASA, ESA, CSA, Jupiter ERS Team; image processing by Judy Schmidt), and in the 5-μm window (right, credit: Gemini Observatory, NOIRLab, NSF, AURA, M.H. Wong *et al.*), where clouds appear in silhouette against the thermal background. Auroral emissions from H_3^+ can be seen in the JWST image, and in the UV in Hubble observations (centre-top and centre-bottom, credit: NASA, ESA. J. Clarke).

2.1 Jupiter's Dynamic Weather Layer

Investigations of Jovian dynamics and meteorology are naturally biased to the dayside top-most clouds, where contrasts in colours, and rapid motions of small-scale meteorological phenomena, reveal the banded structure of winds, aerosols, temperatures, and gaseous composition. This two-dimensional perspective samples a relatively unique interface, where the condensate cloud decks start to mingle with sunlight; where adiabatic lapse rates (both dry and saturated) become influenced by radiative heating to produce the statically-stable upper troposphere; and where photolysis of gaseous compounds by ultraviolet light can produce colourful hazes. Despite this complexity, visible-light images of this region surrounding the top-most clouds informs much of what we know today about atmospheric dynamics on Jupiter-sized worlds (Ingersoll et al. 2004; Vasavada and Showman 2005; Sánchez-Lavega et al. 2019). However, spectroscopy from the UV to the sub-millimetre (Fig. 3) provides an invaluable tool to access the vertical dimension, probing the depths below the visible cloud tops ($\sim$ 500 $-$ 1000 mbars), and extending measurements through the cold-trap of the tropopause ($\sim$ 100 mbar), the radiatively-controlled stratosphere (mbar-μbar pressures), and into the ionosphere and thermosphere (nbar pressures). Spectroscopy from JUICE will exploit reflected sunlight, i.e., the solar spectrum with significant absorption from methane and other species to sound the vertical distribution of aerosols, and thermal emission, i.e., hydrogen-helium collision-induced opacity overlain by tropospheric absorption and stratospheric/ionospheric emission bands. JUICE will use nadir views, limb views, and solar/stellar occultations, to probe the

vertical domain and the transfer of energy, momentum and material between adjacent atmospheric layers.

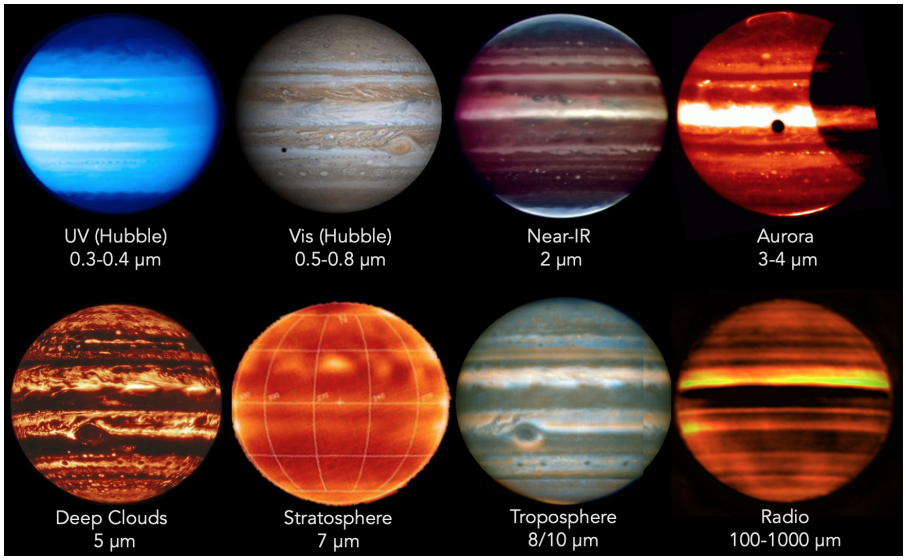

Fig. 2 Multi-wavelength remote sensing of Jupiter provides access to both reflected sunlight (UV to near-IR) and thermal emission (mid-IR to radio). These false-colour images demonstrate the appearance of the atmosphere at different wavelengths. JUICE UVS will measure scattered sunlight from upper-tropospheric aerosols. JANUS and MAJIS observations (below approximately 3 μm) sense clouds, chromophores and winds using both the continuum and strong CH_4 absorption bands (Hueso et al. 2017; Grassi et al. 2020). MAJIS will be able to observe H_3^+ emission from Jupiter's ionosphere and auroras between 3-4 μm (VLT/ISAAC observations, Credit: ESO), as well as thermal emission from the deep cloud-forming layers near 5 μm (Gemini/NIRI observation, Wong et al. 2020). Although JUICE lacks mid-IR capabilities (VLT/VISIR observations, Fletcher et al. 2017a) and radio-wavelength capabilities (VLA observations, de Pater et al. 2016), sub-millimetre sounding by SWI will probe the stratospheric temperatures and winds.

This capability to view the Jovian atmosphere in three dimensions will be exploited over a variety of spatial scales, from the largest circulation patterns, to the smallest storm systems and waves.

2.1.1 Belt/Zone Circulation

The dominance of the Coriolis force in the momentum balance on a rapidly rotating planet leads to the generation of a system of planetary bands. Jupiter's system of zonal (east-west) jets has been remarkably stable over multiple years (García-Melendo and Sánchez-Lavega 2001; Porco et al. 2003; Hueso et al. 2017; Tollefson et al. 2017), despite significant variability in cloud coverage and aerosols. The jets themselves appear to be maintained by an upscale flow of energy, from the smallest scales to the largest scales, with eddies and storms feeding momentum into the zonal flows (Sánchez-Lavega et al. 2019). Given Jupiter's rapid rotation, the jets are in geostrophic balance, as the Coriolis force is in balance with the forces exerted by

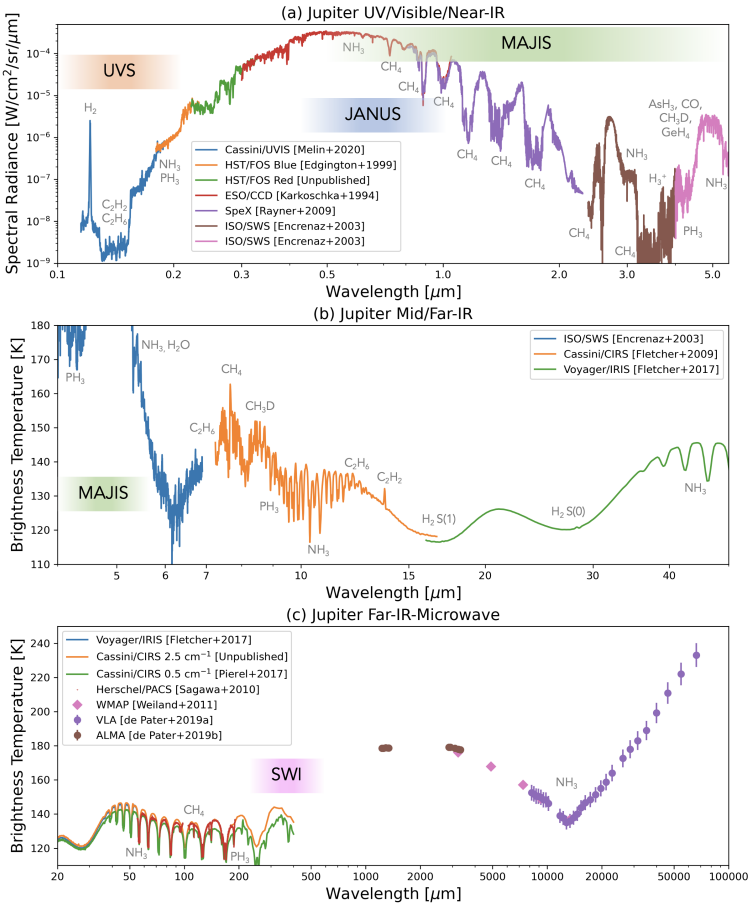

Fig. 3 Overview of Jupiter's reflected ($\lambda < 4$ μm) and thermal emission ($\lambda > 4$ μm) spectra, with key molecular features labelled, and the approximate ranges covered by UVS, JANUS, MAJIS and SWI. UV, visible, and near-IR spectra in (a) were created from a low-latitude spectrum from Cassini/UVIS (Melin et al. 2020); Hubble FOS spectra at $6 - 20^{\circ}$N acquired in November 1992 with the blue and red detectors (Edgington et al. 1999); disc-averaged measurements from the European Southern Observatory (Karkoschka 1994) converted from albedo to spectral radiance assuming the solar spectrum of (Meftah et al. 2018); disc-averaged measurements from IRTF SpeX instrument (Rayner et al. 2009) approximately scaled to match adjacent datasets; and disc-averaged ISO/SWS measurements from Encrenaz (2003). Mid- and far-IR spectra in (b) were from ISO/SWS, plus low-latitudes averages from Cassini/CIRS (Fletcher et al. 2009) and Voyager-1/IRIS (Fletcher et al. 2017b). Far-IR to microwave spectra in (c) were from averaged Cassini/CIRS spectra (Pierel et al. 2017), Herschel/PACS observations (Sagawa et al. 2010); and disc-averaged brightnesses from WMAP and ALMA in the millimetre (Weiland et al. 2011; de Pater et al. 2019a) and VLA in the centimetre (de Pater et al. 2019b).

the pressure gradient, and the thermal wind equation (Holton 2004) relates the vertical shear on the winds to latitudinal temperature contrasts in the upper troposphere. At altitudes above the top-most clouds, the tropospheric winds are found to decay with increasing height (Pirraglia et al. 1981; Flasar et al. 2004; Fletcher et al. 2016), and the temperature gradients and zonal jets are so well co-aligned that both are used

to define the latitudes of Jupiter's canonical warm, cyclonic 'belts' and cool, anticyclonic 'zones.' These axisymmetric bands sometimes (but not always) exhibit contrasts in aerosol properties - zones are often considered to be bright and reflective, as volatile species like ammonia become saturated and condense to NH_3 ice at the cool temperatures of the zones. Conversely, aerosols evaporate/sublime in the warmer and typically cloud-free belts. But this correspondence between aerosols and the belt/zone boundaries is only well defined around the equator, with its typically-white Equatorial Zone (EZ) bordered by the typically-brown North and South Equatorial Belts (NEB and SEB). At mid-latitudes, the banding becomes more tightly packed, with Tropical Zones giving way to a series of Temperate Belts in each hemisphere, each bordered by prograde (eastward) jets on the equatorward edge, and retrograde (westward) jets on their poleward edge. Here the correspondence between the thermal/wind banding and the aerosol properties begins to break down (Fletcher et al. 2020). The last detectable zonal jets, around $65 - 70^{\circ}$ in each hemisphere, give way to a polar region dominated by smaller-scale vortices and large cyclones (Orton et al. 2017; Mura et al. 2022), albeit still with some form of latitudinal organisation (see Section 2.1.2). A diagram presenting the zone/belt structure is shown in Figure 4.

Jupiter's belts and zones therefore appear to differ as a function of latitude, and their appearance at least at wavelengths sensitive to aerosols appears to change over poorly understood timescales (Fletcher 2017; Antuñano et al. 2018, 2019). To better understand the circulation patterns associated with the planetary banding, JUICE will probe their vertical aerosol and gaseous structures via spectroscopy, and characterise the fluxes of momentum and energy into the zonal jets. Crucially, the JUICE orbital tour enables long-term monitoring of the winds, clouds, and composition, to see how they change along with the axisymmetric 'upheavals' to their appearance. For example, the North Equatorial Belt undergoes periods of northward expansion and contraction with a 4-5 year period (Fletcher et al. 2017a); the Equatorial Zone exhibits periodic clearings of clouds with a 6-7 year period (Antuñano et al. 2018); the North Temperate Belt exhibits spectacular plume activity on a 4-5 year period (Sánchez-Lavega et al. 2016); and the South Equatorial Belt displays disturbances, fades (whitening) and revivals with periods of 3-7 years (Sánchez-Lavega and Gomez 1996; Fletcher et al. 2017c). These timescales, or at least their half-cycles, are within reach of the JUICE mission.

Measuring Winds:. Determination of wind speed and direction requires the monitoring of cloud tracers (Sánchez-Lavega et al. 2019), usually over one Jupiter rotation (10 hours), but sometimes over smaller time-scales (0.5-2.0 hr) on particularly active regions in convective storms, turbulent regions or inside vortices. Continuum-band imaging, i.e., away from strong methane absorption, where the atmosphere is relatively transparent down to the NH_3-ice cloud tops, and methane-band imaging (i.e., sensing the upper tropospheric hazes) can be used to determine how winds vary with altitude, a direct measure of the vertical wind shear that can be compared to maps of tropospheric temperatures derived from continuum spectra measured in the submillimetre. The resultant wind maps can reveal zonal and (weak) meridional motions, and resolve the motions of individual eddies to understand momentum convergence on the zonal jets (Salyk et al. 2006), as well as the kinetic-energy and turbulence spectra at the cloud tops. By observing how this changes with time, such maps will

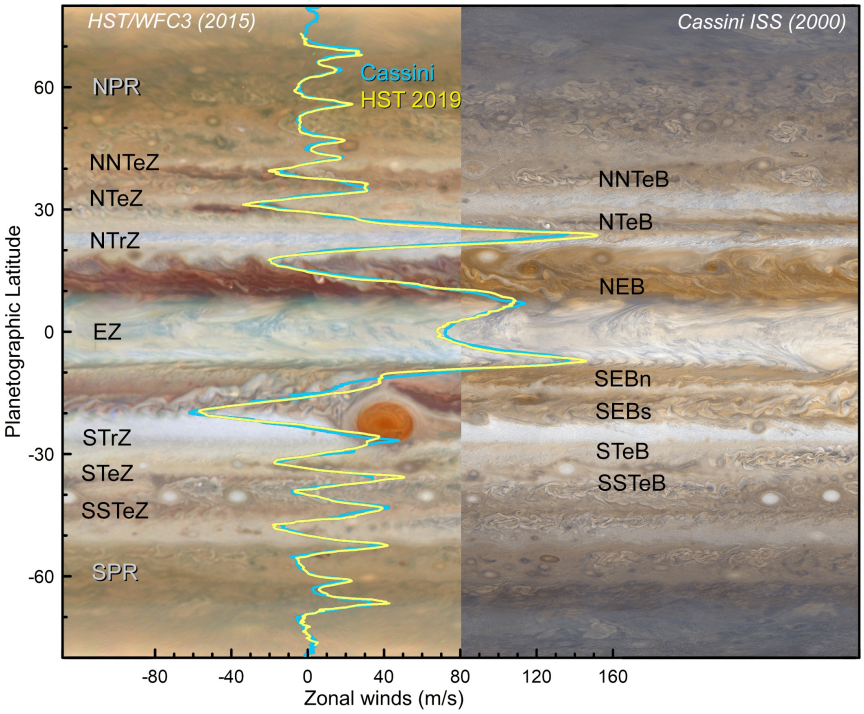

Fig. 4 Jupiter belts and zones, defined by the zonal winds, compared to contrasts in colour and reflectivity. White zones and reddish belts alternate in latitude following the anticyclonic and cyclonic shear of the zonal jets. The locations and overall characteristics of the jets and the bands are stable in time, but the magnitude of the winds and the intensity of the belt/zone colors are variable. Zonal winds in this figure come from Cassini in 2000 (Porco et al. 2003) and from Hubble images from 2019 following an equivalent analysis to that presented in Hueso et al. (2017). The conventional names of zones (left) and belts (right) are given. The HST background on the left comes from the HST/OPAL program and is available at http://dx.doi.org/10.17909/T9G593. The Cassini map is available at NASA photojournal as image PIA02864.

allow JUICE to explore the variability of the energetics of the jets, particularly in relation to discrete storm activity and planet-wide changes. JUICE was therefore required to **'globally determine the vertical structure of zonal, meridional and vertical winds and eddy fields to understand the mechanisms driving zonal jets and meteorological activity (R1-J-5).'** The close-in orbit of Juno, whilst providing high-resolution regional views of atmospheric phenomena with JunoCam (Hansen et al. 2017a), cannot provide the global temporal coverage needed to study the global windfield.

This discussion naturally raises the question of how the windspeeds change as a function of depth. Infrared imaging, particularly in the 4.5-5.7 μm range, senses thermal emission from the 2-6 bar region, with clouds in silhouette (i.e., absorbing) against the bright background. Tracking of cloud tracers at these longer 'M-band' wavelengths may enable JUICE to measure windshear immediately below the NH_3 ice clouds, down to the levels where the NH_4SH cloud forms via combination of NH_3

and H_2S, and possibly the condensation levels of H_2O clouds (see Figure 5). The Galileo probe revealed that winds appeared to strengthen from the cloud tops to the 5-bar level (Atkinson et al. 1998) for a single location (the jet stream separating the NEB and EZ), whilst microwave contrasts measured by Juno (Oyafuso et al. 2020) were suggestive of the same strengthening of zonal winds at all latitudes down to the $\sim$ 6 bar level of the H_2O cloud (Fletcher et al. 2021). However, degeneracies between ammonia absorption and physical temperatures prevent a unique interpretation of microwave data, so JUICE will attempt to use visible and near-infrared observations to directly determine windshear and atmospheric stability across all of Jupiter's belts and zones down to approximately $\sim$ 5 bars.

Clouds and Hazes: JUICE has two further techniques to determine the properties of the belts and zones - by mapping the distributions of aerosols and gases. The vertical distribution of aerosols - both condensed volatiles like NH_3 ice, and photochemical hazes like hydrazine N_2H_4 - can be derived by modelling reflected-sunlight spectra in the near-infrared, as the differing strengths of gaseous CH_4 absorption provide sensitivity across a range of altitudes. The phase function of aerosol scattering can be used to investigate the size, shape, and possible chemical composition of the aerosols. This remains a considerable unknown - the clouds are certainly not pure condensates (e.g., Sromovsky and Fry 2010a; Pérez-Hoyos et al. 2020), but could be aggregates of multiple compounds, seeded around a cloud-condensation nucleus that could be photochemical in origin (e.g., West et al. 2004). However, breaking the degeneracies between the optical properties, composition, and vertical structure requires sampling the aerosol population under a range of illumination conditions and viewing geometries, from nadir low-phase imaging in noon sunlight, to observations of the dawn and dusk terminator regions. Darkening as observations approach the planetary limb and terminator can provide invaluable constraint on the aerosol properties. Diagnostic spectral signatures of pure NH_3 ices, H_2O ice and NH_4SH all exist in the near-infrared accessible to MAJIS, particularly near 2-3 μm (Baines et al. 2002; Sromovsky and Fry 2010a, 2018), which can be used to understand the existence of fresh ices in regions of strong convective activity.

The JUICE orbital tour was required to **'provide sufficient spectral, latitudinal, illumination and phase angle coverage to investigate Jovian aerosols from the condensation clouds to upper tropospheric and stratospheric hazes (R1-J-10).'** The nature of these Jovian aerosols is expected to be tied to their formation environments, such as fresh white condensates in cold zones, or stagnant UV-photolysed hazes in quiescent vortices, so JUICE will **'relate the global temperature and wind structure to visible properties (albedo, winds, clouds) and atmospheric chemistry (R1-J-3).'** Finally, the ability to view the limb of Jupiter at high spatial resolution, using visible images and infrared spectral maps, could also provide access to thin, tenuous haze layers in the lower stratosphere, which in turn can be tied to the vertical thermal structure derived via sub-millimetre sounding the solar/stellar occultations. Figure 5 shows the various altitudes and cloud layers probed by the remote sensing instruments.

Volatiles and Disequilibrium Species:. Clouds are intricately linked to the supply of volatile species (NH_3, H_2S , H_2O) to condense on condensation nuclei, and colourful aerosols are linked to the supply of chemicals (e.g., PH_3, NH_3, sulphur-

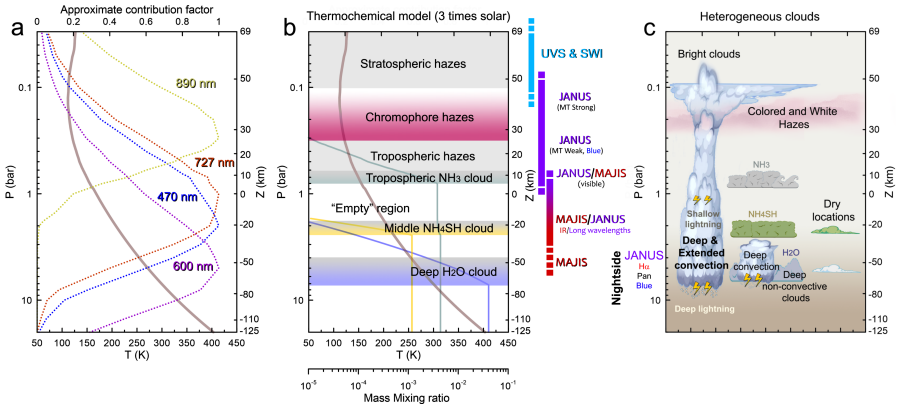

Fig. 5 Vertical structure of Jupiter's troposphere and lower stratosphere. Deriving the vertical cloud structure at different locations from JANUS/MAJIS data will require the use of radiative transfer models. Reflected-sunlight bservations will be sensitive to levels from $\sim$ 100 mbar (in the methane absorption band with JANUS) to at least 2.5 bar (in the IR images from MAJIS) with some contributions from deeper layers (Wong et al. 2023). (a) In a cloudless atmosphere imaging filters from the blue to red wavelengths can penetrate deep in the atmosphere limited by Rayleigh scattering and methane absorptions at specific wavelengths such as in 727 and 890 nm (contribution functions for single wavelengths from Dahl et al. 2021). (b) The nominal cloud structure in Jupiter consists of layers of ammonia, ammonia hydrosulphide and water clouds with approximate cloud bases at around 0.7, 2.5, 5-7 bar, respectively, depending on the local abundance of condensables (the thermochemical calculation shown here assumes 3 times solar abundance of condensables; see Atreya et al. 1999 for details). The upper ammonia cloud limits the penetration depth of visible light. Above the condensate clouds are higher-altitude hazes with varied properties in different Jupiter regions that can be sampled with a combination of methane band images and observations in near-IR wavelengths. (c) The real cloud structure is probably very heterogeneous with locations of deep convection, dry areas and intermediate cloud systems.

bearing species) that can be photolysed by UV irradiation above the clouds. The strength of vertical mixing within the belts and zones is a crucial missing piece to understand this puzzle. Upper tropospheric PH_3 and NH_3 are known to be elevated in the anticyclonic zones and depleted in the cyclonic belts (Gierasch et al. 1986; Achterberg et al. 2006; Fletcher et al. 2009; Grassi et al. 2020). The EZ is the only region with a significant deep column of NH3 gas below the ammonia clouds (de Pater et al. 2016; Li et al. 2017). The ammonia rich EZ renders this region dark at microwave wavelengths sensitive to depths from 1 bar all the way down to 100 bar. Saturn displays a similar connection between gaseous species and the meridional circulation on the scale of the belts and zones (e.g., Fletcher et al. 2011; Laraia et al. 2013).

The meridional circulation derived from temperature measurements and jet decay was first explored during the Voyager era (Pirraglia et al. 1981; Conrath and Pirraglia 1983). The circulation associated with the equatorial zones and belts has been likened to the Earth's Hadley circulation (Barcilon and Gierasch 1970). On the other hand, the mid-latitude jets may be similar to Earth's Ferrel-like circulations (Fletcher et al. 2020) that may exhibit different directions (upwelling, downwelling) above and below the water-condensation level (as revealed by contrasts in microwave brightness associated with NH_3 and temperatures in the 0.1-100 bar region, Duer et al. 2021;

Fletcher et al. 2021). This hypothetical vertically-stacked series of cells with different circulation regimes is testable using measurements of gaseous species as tracers and the distribution of moist convection inferred from lighting (Ingersoll et al. 2000; Fletcher et al. 2020). However, the belt/zone variability of several gaseous species accessible in the 4.0-5.7 μm range, including AsH_3, GeH_4, CO, and H_2O, remains unclear, largely due to the challenge of accessing the trace abundances, and degeneracies associated with the distribution of aerosols (Giles et al. 2017; Bjoraker et al. 2018; Grassi et al. 2020). Both PH_3 (160-180 nm) and NH_3 ($>$ 160 nm) also provide absorption in the ultraviolet (Edgington et al. 1998; Melin et al. 2020), sensing higher altitudes of the upper troposphere where photochemical depletion dominates. It is possible that vertical motions, and associated transport of materials, is localised within discrete meteorological features (see Section 2.1.3), rather than being elevated over an entire planetary band. JUICE will map the spatial distributions of each of these species, and monitor their variation over months and years, in an effort to understand the belt/zone circulation patterns within and above the cloud-forming region of the troposphere.

At even higher pressures, below the cloud-forming layers, Juno has revealed that the cloud-level winds persist down to approximately 3000 km depth, decaying away before reaching the transition to metallic hydrogen (Kaspi et al. 2018, 2020; Guillot et al. 2018). The truncation of these winds could potentially be due to stabilising compositional gradients or radiative zones at great depth (Christensen et al. 2020), but must occur before differential winds reach the conducting, uniformly rotating interior where the dynamo originates (Cao and Stevenson 2017). Juno's microwave radiometer can probe below the clouds to depths of $\sim$ 300 km, but unexpectedly found that NH_3 still showed spatial belt/zone variability and global depletion (Ingersoll et al. 2017). The absence of microwave remote sensing and close-perijove gravity measurements on JUICE means that it will not directly reproduce these Juno discoveries, but it will scrutinise the interface region down to $\sim$ 5 bars - the weather layer sitting above the deeper troposphere - using infrared spectroscopy to understand how it couples to the deeper circulation patterns revealed by Juno.

2.1.2 Vortices

Jupiter's banded appearance is disrupted by the presence of a diverse collection of geostrophic vortices, both anticyclones (high-pressure centres, with anticlockwise circulation in the southern hemisphere) and cyclones (low-pressure centres, with clockwise circulation in the southern hemisphere), as displayed in Figure 6. These vortices possess the same sign of vorticity as the environment in which they are embedded, and are prevented from migrating with latitude by the strong shears associated with the system of zonal jets. Jupiter displays a fundamental asymmetry between the two types - anticyclones appear larger and more numerous than cyclones. Anticyclones appear to grow at the expense of other anticyclones, as was the case for Oval BA, which formed from three smaller anticyclones in the South Temperate Belt (Sánchez-Lavega et al. 2001). These vortices are relatively shallow 'pancake-like' structures, with horizontal extents orders of magnitude greater than their depths. They are thought to possess a midplane somewhere in the cloud-forming region (Dowl-

ing 2014; Lemasquerier et al. 2020), where tangential velocities and the pressure differences are at a maximum. Their windspeeds decay via the thermal wind equation (a 'despinning') with both altitude and depth. Thus an anticyclone will exhibit a cold anomaly in the upper troposphere, a cyclone will exhibit a warm anomaly, and such thermal contrasts have been confirmed by mid-infrared thermal imaging (e.g., Fletcher et al. 2010; Wong et al. 2020). Below the vortex midplane, there is evidence from Juno for warm cores beneath anticyclones, and cold cores beneath cyclones (Bolton et al. 2021; Parisi et al. 2021). However, these deep levels will not be accessible to JUICE.

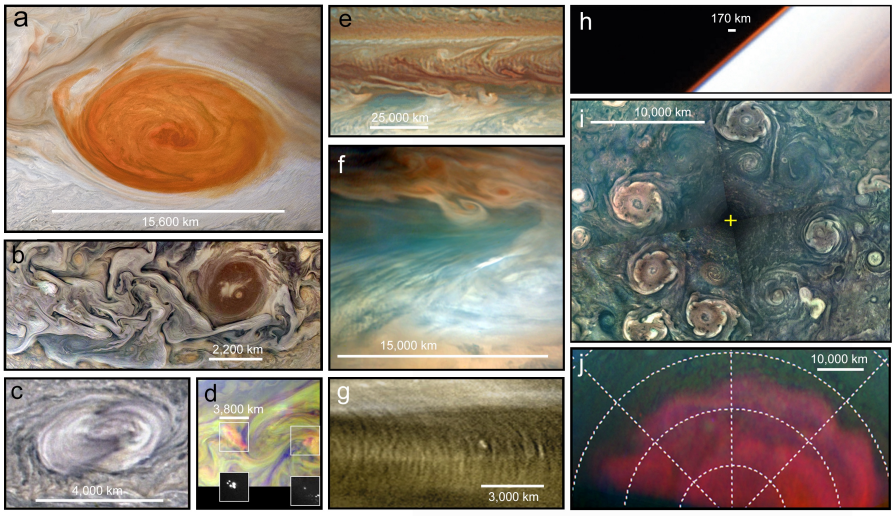

Fig. 6 Jupiter atmosphere: Morphology and variety of atmospheric features at different spatial scales: (a) Jupiter's Great Red Spot. (b) Turbulent features at a 55°N. (c) Convective storm at 31°S. (d) Dayside storms with lightning observed at the same location on the nightside. (e) Series of short-scale gravity waves in Jupiter's cloud at 17°N above a series of large dark features at 8°N in Jupiter's North Equatorial Belt. (f) One of the dark projections of the North Equatorial Belt, sometimes known as a 5-μm hotspots. (g) New Horizons observation of small-scale gravity waves in Jupiter's atmosphere. (h) Galileo observations of Jupiter's limb in violet and near infrared light at 756 nm. (i) Composite map of Jupiter's North polar region in polar projection from Junocam observations obtained on different perijoves. (j) combination of visible and near IR observations of Jupiter's South polar region sampling polar hazes structured as a circumpolar wave. Latitudinal grid is superimposed each 10°. Credits and sources: (a) and (b). Junocam images acquired on February 12, 2019 with credits: NASA / JPL-Caltech / SwRI / MSSS / Kevin M. Gill. (c) Excerpt from a Junocam observation obtained on June 2, 2020. (d) Combination of Galileo SSI images obtained on May 4, 1999. NASA / JPL-Caltech. Image (e) is an HST observation from April 1, 2017 from Simon et al. (2018a). Image (f) is a Junocam observation obtained on Sept. 16, 2020. (g) New Horizons views from the MVIC instrument of equatorial waves on Feb. 28, 2007 with credits from NASA/Johns Hopkins University Applied Physics Laboratory/Southwest Research Institute. (h) Galileo December 20, 1996; NASA / JPL-Caltech. (i) Image composite from Junocam images obtained on Feb. 17, April 10, June 2, and July 25 of 2020. NASA/JPL-Caltech/SwRI/MSSS / Gerald Eichstädt, John Rogers. (j) Adapted from Barrado-Izagirre et al. (2008a).

Anticyclones: The Great Red Spot (GRS) (Figure 6a) is the largest and longest-lived of all the vortices observed in planetary atmospheres (Rogers 1995). Internally

the GRS exhibits a variety of meteorological phenomena (Sánchez-Lavega et al. 2018), and the interaction of these large-scale vortices with the surrounding environment also has a significant effect on Jovian dynamics. The Great Red Spot deflects jet streams to the north and south, which generate a 'wake' of turbulent activity that promotes moist convective plumes (see Section 2.1.3). The peripheral winds appear to entrain material within the GRS (Sánchez-Lavega et al. 2021), such that the unidentified compounds responsible for the orange-red haze (Baines et al. 2019) are either irradiated for longer within the stagnant top of the anticyclone, or some unusual chromophore is supplied from below via secondary circulation with the vortex itself. UV and infrared spectroscopy will be able to compare aerosols and gaseous composition in the GRS compared to its surroundings, and to compare this largest anticyclone to smaller white anticyclonic ovals (Anguiano-Arteaga et al. 2021). Furthermore, the GRS has been steadily shrinking from ∼40000 km in 1879 to its current value of ∼15000 km (Simon et al. 2018b), resulting in changes to its velocity field, vorticity, and temperature structure at the upper cloud level. Another large anticyclone, Oval BA, undergoes colour changes, from white to red and back again (Cheng et al. 2008a). By the early 2030s, JUICE will be able to assess any changes to velocities, vorticity, aerosol coverage and gaseous composition associated with these variable anticyclones.

Cyclones: Temporal variability is not just a feature of anticyclones. Cyclonic vortices come in diverse shapes and sizes, from elongated and quiescent brown barges, to chaotic 'Folded Filamentary Regions' (FFRs) at mid-to-high latitudes, to organised arrays of circumpolar (CPCs) and polar cyclones (PCs) at both poles (Figure 6i). The connections between the dynamics of these different types of cyclones remains unclear, but cyclones do appear to promote moist convective activity (see Section 2.1.3), which may be partially responsible for the chaotic and ever-changing appearance of the FFRs. The CPCs and PCs revealed by Juno (Adriani et al. 2018a) challenge our understanding of Jupiter's polar domain - an octagonal arrangement at the north pole, and a pentagonal (sometimes hexagonal) arrangement at the south pole, whose long-term stability reveals the dynamics of atmospheric turbulence and the 'beta-drift' of cyclones (Gavriel and Kaspi 2021). The inclined phase of JUICE, with sub-spacecraft latitude reaching up to 33°, will provide a new glimpse of the polar domain, with its FFRs and polar cyclones, several years after the culmination of the Juno mission. Whilst the JUICE inclination (see Section 9) does not match the polar orbit of Juno, it does provide a long-term vantage point to observe how these polar features move and change over daily or weekly timescales, and a broader infrared spectral range to study their aerosols and composition. Thus the JUICE mission is designed to **'determine the three-dimensional properties of discrete atmospheric features at high spatial resolution and track them over time (e.g., Great Red Spot, vortices, atmospheric plumes, 'brown barges') (R1-J-6)'.**

2.1.3 Convective Storms and Lightning

On the smallest scales, the high-resolution imaging and spectroscopy of JUICE will be able study individual storm cloud features as a window onto moist convection in hydrogen-rich atmospheres. Although latent heat release at phase transitions can

drive heat transport in atmospheres, the high molecular weight of condensates (compared to the hydrogen atmosphere) can have an inhibiting effect on convection, which must be overcome (Guillot 1995; Hueso et al. 2002; Leconte et al. 2017) to generate the storms that we see. Such storms may help to regulate heat flux through the tropospheric layers, and as such may play a role in the thermal evolution and banded structure of Jupiter.

Storm plumes are observed as small white spots in dynamically-active domains (Figure 6c), such as the centres of cyclonic vortices (Hueso et al. 2022), or the wake of the GRS (Baines et al. 2002). Individual cumulus-like clouds can be seen in Juno high-resolution imaging, often adding texture to larger-scale stratiform clouds. These cumulus clouds are most likely powered by the latent heat release of water condensation in the $\sim$ 6-bar region, providing enough buoyancy to rise through the hydrogen-rich air. Shallow convection, at altitudes too cold for liquid water and potentially associated with latent heat release in NH_3-ice cloud layers, may also be occurring (Becker et al. 2020a; Hueso et al. 2022), and the complex blend of water and ammonia ice may be forming slushy 'mushballs,' (Guillot et al. 2020a), which trap NH_3 gas, precipitate, and then release their payload at several tens of bars (Guillot et al. 2020b). Thus convective motions, and associated precipitation, play a vital role in shaping the vertical structure of aerosols and gaseous composition, both on the largest scales (belts and zones) and smallest scales (surrounding individual storm plumes).

Remote sensing from JUICE will examine these thunderstorms, determining the vertical aerosol structure in the upper troposphere, and the spatial distribution of volatiles (e.g., NH_3 and H_2O) and disequilibrium species (e.g., PH_3, AsH_3, GeH_4, CO) as tracers of vertical motions. Spectroscopic maps in the UV and infrared will be compared to the morphology of the cumulus clouds at the highest spatial resolutions.

JUICE will also examine the distribution and energetics of Jovian lightning, using nightside imaging to detect flashes (e.g., Borucki and Williams 1986; Little et al. 1999; Dyudina et al. 2004; Baines et al. 2007), and listening for radio emissions generated by electrical discharges in the Jovian atmosphere and propagating through the plasma environment. Using this technique during the first quarter of the Juno mission, the Waves instrument has made about two thousand lightning detections. This represents the largest data set on Jovian lightning processes collected to date. Close to Jupiter, low dispersion rapid whistlers occurred at frequencies from 50 Hz to 20 kHz (Kolmašová et al. 2018), and the so-called Jupiter dispersed pulses (JDPs) were recorded at frequencies between 10 kHz and 150 kHz (Imai et al. 2019). The rapid whistlers have dispersion from units of milliseconds to a few tens of milliseconds, and the dispersion of JDPs is even lower. The latter might propagate in the free space ordinary mode through low density regions in Jupiter's ionosphere (Imai et al. 2019). The third kind of Jovian lightning radio bursts are long dispersion whistlers lasting for several seconds, which were previously detected at frequencies of several kHz in different regions of the Io torus between 5 and 6 Jovian radii using Voyager 2 measurements (Gurnett et al. 1979; Kurth et al. 1985). Due to the larger periapsis distances of JUICE ($\sim$9 to 20 Jovian radii, see Section 3) compared to Juno or the Voyagers, it will be more difficult for JUICE RPWI to detect lightning radio pulses.

However, lightning whistlers from very high latitudes as well as JDPs going through the ionospheric low-density patches might propagate that far and be recorded.

In Jupiter's atmosphere, lightning activity is predicted to show the largest emission in the Hα line at 656-nm (Borucki et al. 1996). However, nightside emissions (Figure 6d) of lightning observed by Galileo at 656-nm were ten times weaker than expected (Dyudina et al. 2013). This can be a consequence of deep lightning at pressures larger than a few bar. Shallow lightning on Jupiter at pressures near 1 bar were discovered by Juno at high latitudes (Becker et al. 2020a) and might be brighter at 656-nm than in clear filters. Dayside lightning in Saturn was observed in blue wavelengths during a large-scale storm (Dyudina et al. 2013). Thus, searches of lightning in Jupiter's atmosphere by JUICE will have to use a combination of filters to test different scenarios of depth and intensity of the lightning. Furthermore, JUICE will search for Transient Luminous Events (TLEs) in the ultraviolet from the night side in Jupiter's upper atmosphere (Giles et al. 2020b). Although lightning statistics from Galileo had suggested that lightning was predominantly found within the Jovian belts (Gierasch et al. 2000), Juno observations of microwave sferics and rapid whistlers indicated increased lightning activity at the middle and higher latitudes (Brown et al. 2018; Kolmašová et al. 2018). These distributions of lightning activity provides constraints on moist convection and the deep abundance of water (Yair et al. 1998; Sugiyama et al. 2014; Li and Ingersoll 2015). JUICE will therefore re-examine the relationships between the distribution of lightning and the distribution of cumulus-like clouds, and **'determine the influence of moist convective processes by mapping the frequency, distribution and depth of tropospheric lightning (R1-J-7).'**

2.1.4 Tropospheric Waves

Jupiter's atmosphere exhibits wave phenomena at a variety of scales, each providing a means of characterising the background atmosphere through which they propagate. Longitudinal waves and curvilinear structures have been observed at the smallest scales of Galileo orbiter (Arregi et al. 2009) and Juno imaging (Orton et al. 2020), and interpreted to be gravity (i.e., buoyancy waves in a stably-stratified atmosphere) or inertia-gravity waves (i.e., sensing the Coriolis effect). Mesoscale waves modulating cloud opacity and reflectivity, often found in regions of cyclogenesis, have been observed by the Hubble Space Telescope (HST, Figure 6e), Juno, and ground-based telescopes (Fletcher et al. 2018; Simon et al. 2018a). And larger planetary-scale waves have been observed at low latitudes, including the equatorially-trapped Rossby wave responsible for the chain of 5-μm hotspots (visibly-dark formations, Figure 6f) on the jet separating the NEB and EZ (Allison 1990; Arregi et al. 2006), and the large-scale thermal waves that often occur over the NEB during periods of expansion and contraction (Fletcher et al. 2017a). Large-scale wave motions were recorded as movies by Cassini over two months in late 2000 (e.g., Choi et al. 2013). The polar regions are covered by high hazes that stand out in images taken in methane absorption filters and in the ultraviolet, with their edge at about 65 deg latitude undulating with wavenumber 12 (Figure 6j, Sánchez-Lavega et al. 1998; Barrado-Izagirre et al. 2008b). These Rossby waves, which require a gradient of the Coriolis parameter as the restoring force, are known to modulate aerosol reflectivity and upper tropospheric

temperatures, but as yet the distribution of gaseous species and their phase speeds remains unclear.

Understanding the origins of the waves (e.g., from instabilities, or arising from convection, or some other means) and the deposition of energy during wave breaking (providing or removing momentum from the zonal flows) requires assessment of their motions. Measuring the phase velocities of waves requires long-term imaging and cloud tracking, with timescales tuned to the phenomenon of interest. A JUICE requirement was therefore to **'classify the wave activity in the Jovian atmosphere, both horizontally (multi-spectral imaging) and vertically (R1-J-11).'** We will return to the influence of wave phenomena on the stratosphere and upper atmosphere in the following sections, as a means to couple the meteorology of the troposphere with the circulations at higher altitudes.

2.2 Chemistry and Circulation in the Middle Atmosphere

The previous section described JUICE requirements for remote sensing of the troposphere, at the interface between the deep interior and the cloud-forming regions accessible to multi-wavelength observations. However, a key strength of JUICE is its ability to probe the radiatively-controlled middle atmosphere, namely the stratosphere above the tropopause. Here the stratified thermal structure is determined by a radiative balance (e.g., Guerlet et al. 2020a) between heating (absorption by CH_4 gas and aerosols) and cooling (thermal emission from ethane, acetylene, and to a lesser extent CH_4), and UV photolysis of methane generates a complex network of hydrocarbon species (Moses et al. 2005a) with emission features throughout the mid-infrared. The JUICE remote sensing payload is required to **'characterise the three-dimensional temperature structure of the upper troposphere, stratosphere, and thermosphere (R1-J-9.5),'** enabling a comprehensive study of the Jovian middle atmosphere.

Stratospheric Temperatures: Jupiter's stratospheric circulation exhibits similar zonal organisation as the troposphere, with bands of warmer and cooler regions revealed via thermal imaging (Figure 7). The zonal organisation is strongest at low-latitudes, where Jupiter's equatorial stratospheric oscillation (often referred to as the Quasi-Quadrennial Oscillation, or QQO, Leovy et al. 1991a; Orton et al. 1991a) modulates the 10-mbar thermal contrasts at the equator on a $\sim$ 4-year timescale. Mid-infrared spectroscopy revealed that this is associated with a downward-moving chain of warm and cool anomalies (and associated changes in stratospheric zonal jets, Flasar et al. 2004; Cosentino et al. 2017a; Giles et al. 2020a), but long-term monitoring reveals that its period and phase can be substantially perturbed by tropospheric upheavals (Antuñano et al. 2021). The vertical structure of this pattern, which is thought to be driven by waves emanating from the troposphere and interacting with the mean flow (Friedson 1999), can be sounded via emission in the sub-millimetre (Cavalié et al. 2021; Benmahi et al. 2021), particularly with CH_4 and H_2O from the lower stratosphere up to 10 μbar, but also via occultations - radio occultations as JUICE passes behind Jupiter as seen from Earth, and stellar/solar occultations as a star or the Sun sets behind the Jovian limb (e.g., Greathouse et al. 2010). These tech-

niques will reveal the vertical structure of the QQO. Given the expected longevity of JUICE, the pattern of stacked wind/temperature anomalies will be monitored during their descent, sampling a full $\sim$ 4-year period over the duration of the mission.

Gaseous Tracers: Moving to mid-latitudes, the stratosphere again demonstrates coupling to the underlying troposphere. The spatial distribution of stratospheric acetylene is asymmetric between the northern and southern hemisphere (Nixon et al. 2010; Fletcher et al. 2016; Melin et al. 2018), possibly due to a difference in the strength of vertical mixing, rather than differences in the efficiency of photochemical production. Furthermore, significant stratospheric thermal wave activity, likely to be near-stationary Rossby waves, are often reported in the northern hemisphere (Fletcher et al. 2017a) where the acetylene is at its maximum. Ultraviolet spectra from Juno, which exhibit strong C_2H_2 absorption, reveal that this abundance declines strongly towards the poles, as expected from the annually-averaged solar insolation, also indicating that horizontal equator-to-pole mixing is not strong enough to distribute C_2H_2 uniformly with latitude (Nixon et al. 2007b; Giles et al. 2021b). On the other hand, the meridional distribution of C_2H_6 does not follow the mean solar insolation and increases towards the poles (Nixon et al. 2007b), and altitude-latitude advective transport models cannot reproduce these C_2H_2 and C_2H_6 distributions (Hue et al. 2018a).

Recent observations of the polar regions have revealed an even more complex situation, in which the distributions of C_2H_x species are not zonal. Local enhancements in abundances are correlated with the location of the diffuse auroras (Sinclair et al. 2017a, 2018a, 2019). Other species, like HCN and CO_2, also show enhancements/depletion in the polar and auroral regions (Lellouch et al. 2006; Cavalié et al. 2022). This is a strong indication that auroral chemistry plays an important role in these regions. Thermal-infrared observations of the polar stratosphere and upper troposphere reveal cold polar vortices (Simon-Miller et al. 2006; Fletcher et al. 2016), possibly as a consequence of efficient radiative cooling from polar aerosols (Guerlet et al. 2020a), for which C_2 species are probable precursors. However, tying the aerosol distribution observed in reflected sunlight directly to the thermal structure will remain a challenge, particularly as a consequence of auroral heating discussed in Section 2.4.2. JUICE will investigate the thermal structure of the stratosphere, as well as the distribution of tracers like C_2H_2 and C_2H_6 (which have signatures in the FUV below 180 nm, Gladstone and Yung 1983). It will also study the distribution of species deposited by Comet Shoemaker-Levy 9 (SL9) like HCN, CO, CS and H_2O (e.g., Lellouch et al. 1995b; Feuchtgruber et al. 1997), to understand the middle-atmospheric circulation, from the equatorial QQO, to the mid-latitude waves, to the polar domain.

Stratospheric Winds: The global stratospheric temperature field, and the distributions of hydrocarbons, are just two ingredients required for understanding the global circulation. Measurements of winds in the Jovian stratosphere have presented a challenge, given the absence of identifiable cloud tracers to monitor the flows at millibar pressures. Indirect determinations via stratospheric temperature gradients and the thermal wind equation (Flasar et al. 2004; Read et al. 2006) are subject to substantial uncertainties, because there is an altitude gap of two scale heights between the level where the cloud-top winds are used as initial condition (in the upper troposphere), and the levels where the winds are derived (in the stratosphere). Direct and

absolute measurement of stratospheric winds relies on high-resolution spectroscopy to reveal the Doppler shifts of individual sub-millimetre emission lines, recently demonstrated using the Atacama Large Millimeter/submillimeter Array (ALMA) (Cavalié et al. 2021; Benmahi et al. 2022). The winds are measured at the levels probed by the spectral lines, usually in the middle stratosphere with the sensitivity of ALMA. The derivation of the full stratospheric wind field then requires near-simultaneous temperature measurements to be combined with the wind observations using the thermal wind equation, as shown in Benmahi et al. (2021). Although it is an essential piece to constrain general circulation models and quasi-periodic stratospheric oscillations like Jupiter's QQO (see Figure 7), such a combination has only been obtained once in ten years of ALMA operations. The JUICE payload will enable the first maps of stratospheric winds, using emission from CH_4, H_2O, CO, HCN and CS lines. Here we take advantage of an influx of chemical species from exogenic sources, such as long-lived oxygen-bearing species (H_2O, CO_2, and CO), HCN, and CS, many of which were deposited by the impact of the SL9 comet in 1994 (Lellouch et al. 1995a; Harrington et al. 2004) and have been slowly diffusing with latitude ever since (Moreno et al. 2003; Lellouch et al. 2006). High-resolution and high-sensitivity spectroscopy of these emission lines enables simultaneous sounding of stratospheric temperatures and direct wind measurements in the 10 μbar to 100 mbar range, with scale-height resolution, a first for an orbiting spacecraft. Combining sub-millimetre sounding, performed every orbit for the entire JUICE tour, with UV, IR and radio occultations will provide significant opportunities for synergistic science for stratospheric circulation (see Section 5), with the goal to **'globally determine the vertical structure of zonal, meridional and vertical winds (R1-J-5).'**

2.3 Global Composition and Origins

The origin and migration of Jupiter played a central role in shaping the present-day configuration of our Solar System. Its bulk chemical composition (in comparison to that of the Sun) provides a window on the composition of the protosolar nebula at the time of planet formation (Atreya et al. 2003; Lunine et al. 2004; Venturini and Helled 2020). JUICE does not aim to reproduce the Juno capabilities of probing the bulk NH_3 (Li et al. 2017) and H_2O (Li et al. 2020) content of Jupiter's deep interior, nor will it perform gravity sounding of the zonal flows and density gradients in the hot and fluid interior (e.g., the diffuse core extending up to 50% of Jupiter's radius into the overlying molecular envelope, Wahl et al. 2017). Furthermore, the picture of a relatively homogeneous hydrogen-helium envelope, mixed by efficient convection associated with its high intrinsic luminosity (e.g., Guillot et al. 2004; Li et al. 2018) is no longer suitable, with a gradient in heavier elements being more likely. However, JUICE will contribute to our understanding of Jupiter's atmospheric composition from the cloud-forming region and upwards, and is specifically required to **'provide estimates of elemental abundances and isotopic ratios in the atmospheric envelope to constrain the composition of the deep troposphere and the origin of external material (R1-J-9).'**

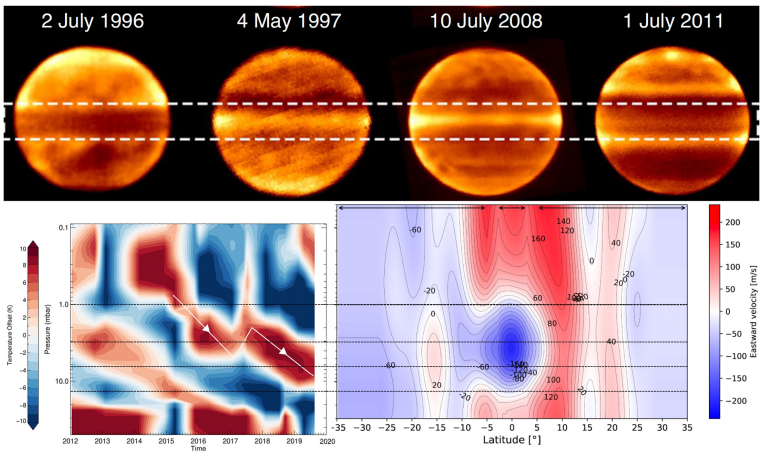

Fig. 7 Jupiter's stratospheric equatorial oscillation was initially discovered from thermal infrared observations similar to those shown in the upper panel (adapted from Antuñano et al. 2021). It is characterised by vertically alternating temperature extrema that descend with time. At a given pressure level (the 3, 6.4, and 13.5 mbar levels are indicated with horizontal dashed lines), positive maxima occur approximately every 4.5 years. Over the years, this oscillation has shown some variability in its periodicity as demonstrated by Giles et al. (2020a) (left panel). The oscillation is not only temporal, but also spatial, as demonstrated on the right panel by the vertically stacked prograde and retrograde jets at the equator (adapted from Benmahi et al. 2021).

2.3.1 Tropospheric Composition and Origins

Thermochemistry in a strongly-reducing environment leads to the most cosmogonically abundant elements (C, N, O, S, P) appearing in their hydrogenated forms (CH_4, NH_3, H_2O, H_2S, PH_3). At the low temperatures of the upper troposphere, the volatile compounds will condense to form clouds (ices of NH_3 and H_2O, and a combination reaction to form NH_4SH, Weidenschilling and Lewis 1973), such that the main reservoirs for these gases are hidden at depth below the clouds. Furthermore, Juno has revealed that NH_3 is not well-mixed even below its $\sim$ 700−mbar cloud base, remaining variable and depleted down to $\sim$ 60 bars (Ingersoll et al. 2017; Li et al. 2017). Spectroscopic measurements from JUICE will sound the abundances above, within, and immediately below the cloud-formation levels. At these altitudes, the abundances are governed by a combination of vertical mixing, saturation, and photolytic destruction (e.g., NH_3 is photolysed to form N_2H_4, a possible contributor to aerosols in the upper troposphere). JUICE contributions are therefore likely to be lower limits for tropospheric volatile enrichments N/H, S/H and O/H. Nevertheless, mapping the latitudinal variability of these species (in relation to the belt/zone structure), and observing how they vary with time, places bulk measurements of these gases into a wider context, to understand how representative they might be of the planet as a whole.

Similarly, disequilibrium species like PH_3, AsH_3, GeH_4 and tropospheric CO can be studied via combination of UV and 4.0-5.7 μm spectroscopy. These species are only present in the upper troposphere as the rate of vertical mixing is faster than the rate of their thermochemical destruction, leading to 'quenched' abundances that are

representative of deeper, kilobar levels (Kaye and Strobel 1984). Their spatial and temporal variability therefore provides estimates of elemental abundances of P/H, As/H, and Ge/H that would be otherwise inaccessible. Furthermore, tropospheric PH_3 and CO are limited by chemical reactions with water, providing an indirect means of estimating the deep water abundance via thermochemistry (Bézard et al. 2002; Visscher et al. 2010; Cavalié et al. 2023). Thus, JUICE can provide indirect constraints on deep elemental abundances, without actually sampling below the cloud-forming layers.

The ratios of isotopes within a particular molecule can also reveal insights into the nature of its original reservoirs, and the proportion of ices incorporated into the forming protoplanets. In particular, Jupiter's deuterium-to-hydrogen (D/H) ratio can be measured in methane (Owen and Encrenaz 2003), using absorption features of CH_3D in the 4.0-5.7 μm range. Separating CH_3D abundances from the properties of aerosols is challenging, and will rely on the techniques described in Section 2.1.1, exploiting reflected sunlight observations under multiple illumination conditions and geometries. Nevertheless, the JUICE estimate of D/H in methane can then be compared to estimates of the D/H in hydrogen (Lellouch et al. 2001a) to understand the fractionation of deuterium between different molecules. It will also be compared to the direct in situ measurement from the Galileo probe (Mahaffy et al. 2000), to assess how well that measurement represents the global composition of Jupiter.

2.3.2 Stratospheric Composition and Evolution

Jupiter's stratospheric composition is determined by photochemistry of methane (which does not condense at Jovian temperatures), alongside the influx of exogenic species from interplanetary dust, bolides and larger impactors (asteroids and comets) entering the upper atmosphere (Moses et al. 2005a; Hue et al. 2018b). As described in Section 2.2, JUICE remote sensing will be able to map the spatial distribution of stratospheric hydrocarbons, primarily C_2H_2 and C_2H_6 in the UV (Melin et al. 2020; Giles et al. 2021b, 2023; Sinclair et al. 2023) as well as CH_3C_2H in the sub-millimetre. An additional goal is to **'constrain the origin of external material (R1-J-9)'** via measurements of abundances and isotopic ratios in externally sourced materials. This includes species like H_2O, CS, CO and HCN originating from the cometary impact (SL9) in 1994. The latitudinal distribution of these species is expected to be governed by stratospheric circulation and diffusion since the time of impact (Moreno et al. 2003; Lellouch et al. 2006), but additional ongoing sources of exogenic materials (e.g., interplanetary dust, connections with Jupiter's rings, or with satellites via magnetic field lines) could be determined via new spatial maps acquired by JUICE in the sub-millimetre (e.g., Connerney 1986; Moses and Poppe 2017). The vertical profiles of H_2O and CO can be mapped with scale-height resolution, providing an indication of the origin of the external oxygen.

JUICE has another technique to determine the origin of these exogenic species - high spectral-resolution observations in the sub-millimetre will provide estimates of isotopic ratios in those molecules, for comparison with the wider Jovian environment. Examples include D/H, $^{16}O/^{18}O$, $^{16}O/^{17}O$ in water and CO; $^{12}C/^{13}C$ in CO; and $^{12}C/^{13}C$ and $^{15}N/^{14}N$ in HCN, each of which may allow us to connect Jupiter's

stratospheric species back to source populations in comets and other icy bodies. For example, if Jupiter's external water originates from interplanetary dust particles and if these particles would enter the planet with slow velocities (so as not to be dissociated by the heat generated during atmospheric entry), then we would expect to find cometary D/H ratios in H_2O, i.e. $1–8\times10^{-4}$ (Anderson et al. 2022). Conversely, if the water were produced by comet impacts and would thus result from the recombination of cometary oxygen with Jovian hydrogen, then the water would exhibit a Jupiter-like D/H ratio, i.e. $\sim2\times10^{-5}$ (Lellouch et al. 2001b). In this case, the ortho-to-para ratio in water would reflect that of Jovian hydrogen and not depart from 3:1. By comparing the potential origins of stratospheric species with what is known of Jupiter's global composition, JUICE will be able to place new constraints on the formation and subsequent evolution of the gas giant.

Finally, JUICE may be lucky and glimpse examples of ongoing evolution in stratospheric composition. The rate of impacts is being refined by Earth-based video monitoring of flashes in the Jovian atmosphere (Hueso et al. 2018b), revealing bolide flashes (i.e., impactors disintegrating in the upper atmosphere) at a detectable rate estimated to be 0.4-2.6 per year. Juno UVS has detected an impactor from orbit, and considering the probabilities of capturing such an event in a UVS scan, estimated a rate that was considerably higher (Giles et al. 2021a). Larger impactors, such as the 1994 Comet Shoemaker Levy 9 (Harrington et al. 2004), or the 2009 'Wesley' asteroidal impactor (Sánchez-Lavega et al. 2010; Hammel et al. 2010), remain much rarer (Zahnle et al. 2003). Each of these events may have observable consequences for atmospheric composition (injecting water and silicate-rich materials, and producing high-temperature shock chemistry within the entry point), and the likelihood of tracking impactors in advance will improve with the commissioning of the forthcoming Vera Rubin observatory (see Section 6). The flexibility and agility of the JUICE spacecraft to react to unique (and potentially unexpected) events will be discussed in Section 3.

2.4 Energetics of the Ionosphere, Thermosphere, and Auroras

Beyond the dynamics of the troposphere, and the circulation and chemistry of the stratosphere, JUICE will explore the interface between the neutral atmosphere and the external charged-particle environment. Jupiter's ionosphere and thermosphere epitomises the JUICE goal of exploring coupling between components of the Jovian system, being influenced by the circulation and wave propagation of the lower atmosphere, and the deposition of energy in the polar region via electrons propagating along magnetic field lines. Particle and fields in situ measurements, by PEP, RPWI and J-MAG, will directly monitor the energy and momentum exchange processes in the magnetosphere responsible for these energetic auroral particles impacting the atmosphere (c.f., Masters et al. in prep.). This gives the electromagnetic energy flux and exact energy distributions flowing downward along the field lines, and can be compared to the auroral emissions detected in the atmosphere at various wavelengths. It will also put further constraints on the ionization, related ion-molecule and thermosphere aerosol formation chemistry, and thermal altitude profiles in the Jovian

ionosphere, and electrodynamic processes that contribute to the atmosphere thermal balance. The locations of the auroral electron acceleration regions and radio emissions from atmospheric lightning can furthermore be remotely monitored by radio wave detections by RPWI.

Above the methane homopause, solar EUV and auroral precipitation shape a region comprising H_2, He and H. The ionosphere is formed from layers of thermal plasma embedded in the neutral atmosphere, from EUV/XUV ionisation or impact ionisation from high-energy precipitating particles. JUICE will explore this upper atmospheric region by means of (i) both radio occultations and stellar occultations to determine electron densities (from refraction and Doppler frequency shifting) and the temperature structure of the neutral atmosphere; and via (ii) imaging spectroscopy (UV and infrared emissions from H_2, H, and the H_3^+ ion) from the auroral regions to low latitudes. Direct measurements of stratospheric winds via sub-millimetre Doppler shifts of spectral lines will also provide constraints on the winds in this region (see Section 5).

2.4.1 Thermospheric Circulation and the Energy Crisis

From stellar occultations and observations of the H_3^+ ion (generated on the dayside via the reaction of H_2 with H_2^+ produced by the ionisation of H_2 under solar Extreme Ultraviolet (EUV) radiation, Drossart et al. 1989), it is known that Jupiter's upper atmosphere and exosphere at low to mid-latitudes are systematically far hotter than can be explained by solar heating alone (Yelle and Miller 2004), a conundrum known as the 'energy crisis.' The auroral regions are bombarded by electrons that cover a broad range of energies, with low energy electrons (eVs) mainly contributing to heating the atmosphere, and the more energetic ones (100 eV and above) producing excitation, ionization, dissociation and subsequent auroral emissions, chemistry, and heating. However, thermospheric circulation models (e.g., Achilleos et al. 1998; Yates et al. 2020) suggest that the strong Coriolis forces associated with Jupiter's rapid rotation should trap this energy at high latitudes. However, recent H_3^+ observations during a potential solar wind compression event have revealed a steady decrease in temperature from the auroral regions to the equator, confirming the potential redistribution of energy from high to lower latitude regions (O'Donoghue et al. 2021). This heating possibly occurs in pulses associated with a solar-wind compression, which facilitates the transport of heat to lower latitudes (Yates et al. 2014). Additional sources of heating from below (e.g., dissipation of gravity and acoustic waves propagating from the troposphere) may contribute to low-latitude variability in H_3^+ emission (Schubert et al. 2003), such as the possible excess heating over the Great Red Spot (O'Donoghue et al. 2016). Such sources, localised and sporadic, also contribute to the highly structured and variable H_3^+ density profile in altitude (Matcheva et al. 2001). Furthermore, heating not only expands the atmosphere but can also drive vertical winds and affect turbulence. The location of the homopause, below which the main atmospheric species are well mixed and above which there is a diffusive separation of species by mass, is hence a tracer of energy deposition and dynamics.

Remote sensing by JUICE will **'characterise the three-dimensional temperature structure of the ... thermosphere (R1-J-9.5)'**. Vertically propagating waves

observed in occultations throughout the atmosphere in the IR and the UV will be directly correlated with potential sources in the lower atmosphere (e.g., moist convective events and plumes) to understand their contribution to the energy budget. The combination of UV and IR occultations is a powerful means to characterise Jupiter's atmospheric vertical structure and composition, the dynamical coupling between layers, and the source of energy sources in the upper atmosphere. They will be complemented by measurements of the stratospheric windfield by SWI, and radio occultations (e.g., Gupta et al. 2022). In addition, UV observations will be critical to derive the global variations of the homopause in terms of height and eddy diffusion coefficient, characterising the amount of mixing, based on hydrocarbon tangential column densities from multiple UV stellar occultations, complemented by dayglow HeI 58.4 nm resonance line observations (e.g., Parkinson et al. 2006, Vervack et al. 1995). Temperature profiles associated with H_2 can be derived from solar and stellar occultations in the UV (Koskinen et al. 2015). Furthermore, UV dayglow maps could help to identify the origin of the H Lyman alpha bulge, its possible connection with the auroral activity or with thermospheric/exospheric circulation, and its relation of any possible longitudinal asymmetry in HeI 58.4 nm.

2.4.2 Jupiter's Auroras

Before the Juno mission, the main emissions (shown in Fig. 8) were thought to be due to co-rotation breakdown in the middle magnetosphere, with emissions related to upward currents (Cowley and Bunce 2001) from the auroral ionosphere. Juno observations have shown that particles and plasma wave phenomena are tightly linked in Jupiter's low-altitude auroral regions (Kurth et al. 2018; Bonfond et al. 2021a; Sulaiman et al. 2022), where different latitudinally separated zones are linked to upward (zone I) and downward (zone II) electric currents (Mauk et al. 2020). Kurth et al. (2018) showed that the electron distributions and significant density depletions corresponding to zone I are coincident with brief but very intense broadband plasma waves propagating downward in the whistler mode at frequencies below 10 kHz. Sulaiman et al. (2022) identified H^+ / H_3^+ cyclotron waves in zone I in the presence of energetic upward H^+ beams and downward energetic electron beams, and large-amplitude solitary waves in zone II. Juno has also detected evidence of large-scale electrostatic potentials above the main aurora, with broad electron energy distributions (Allegrini et al. 2020). Hence, we still probably lack a complete understanding of all the phenomena that produce the aurora.

The variable magnetic footprints of Io, Europa, and Ganymede are visible equatorward of the main oval (Fig. 8, Grodent et al. 2008), associated with Alfvén, ion cyclotron, and whistler mode waves (Sulaiman et al. 2020), but the complex nature of their morphology and hence of the moon-plasma interaction, revealed by Juno close-in observations (Mura et al. 2018), is still to be fully understood. A magnetic footprint of Callisto was tentatively observed by Bhattacharyya et al. (2018) and further observations are necessary to confirm it. Interior to the main oval, the acceleration of charged particles may be responsible for the fluctuating polar-cap aurora (e.g., Grodent et al. 2003), with signatures of flares associated with magnetic reconnection on the dayside magnetopause being observed (e.g., Ebert et al. 2017), but the

debate about whether the polar region is open or closed to the solar magnetic flux remains unresolved. These auroral signatures, from the polar cap, to the main oval and satellite footprints, are all highly variable on timescales of minutes and hours (Clarke et al. 2004); signatures of possible substorm-like injections have been proposed (Bonfond et al. 2021a). Greathouse et al. (2021) reported that the bright polar emissions observed by the HST and Juno UVS on the day side dim substantially or disappear between midnight and dawn. The JUICE UVS will have extended periods of time to scan the aurora on the night side to study this dimming in more detail, especially during the high inclination phase. Long-term HST imaging programmes (Nichols et al. 2009; Clarke et al. 2009; Nichols et al. 2017), as well as Juno IR and UV imaging (Mura et al. 2017a; Bonfond et al. 2017), have provided substantial increases in our understanding of auroral morphology. In particular, the comparison between UV and IR is crucial to understand the complexity of the auroral-related energization processes (Gérard et al. 2018, 2023), but a long-term programme of JUICE auroral monitoring will provide vantage points that are not possible from Earth-based facilities.

Visible light studies with JANUS will greatly enhance our understanding of the aurora in this wavelength range, which, unlike the IR and UV emission, cannot be observed on the dayside of Jupiter, thus ruling out studies from the Earth or its vicinity. Limited visible light observations by the Galileo solid-state imaging (SSI) system (e.g. Fig. 8) captured several classes of auroral features from a survey of the northern auroral region (Vasavada et al. 1999). These included a continuous primary arc a few hundred km wide, observed at around 245 km above the 1-bar level. This varied in morphology with local time between a single arc and a multiply-branched feature. A variable secondary arc, associated with the region just beyond Io's torus was also visible, plus a diffuse "polar cap" emission. A spot and tail associated with the magnetic footprint of Io was also observed. As the visible emission is too faint for Juno's JunoCam, JANUS will provide unprecedented data, at spatial resolutions as small as tens of km per pixel, and occasionally at high cadence, allowing the dynamics of these features to be captured.

The vertical structure of the auroral curtain, and its spectral properties, have been explored at high spatial resolution in the ultraviolet (Bonfond et al. 2017; Mauk et al. 2020), infrared (Adriani et al. 2017; Dinelli et al. 2017) and visible (Vasavada et al. 1999), which sense different altitudes and chemical compounds. With JANUS and MAJIS imagery at perijove, along with MAJIS and UVS occultations, JUICE will study the dynamic auroras in three dimensions and their temporal evolution.

Auroral Coupling to the Stratosphere: Ion-neutral chemistry at high latitudes may be responsible for the unusual nature of upper tropospheric and stratospheric aerosols in the polar hazes (Friedson et al. 2002a; Wong et al. 2000), possibly fractal aggregates (Li et al. 2013) that are numerous and reflective in the infrared (Barrado-Izagirre et al. 2008a), and dark and absorbent in the ultraviolet. Remote sensing in the UV and infrared will characterise the composition and scattering properties of these polar hazes, to understand their asymmetric properties between the northern and southern poles, and their influence on radiative balance. The consequences of auroral heating are visible at stratospheric altitudes (e.g., Sinclair et al. 2018b), possibly via direct Joule heating or radiative effects in the auroral-associated hazes. Sub-

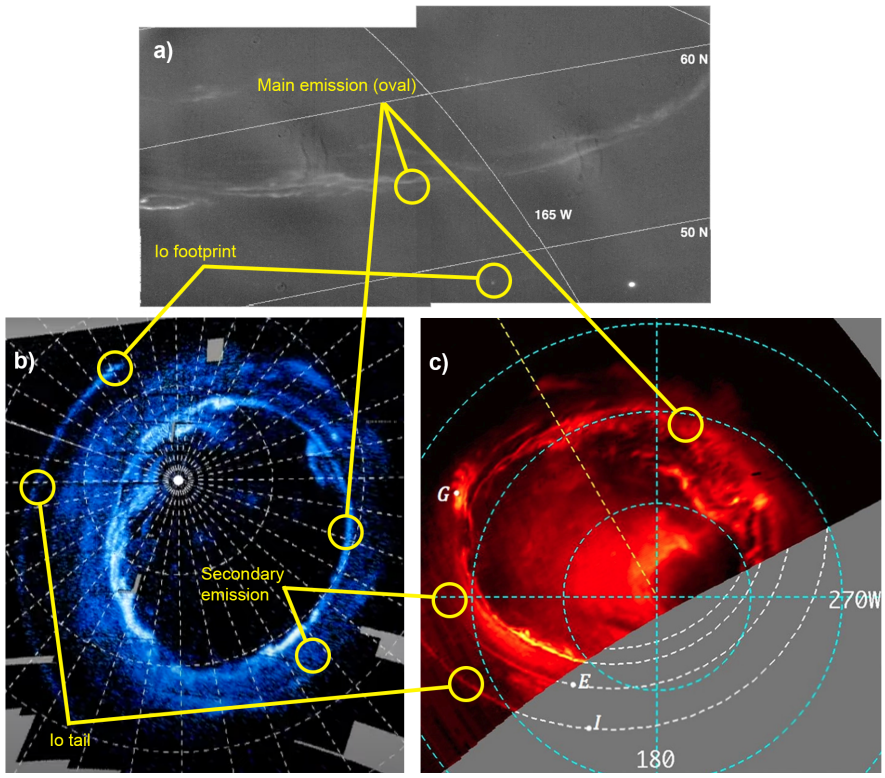

Fig. 8 Example auroral images obtained from Jovian orbit at three wavelengths, at different epochs and orientations, with some key features labelled. Lines of System-III longitude and latitude are shown on each. See Fig. 2 of Grodent (2015) for a comprehensive overview of features at UV wavelengths. a) Galileo SSI visible light image of the northern aurora, at a spatial resolution ∼26 km/pix, obtained in November 1997; presented in Fig. 1 of Vasavada et al. (1999), and released as NASA PIA01602 (Credit: NASA/JPL-Caltech). b) Polar projection of May 2017 data from Juno UVS, here showing the southern aurora, presented in detail in Fig. 2 of Bonfond et al. (2021b) (Credit: NASA/JPL-Caltech/SwRI/UVS/ULiège). c) Juno JIRAM mosaic map of the southern auroral oval, taken during August 2016. White points are predicted footprint positions indicated by letters I, E, and G for the moons Io, Europa, and Ganymede, respectively. Presented in detail by Mura et al. (2017b), Fig. 2 (credit: NASA/JPL-Caltech/SwRI/ASI/INAF/JIRAM).

millimetre observations will enable joint measurements of stratospheric temperatures and winds within these auroral zones, to assess the penetration levels of auroral energy into the stratosphere. Measuring the distributions of species like C_2H_2 and C_2H_6 (e.g., Sinclair et al. 2018b, 2023; Giles et al. 2023), H_2O, HCN and CO_2 (Benmahi et al. 2020; Cavalié et al. 2022; Lellouch et al. 2006), will also help shed light on chemistry occurring in the auroral regions, like aerosol production (Perry et al. 1999; Wong et al. 2000, 2003; Friedson et al. 2002b) and heterogeneous chemistry involving them (Perrin et al. 2021).

JUICE is required to **'investigate the unique atmospheric properties of Jupiter's polar regions, including the influence of auroral energy deposition and ion chem-**

istry on the atmospheric temperatures, energy budget, chemistry and cloud/ haze formation (R1-J-4)'. As we discuss in Section 3, the JUICE tour enables a long-term study of the Jovian auroras across multiple wavelengths, with observations tuned to the timescales of the various phenomena, observing variable emissions over minutes, hours and days as the conditions within the solar wind fluctuate. The auroras will be particularly scrutinised as JUICE reaches higher orbital inclinations.

2.5 Summary of Objectives

The JUICE science case is summarised by the eleven objectives listed in Table 1, and by the boldface science requirements included in the text above. The requirements state that the mission **'shall have the capability to investigate the spatial variability of Jovian dynamics, chemistry and atmospheric structure in three dimensions (R1-J-1)'**, and must provide **'long-term time-domain investigations of atmospheric processes over** $2+$ **years, with a frequency tuned to the timescales of interest (R1-J-2).'** To do so, JUICE **'must support global and regional spectroscopic mapping of the sources and sinks of key atmospheric species tracing atmospheric circulation and chemistry with spatial resolution** $<$ 200 **km/px in the VIS-NIR range,** $<$ 1000 **km in UV and with about a scale height vertical and 2000-4000 km horizontal resolution in the sub-millimeter range, repeated over a range of timescales from days to years (R1-J-8).'** All other science requirements (R1-J-1 to J-11) are recorded in the previous sections. An overarching theme of the JUICE science case is that the different regimes (the interior, atmospheric layers, and magnetosphere) are not decoupled from one another, so cannot be investigated in isolation - JUICE will explore the connections between all of the components within this system. We now turn to how the payload and Jupiter tour have been designed to meet these objectives.

3 JUICE Tour: Jupiter Observing Opportunities

To meet the Level-1 science requirements described in Section 2, Level-2 requirements on the mission and spacecraft design were identified (Science Requirements Document JUI-EST-SGS-RS-001). To summarise those relevant to Jupiter science, the mission and spacecraft were designed to:

- Support inertial pointing for solar and stellar occultations [...] in orbit around Jupiter.
- Support nadir and off-nadir pointing for imaging.
- Support raster pointing for Jupiter [...] when objects are larger than fields of view.
- Support a spot-tracking mode for Jupiter.
- Perform limb tracking manoeuvre during radio occultations of Jupiter.
- Support instrument pointing needs according to [their] requirements.
- Provide sufficient temporal coverage for Jovian atmospheric and magnetospheric science, [with a] Jovian tour [that] shall be at least 2.5 years.

- Start Jupiter atmosphere observations 6 months before the Jupiter Orbit Insertion and continue during the Ganymede phase.
- Provide an orbit with inclination of at least 30° with respect to the Jupiter equatorial plane.
- Co-align the boresights of instruments JANUS, MAJIS, UVS, GALA and SWI.
- Provide repeated observations of the same latitudes and cloud features with frequencies tuned to the timescales of interest (hours to months).
- Enable complete latitudinal, phase angle and local solar time coverage of Jupiter by remote sensing instruments.
- Provide at least two opportunities for remote sensing of Jupiter during the Europa phase when the distance to Jupiter is at a minimum.
- React on short timescales to new and unexpected events in the Jovian atmosphere, such as major storms or impacts. JUICE pointing can be updated up to one week in advance, and commanding up to 3 days before the uplink, both in exceptional cases.
- Enable sounding of the Jovian atmosphere in radio-, stellar and solar occultations at all latitudes, repeating observations at regular times during the mission.
- Provide capabilities for (1) global mosaics/scans of Jupiter repeated once every 2.5 hours to build up 360-degree longitude coverage during a ten-hour rotation, and (2) repetitive imaging of discrete cloud features/ region with hourly frequency for cloud feature tracking while the feature transits from west to east (full rotation in 10 hours), repeated on subsequent rotations.
- Enable joint observation campaigns with remote sensing instruments (submm, IR, visible and UV), as well as ENA and Radio observations for the study of the auroral region of Jupiter, as well as the coupling between the Galilean satellites, the Jovian magnetosphere, and the high latitude regions of Jupiter (thermosphere, ionosphere and magnetosphere).

The JUICE orbital tour of the Jovian system is described by Boutonnet et al. (in prep.), and was designed to meet these requirements and enable the activities of the comprehensive payload discussed in Section 4. The JUICE orbit differs substantially from that of Juno, enabling global views over longer duration from a low-inclination orbit, and with an inclined phase offering high-resolution views of the southern hemisphere. Unlike Juno, JUICE does not spin, therefore simplifying some of the remote sensing observation sequences described in Section 4. Here we briefly describe the different phases of the tour of interest to Jupiter science, which are shown in Figs. 9 and 11.

Phase One begins some six months before Jupiter Orbit Insertion (JOI) in July 2031 according to the Crema 5.0 (Consolidated report on mission analysis) trajectory, and encompasses the first elliptical orbit around Jupiter until February 2032. The long approach to Jupiter will permit atmospheric monitoring and the generation of low-resolution movies, with the spatial resolution afforded by the JANUS camera exceeding the 150 km/pixel of the HST WFC3 instrument some 11.0 days before JOI and will exceed JWST spatial resolution at 8.5 days before JOI, respectively (see Figure 10). For much of the long first orbit, the resolution will be 200-300 km/pixel, enabling global monitoring of atmospheric phenomena. Higher-resolution observa-

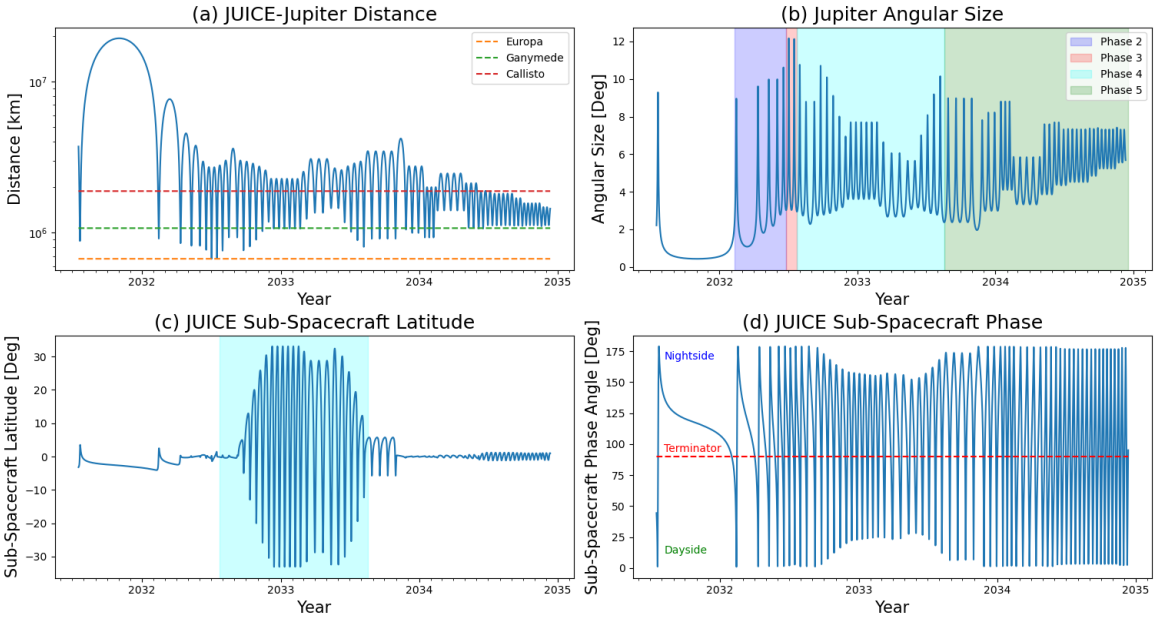

Fig. 9 Overview of the JUICE orbital tour of Jupiter using Crema 5.0, showing (a) the distance to Jupiter in km; (b) the angular size of Jupiter from JUICE's vantage point; (c) the sub-spacecraft latitude; and (d) the phase angle (low phase implies dayside, high phase implies nightside). In (a) we show the mean orbital distances of Europa, Ganymede and Callisto for comparison. In (b) we highlight phases 2, 3, 4 and 5 of the tour.

tions begin in earnest in **Phase Two,** between February and June 2032, as the JUICE orbital energy is reduced. Five close flybys of Jupiter occur during this phase (perijoves 2-6, with perijove 1 being orbit insertion in July 2031), and provide the first real opportunity to test the JUICE remote sensing investigations with distances down to 11–13 R_J from Jupiter (Figure 9). Jupiter remote sensing will work in tandem with satellite remote sensing and magnetospheric measurements during this period, with four Ganymede flybys and one Callisto flyby during Phase 2.

Phase Three provides the highest spatial-resolution Jupiter observations of the entire tour, as JUICE performs two close flybys of Europa in July 2032. Although much of the spacecraft resources and data volume will be dedicated to the Europa encounters, Jupiter science activities will aim to take advantage of these high-resolution opportunities at perijove 7 and 8 (9.4 R_J from Jupiter).

Following the Europa encounters, JUICE then uses multiple flybys of Callisto to increase its orbital inclination up to $\gtrsim 33^\circ$ during **Phase Four**, the inclined phase between July 2032 and August 2033 (Figure 9c). With $\sim$ 23 perijoves during this period, with distances ranging from 11-20 R_J from Jupiter, JUICE will be afforded with improved views of the atmosphere and auroras in the polar domains. The maximum orbit inclination will be attained between December 2032 and February 2033 and the highest sub-spacecraft latitude at perijove of $\gtrsim 33^\circ$ will be reached in May-June 2033 (perijoves 26 and 27). JUICE will spend more than 6 months with an orbit more

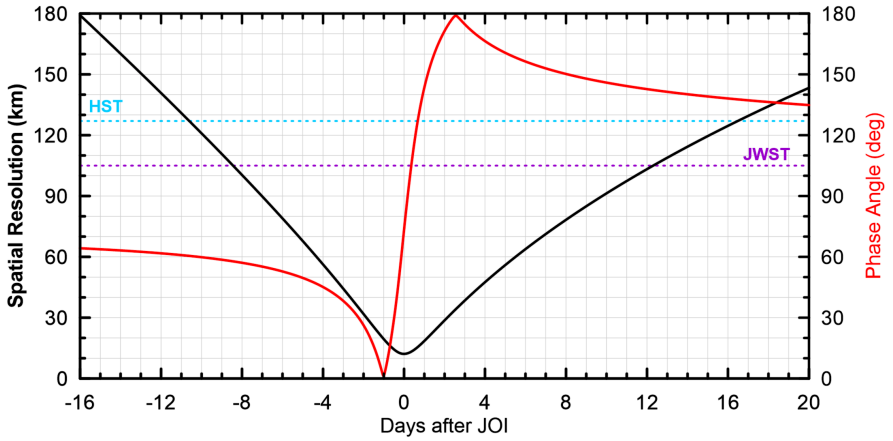

Fig. 10 Spatial resolution of JANUS (black line) in the days surrounding JOI and compared to HST and JWST resolutions (cyan and purple lines, respectively). Phase angle is also plotted (red line).

inclined than 30°. Furthermore, JUICE closest approaches and highest spatial resolutions during the inclined phase will be in the southern hemisphere, complementing the northern-hemisphere perijoves of Juno's extended mission.

As JUICE returns to the equatorial plane, it commences the low-energy **Phase Five**, circularising the orbit and providing perijoves that are much more frequent, approximately every two weeks between August 2033 (perijove 32) and December 2034 (perijove 67). Spatial resolutions of visible images match those of the best Galileo images (10 to 40 km/pixel) throughout this phase, with closest approaches varying between 12-20 R_J before reaching Ganymede's orbit at 15 R_J. Fewer satellite encounters are envisaged during this period (four for Callisto, seven for Ganymede), leaving a number of uninterrupted orbits for Jupiter science. Finally, in December 2034, JUICE enters orbit around Ganymede, with **Phase Six** completing its primary mission by September 2035. Short time periods during the Ganymede orbital phase will be devoted to the monitoring of Jupiter's atmosphere, following up on dynamical, chemical, and meteorological phenomena discovered during Phases 1 through 5.

3.1 Segmentation of the Tour

Given the wide-ranging objectives of JUICE, and the wealth of opportunities provided by the orbital tour, a preliminary architecture for scientific operations and scheduling had to be developed so that requirements on spacecraft resources (telemetry, power, pointing, etc.) could be better understood. Each scientific discipline, including Jupiter science, evaluated the observing opportunities during the tour. This included identifying repeated observations of the Jovian atmosphere and auroras, time-critical opportunities for occultations (radio, stellar, and solar), and any unique observational geometries for Jupiter science. Having identified optimal windows of obser-

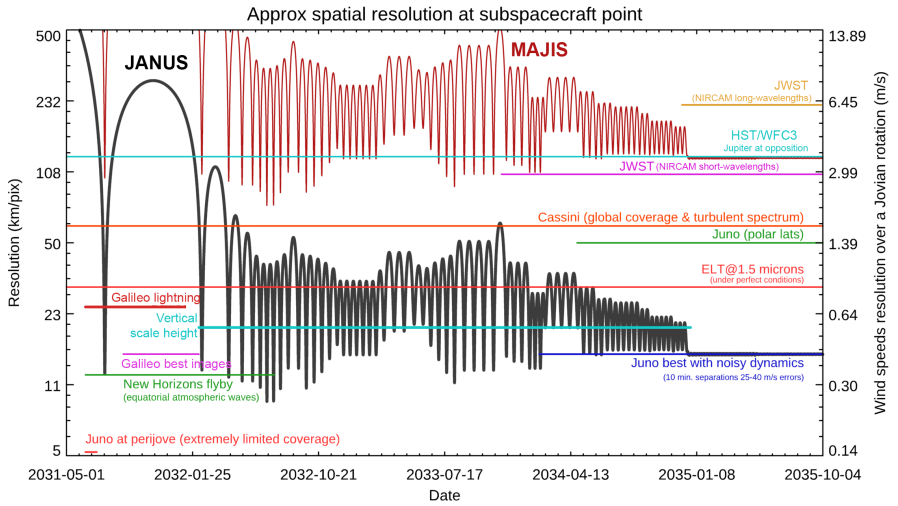

Fig. 11 Spatial and wind speed resolutions of JANUS and MAJIS as a function of time, based on the Crema 5.0 trajectory and compared to instrumentation on other facilities.

vations for all disciplines, a preliminary 'level-0' segmentation plan for the tour was developed, with specific disciplines being assigned the lead for pointing/operations during different segments. Jupiter science segments had to be balanced against opportunities for magnetospheric science, satellite encounters (typically within a $\pm$12-hour window around closest approach to a moon), windows for data downlink (typically 8 hours per day), and other segments for navigation, calibration, and distant investigations of the wider Jovian system. An example is shown in Figure 12 for PJ12 in September 2023. Operations will naturally be more complex during the Jupiter tour, with instruments operating as 'riders' during science segments devoted to other disciplines. Potential disruption of the established observation plan may occur with a time response of a few days only in case of e.g. unexpected events like large asteroid or comet impacts. Nevertheless, this approach enabled a thorough assessment of JUICE's capabilities to meet the original science requirements.

Proposed Jupiter science investigations mainly fall into the following segment types:

- **Perijove Windows:** Jupiter science operations will focus on the $\pm$50-hour window surrounding closest approach, with different types of observations planned for dayside, terminator, or nightside encounters. The highest spatial resolution observations are possible during these windows (particularly during Phase 3), with numerous opportunities for stellar occultations also possible. Jupiter science will be interrupted by satellite flybys and windows for downlink, but otherwise these segments will be the top priority for Jupiter science.
- **Monitoring Observations:** Outside of the perijove windows, JUICE is required to provide frequent opportunities to track the evolution of atmospheric phenomena. Monitoring will likely be organised into campaigns focusing on specific targets (e.g., tracking the changes to a storm or vortex, high-frequency auroral obser-

vations, etc.), but preliminary segmentation places a 10-hour monitoring window once every three days (approximately), with significant flexibility in scheduling.

– **Phase-Angle Windows:** When not already covered by perijove or the monitoring windows, JUICE will observe Jupiter within $\pm$5 hours of minimum phase (i.e., dayside), the terminator crossing (90° phase angle), and at maximum phase (i.e., nightside). These illumination conditions (and phase angles in between) are required to characterise the scattering properties of aerosols, and to provide nightside opportunities for lightning imaging and thermal emission measurements in the absence of scattered sunlight.
– **Inclined Windows:** When not already covered by perijove windows, and when the sub-spacecraft latitude exceeds $\pm$5° during Phase 4, JUICE will observe for $\pm$10 hours either side of the locations of maximum northern and southern sub-spacecraft latitude. This will enable long-term monitoring of the polar atmosphere and auroras during Phase 4. Indeed, a special 'inclined aurora' segment is also planned for when the phase angle exceeds 160°. These inclined windows will be planned on a case by case basis, as overlap with magnetospheric science segments is highly likely during Phase 4.
– **Occultation Windows:** These time-critical events are scheduled independent of the perijove windows, but sometimes occur within them. A window is reserved for radio occultation ingress and egress, as the spacecraft moves behind the planet as seen by Earth. Similarly, a $\pm$1 hour window is reserved for solar occultations. Stellar occultations are extremely numerous, with optimal stellar types selected by the UV and IR instrument teams, and a subset of these will be scheduled throughout the tour.

These generic Jupiter science segments are driven by the tour geometry, and although monitoring of atmospheric and auroral variability is a high priority, the detailed science operations plans will remove any unnecessary redundancies. Furthermore, new segments that cover multi-instrument campaigns for specific phenomena (Section 5) will be built into the plan. A generic Jupiter orbit is shown in Figure 12, highlighting a proposed sequence of activities. This 'level-zero' plan for segmentation of the JUICE orbit will be the basis of a rigorous activity plan that ensures proposed observations remain within the resource envelope (data volume, power, etc.) for JUICE.

To aid in the assessment of different tours, Figure 13 shows the amount of time available to Jupiter remote sensing observations during each of the $\pm$50-hour perijove windows. Once the satellite encounters, spacecraft navigation images, wheel off-loading, and downlink windows are all removed, this leaves approximately 50% of the available time for science. During phase 4, we envisage sharing of perijoves with magnetospheric science, further reducing the time available for remote sensing. However, Jupiter observations are more likely to be data-volume limited rather than time-limited, and as Figures 13 and 14 reveal, there are plentiful opportunities for observations within the 'level-0' segmentation from (i) close proximity to Jupiter during perijoves; (ii) a range of phase angles from dayside to nightside; and (iii) a range of local times. The JUICE tour therefore fulfils the requirements listed at the start of this Section.

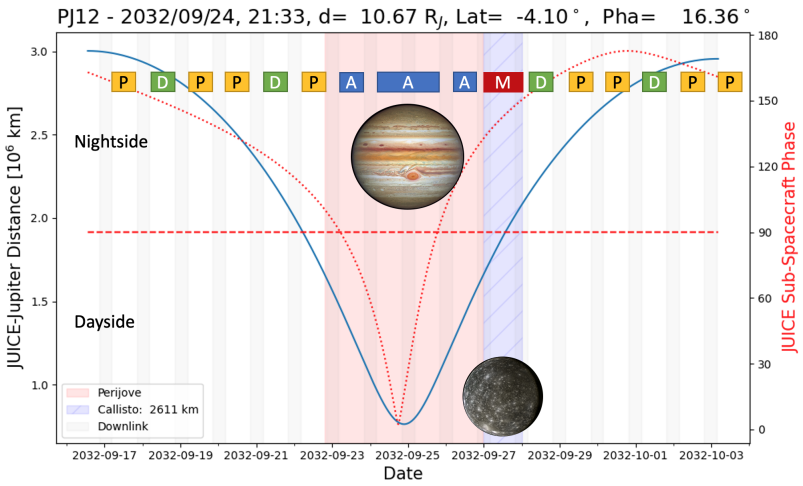

Fig. 12 Perijove 12 is used as a generic orbit, from apojove to apojove, to demonstrate the segmentation of the tour. Satellite observations (labelled 'M') are prioritised during the ±12 hours surrounding closest approach. Jupiter atmosphere and auroral science blocks during the ±50 hour perijove windows (red shading, with specific observations in boxes labelled 'A') are interspersed with downlink windows (grey shaded boxes). Atmospheric monitoring ('D') is interspersed with dedicated magnetospheric and plasma observations ('P') during more distant periods of the orbit. Magnetospheric observations ride along with remote sensing observations during the perijove encounters.

4 JUICE Instrumentation

Based on the tour phases and high-level segmentation described in Section 3, the instrument teams developed a number of observing modes that can be used in an interchangeable fashion, serving as the building blocks to develop the operations plan. In this section, we provide brief overviews of the instruments and their capabilities for Jupiter science, describing how they will operate in the Jovian system.

4.1 UVS

4.1.1 UVS Description

UVS (the Ultraviolet Imaging Spectrograph, Gladstone et al. in prep.) observes photons in the 50-204 nm range of the far-UV. The UVS field of view is defined by its slit, which comprises a 7.3°×0.1°rectangular section with an additional 0.2°×0.2°box at one end for solar occultation observations (see Figure 15e), giving a total slit length of 7.5°. Spectral images of larger regions are built up by scanning across the target in the direction perpendicular to the long axis of the slit. Observations use a series of 'ports', including the main 4 cm × 4 cm airglow port (AP) for auroral observations, stellar occultations (Figure 16), and nadir view; a 1 cm × 1 cm high- resolution port (HP) that allows observations of bright targets with improved spatial resolution at the expense of a 16× reduction in the light collected; and a solar port (SP) offset from

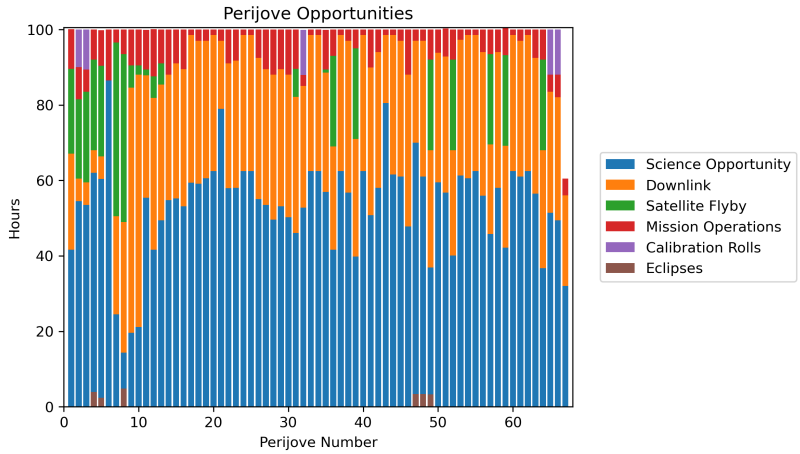

Fig. 13 For each perijove, the ±50-hour perijove windows are subdivided into sub-segments - time available for science observations, time devoted to satellite encounters, telemetry downlink, mission operations (such as navigation images and wheel off-loading), calibration of the magnetometer, and time removed due to Jupiter eclipses.

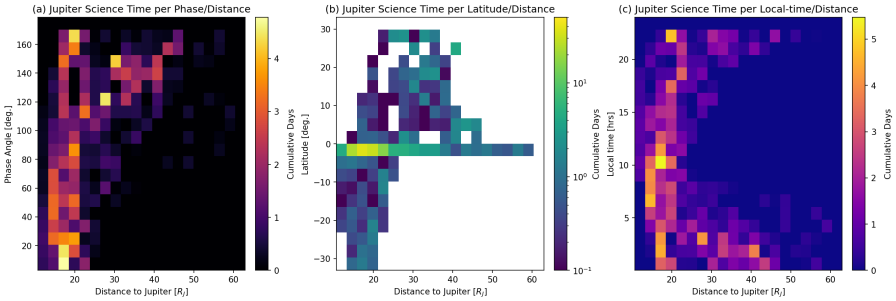

Fig. 14 The cumulative time in days spent in different locations within the jovian system, showing the phase-angle versus distance to Jupiter in (a); the sub-spacecraft latitude versus distance in (b); and the local time versus distance in (c). Note the logarithmic colour range in (b) to display time spent in the high-inclination phases. Times are only counted if they fall within the Jupiter working group segments.

the main instrument aperture, which uses a 0.25 mm diameter pinhole and additional pick-off mirror to reduce the solar flux to a suitable level for UVS solar occultation observations.

The spatial resolution of UVS varies with wavelength and with position along the slit, with the best resolution achieved near the center of the slit (the on-axis position). The AP resolution is $<0.3^\circ$ at all wavelengths and along-slit positions and is $<0.16^\circ$ at most field positions for wavelengths in the range 70 – 130 nm (Davis et al. 2020). The HP resolution ranges from 0.038° to 0.12°; again, the highest spatial resolution is achieved for wavelengths near 70–130 nm. The point source spectral resolution is <1 nm at all wavelengths when observing on-axis light (Davis et al. 2020).

UVS aims to study how Jupiter's upper atmosphere interacts with the lower atmosphere below and the ionosphere and magnetosphere above. Unlike the spinning

Juno spacecraft, JUICE will enable UVS to perform 'point and stare' observations, revealing fainter auroral features, and allowing synoptic-scale imaging of the polar auroras. However, as the minimum JUICE-Jupiter distance is considerably larger than the Juno perijove distances the spatial resolution of JUICE UVS auroral images will be degraded relative to Juno UVS images (see comparison in Figure 17). JUICE UVS will also perform stellar occultation measurements, which are not possible with Juno UVS. These observations use inertial pointing to observe UV-bright stars as they are occulted by Jupiter, providing measurements of atmospheric structure, composition, and variability.

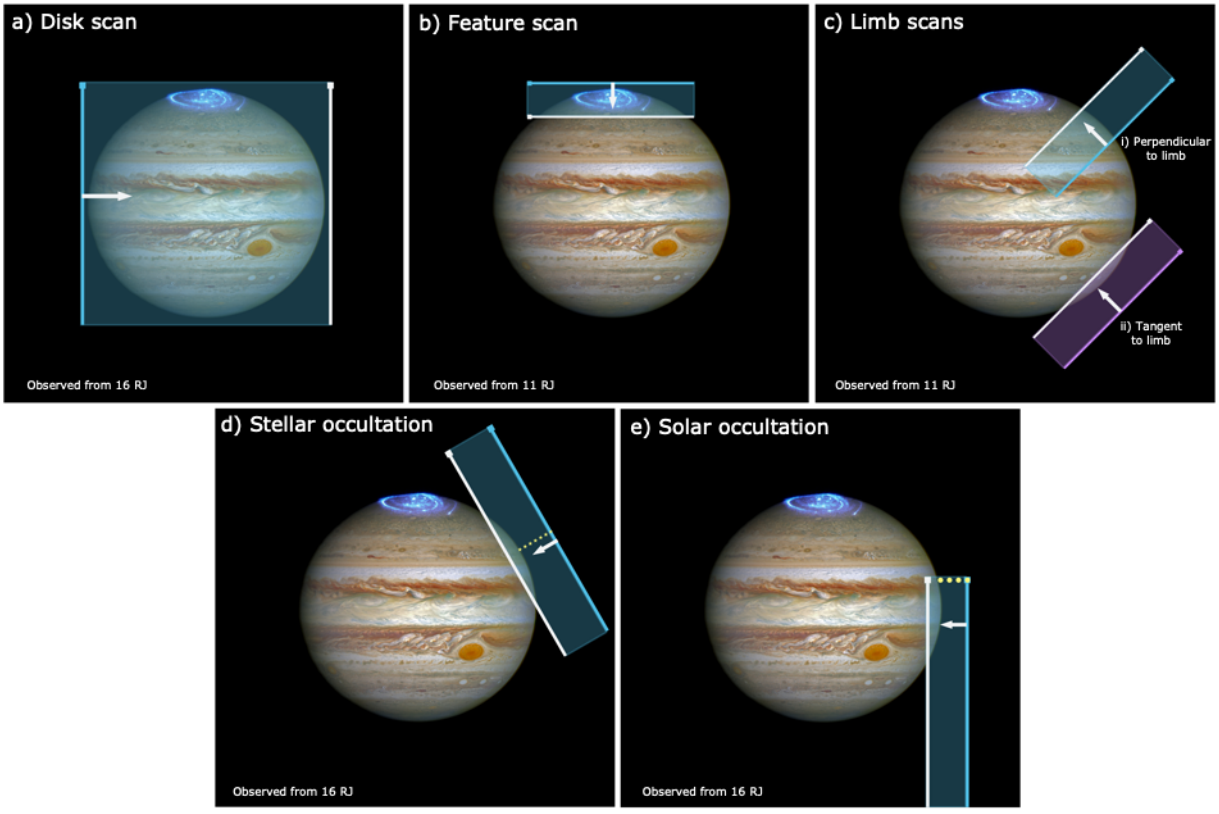

Fig. 15 Examples of JUICE UVS observation techniques at Jupiter. In each example the UVS slit is scaled to its projected size when observing from the distances shown in the bottom left of each panel. The start and end position of the slit is shown, with arrows indicating the direction of slit motion.

4.1.2 UVS Operations

During the $\pm$50-hour period around each JUICE perijove, UVS will use the spacecraft motion to perform a series of scans of Jupiter's disk using both the AP and HP

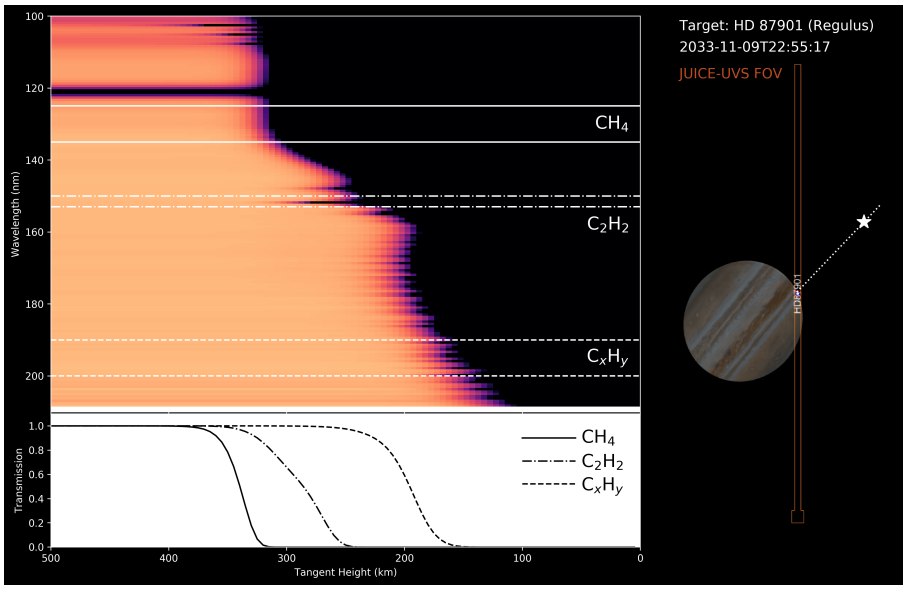

Fig. 16 Simulation of a Jupiter occultation of bright star Regulus from JUICE UVS. JUICE would hold Regulus fixed in the center of the UVS slit starting a few minutes before ingress until all of its light is blocked by Jupiter. The panels on the left show the ingress occultation light curves spectral resolved (above) and binned over wavelength and labeled by dominant absorber (below). Starting on the left with no light blocked and moving to the right we observe the absorption of the shortest wavelengths first due to H_2 and CH_4 and then followed at longer wavelengths by absorptions by C_2H_2, C_2H_6 and a mix of higher order hydrocarbons (C_xH_y).

ports (with the choice of port depending on distance and illumination) to map the aurora and airglow (Figure 15a). High-resolution feature scans of smaller areas will be performed when key regions of interest are visible (Figure 15b), and scans along Jupiter's limb will be used to study the structure and variability of the upper atmosphere (Figure 15c). In both feature scans and limb scans, the region of interest is placed in the center of the slit to achieve the best possible spatial resolution. UVS does not possess an internal scan mechanism, but instead relies on spacecraft slews to perform these observations. The orientation of the UVS slit during scans is not strongly constrained, provided that the scan motion is in the direction perpendicular to the slit as indicated by the arrows in Figure 15. Disk scans may be performed North-South, East-West or at any intermediate pointing, while limb scans at different orientations provide different information: scans with the slit pointed perpendicular to the limb probe the vertical structure at high resolution while scans at a tangent to the limb provide larger instantaneous latitude coverage.

UVS also aims to observe ∼4 stellar occultations per perijove (Figure 15d), targeting a range of longitudes, latitudes, and local times, including repeat measurements of the same regions to assess temporal variability. Occultations in the auroral regions are a high priority, as are events where two UV bright stars may be observed simultaneously at different positions along the UVS slit. Some nightside perijoves include opportunities to observe solar occultations (Figure 15e); UVS aims to observe

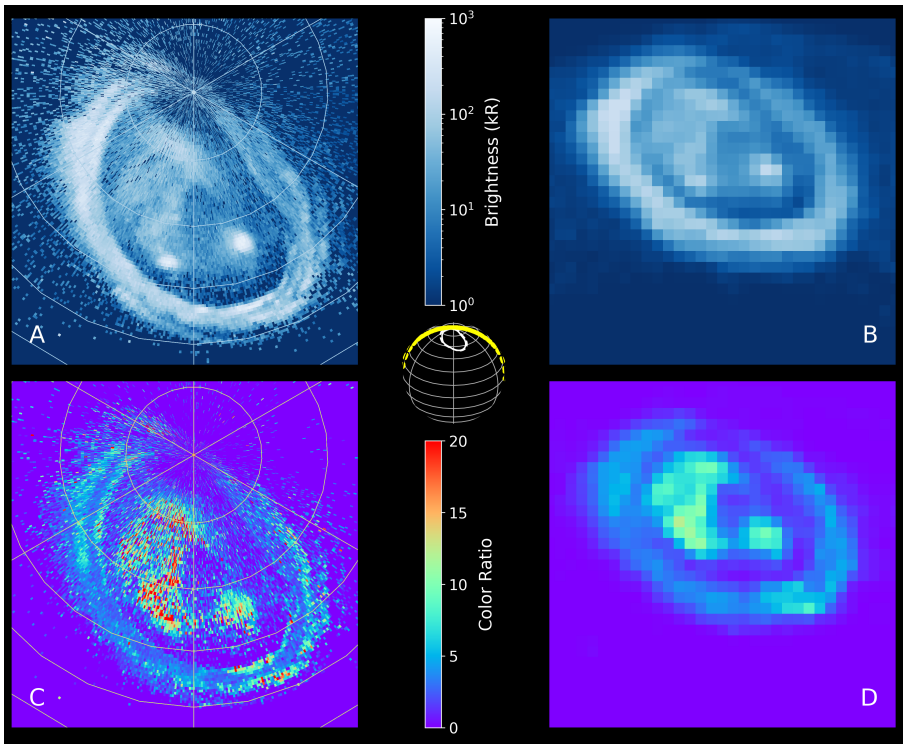

Fig. 17 Juno UVS maps from Perijove 3 display the brightness (A) and color ratio (C) of the emissions from Juno's polar orbit vantage point taken (from supp. in Greathouse et al. 2021). The wire frame model in the center shows the view of Jupiter from JUICE during the high inclination phase and the orientation of the aurora and terminator for the time of the UVS observations (aurora on the night side). Even from a much greater distance, JUICE UVS simulations of the same observation from Juno now displayed in B and D will allow for detailed study of the auroral night side emissions unobservable by Earth-orbiting observatories.

a minimum of four of these events, which are particularly important for investigating atmospheric absorption at the short end of the UVS bandpass, where stellar flux is typically very low.

UVS will perform scans of both the dayside and nightside of Jupiter, with the dayside observations providing the best signal-to-noise ratio for airglow observations and the nightside observations allowing auroral emissions to be devoid of reflected sunlight background. Juno UVS observations of Jupiter's nightside proved unexpectedly interesting, detecting bright flashes associated with Transient Luminous Events (Giles et al. 2020b) and a bolide (Giles et al. 2021a). JUICE UVS will likely not achieve the required spatial resolution to detect similar events, but full disk nightside scans will facilitate searches for tropical nightglow arcs that might be detectable along/near the dip equator, similar to the infrared H_3^+ feature detected by (Stallard et al. 2018).

Outside of the perijove periods, UVS will continue to regularly (1–2 times per week) monitor Jupiter's airglow, aligning the slit along Jupiter's North-South axis

and staring for ∼10 hours to build up maps over a full Jupiter rotation period. Additional stellar occultation measurements will also be performed whenever suitable opportunities are identified, since the JUICE-Jupiter distance is not an important constraint for these observations.

4.2 MAJIS

4.2.1 MAJIS Description

MAJIS (Moons And Jupiter Imaging Spectrometer, Poulet et al. in prep.) is the visible and near-infrared imaging spectrometer for JUICE. It performs global imaging spectroscopy from 0.49 to 5.56 μm across all local times. The MAJIS spectral range is divided in two separate channels: the VIS-NIR, covering the 0.49-2.36 μm region with a spectral resolution of about 4 nm, and the IR, covering the 2.27-5.56 μm region with a spectral sampling of about 6 nm. In typical operating conditions, MAJIS observes a line of 400 spatially-contiguous pixels (a 'slit') and a spectrum is recorded simultaneously for each pixel, in the entire spectral range. The instantaneous field-of-view (IFOV) of an individual pixel is 150 μrad, providing therefore a spatial resolution of about 150 km over the Jupiter's disk at the typical distance of perijove passages ($\sim 10^6$ km, see Figure 11).

The design of the instrument enables a large number of operative options, conceived to optimise science return. Notably, the size of MAJIS cubes can be reduced by masking (i.e., selective removal) along both the spatial and the spectral dimensions, in order to reduce the downlink burden. On the other hand, spectral regions of special interest (e.g., absorption lines) can be observed with a 2× spectral oversampling.

Usually, during Jupiter observations, a mosaic of spatially-contiguous slits (a 'cube') is created by repointing the instrument between consecutive acquisitions. This technique eventually produces a 3D hyperspectral image of the observed scene. The spatial repointing required between different slits can be achieved either by means of a slow spacecraft slew or, more commonly, by the motion of MAJIS' own internal pointing mirror. This device has one degree of freedom and can shift the slit position in the sky parallel to its longer axis.

Specific techniques (summing and comparison of several individual observations for a single slit) have been developed to reduce the adverse effects by impinging energetic particles (mostly electrons) upon the instrument and to improve, at the same time, the signal-to-noise (SNR) ratio. In the case of the brightest infrared hot spots observed between the Equatorial Zone and the North Equatorial Belt (Grassi et al. 2017), MAJIS SNR is expected to exceed 1000 at 4.7 μm.

The radiance observed by MAJIS in a single cube is determined by a range of phenomena, and therefore allows one to address a variety of scientific objectives:

– Properties, distribution and variability of hazes and clouds on Jupiter offers key insights on the vertical and horizontal dynamics of the troposphere. Indeed, dynamics drives the distribution of condensable species (H_2O, H_2S, NH_3) that forms clouds and the transport of gases that, by photodissociation and through complex chemical patterns, produces the tropospheric and stratospheric hazes. The signal

measured by MAJIS between 0.4 and 3.2 μm is dominated by the scattering of solar radiation by aerosols and, in lesser extent, by atmospheric gases (Rayleigh scattering). The large variability of gas opacity (mostly due to methane) within this spectral range determines different effective sounding altitudes at different wavelengths and, in turn, offers a method to probe the vertical structure of clouds and hazes (Sromovsky and Fry 2010b; Braude et al. 2020; Pérez-Hoyos et al. 2020; Grassi et al. 2021; Anguiano-Arteaga et al. 2021). These observations will be instrumental in addressing objectives R1-J-6 and R1-J-10 mentioned in Section 2. Maps presented in Grassi et al. (2021) on the basis of JIRAM data demonstrated the high spatial variability of cloud properties - as retrievable from IR-spectroscopy – at least down to scales of few hundreds of kilometers (see their Figures 8.c and 8d). On the other hand, latitudinal mean profiles are clearly detected (see their Figures 8a and 8b), revealing contrasts in aerosols over several thousands of kilometres. In MAJIS observations, it is therefore important to pursue - at the same time - the highest spatial resolution and largest spatial coverage made possible by available data volume. Notably, the observations presented in the Juno JIRAM study (Grassi et al. 2021) remains both extremely sparse in space as well as limited to a single perijove passage. The latter issue justifies a specific MAJIS strategy aimed to characterise the time variability of aerosol properties at least down to a frequency of a few days.

– Distribution and variability of minor atmospheric components is another strong experimental constraint to dynamic models. Measurement of disequilibrium species (PH_3, GeH_4, AsH_3) is of special interest in assessing the nature of vertical motions (Section 2.1). The signal measured by MAJIS at $\lambda > 4\,\mu$m is mostly driven by the thermal emission of the atmosphere. This spectral range hosts vibro-rotational bands of several compounds such as water, ammonia, phosphine, arsine and germane. In cloud-free regions, the mixing ratios of these molecules can be retrieved down to 5-6 bars (Irwin et al. 1998; Grassi et al. 2010, 2020). These observations will be instrumental in addressing objectives R1-J-8 and R1-J-9 mentioned in Section 2. Spatial and temporal desiderata for the investigation of minor species are similar to the ones implied by aerosol studies, given the intertwined nature of underlying phenomena. Moreover, Grassi et al. (2020) separately demonstrated the variability of minor species mixing ratios at least down to scales of few hundreds of kilometers (see their Figures 7.c and 8.c) as well as consistent spatial patterns over features with dimensions of several thousands of kilometres, such as the hot-spots and the warm ring around the Great Red Spot.
– Physical conditions in the upper stratosphere and thermosphere of Jupiter are strongly coupled with the magnetosphere of the planet, which provides a substantial energy deposition at these altitudes, especially at polar latitudes. The spectral region between 3.2 and 4.0 μm hosts a very opaque methane band, that precludes photons to emerge below the approximate level of 30 mbar (Sromovsky and Fry 2010b) without being absorbed. Here, auroral emission from H_3^+ (ultimately, a by-product of the impinging of electrons over the upper atmosphere, Drossart et al. 1989, Dinelli et al. 2017) or non-LTE emission by methane (Moriconi et al. 2017) can be investigated, providing a method to map phenomena occurring in the magnetosphere (Mura et al. 2018; Moirano et al. 2021). These observations

will be instrumental in addressing objectives R1-J-4 and R1-J-9.5 mentioned in Section 2. While MAJIS data cannot match the spatial resolution of JIRAM auroral observations (that reach in most favourable cases values close to 10 km), they will allow one to explore feature variability at time scales of few hours. This is a frequency regime not probed by fast JIRAM passages over the poles and therefore particularly important to characterise interactions with rapid magnetospheric phenomena.

A particular strength of MAJIS, unlike previous imaging spectrometers, is access to the full M-band window of thermal emission, sculpted by PH_3 on its short-wave side, and NH_3 on its long-wave side. The extension to 5.57 μm, rather than curtailing near 5.1 μm, provides significantly stronger constraints on NH_3 and H_2O than previous instruments (Grassi et al. 2010). Unlike Juno/JIRAM, MAJIS also extends to shorter wavelengths below 2 μm, enabling stronger constraints on aerosol properties than possible with JIRAM.

4.2.2 MAJIS Operations

MAJIS operations are driven by the following requirements:

- To provide continuous coverage of Jupiter's disk, with a time sampling rate as uniform as possible, with periods complementary to those provided by Juno/JIRAM (from timescales from hours to months).
- To provide coverage of Jupiter's limbs at each JUICE perijove, with focus on the comparisons of morning vs. dusk and solar vs. antisolar conditions.
- To provide coverage of Jupiter's polar regions, with much longer exposure times (5 or more seconds) and specific acquisition modes designed for auroral observations, in the vicinity of each perijove.

These requests are translated in a set of observations types and corresponding rules:

1. Observations of Jupiter disk ('MAJIS_JUP_DISK_SCAN') will be performed every three earth days, with small time adjustment performed at each orbit in order to have always an observation around the time of the perijove. Each of these observations will cover the hemisphere of Jupiter visible from JUICE, with a variable number of cubes (from 1 to 4), depending on distance (Figure 18). After the third perijove passage, the MAJIS IFOV will vary between 140 and 680 km along a typical orbit. The main focus will be toward equatorial regions (30°S–30°N), that will benefit of better visibility (lower emission angles) for most of the Jupiter tour (i.e., when not in the high-inclination phase). However, more complete latitudinal coverage (implying the acquisition of lines for each cube) or longitudinal coverage (implying the acquisition of more cubes) can be pursued, as far as feasible within data volume constrains imposed by mission resources.
2. Observations of Jupiter's limb ('MAJIS_JUP_LIMB_SCAN') will consist in a series of cubes (typically eight), acquired while keeping the MAJIS slit parallel to the limb, in order to minimise possible straylight from Jupiter's disk (Figure 19). Such a set of cubes will be acquired three times per orbit, at phase angles of 0°

and 90°. Each cube will cover the tangent altitude between 0 and 3000 km above the nominal 1-bar level. Notably, during these scans, consecutive individual lines will be largely spatially overlapped (up to 90% in area), in order to achieve a substantial spatial supersampling and to allow, by deconvolution, a reconstruction of the vertical profile of the signal with an effective resolution better than IFOV size. Only the central part (40 pixels) of each line will be transmitted to Earth, to cope with data volume limitations.

3. Observations of auroras ('MAJIS_JUP_AURORAL_SCAN') will usually consist of a set of four cubes over the northern polar region (north of 50°N), acquired in proximity of each pericenter passage when sub-spacecraft longitude is closer to 190°W, to ensure better visibility of the northern polar oval. Southern polar oval is more symmetric around the pole and will be better observed with during the high inclination phase. Cubes during each perijove will be taken with gaps of approximately 40 minutes, to monitor the rapid variability of auroral structures.

Although the types of observations mentioned above will represent most of the entries in MAJIS Jupiter dataset, they will be nonetheless complemented by other types, to be performed more rarely during the mission. This latter group includes: a global complete mosaic at full spectral coverage (to be acquired just once during the mission, given the massive data volume output), limb observations while in eclipse, stellar occultations and 'tracking' observations (repeated observations of the same area at the relatively short period of several minutes).

4.3 SWI

4.3.1 SWI Description

The Sub-millimetre Wave Instrument (SWI, Hartogh et al. in prep.) is a passively cooled radio telescope with a 29-cm primary mirror that will be sensitive to radiation produced in Jupiter's atmosphere from its upper troposphere to its lower thermosphere. It will be an ideal instrument to constrain the chemistry and dynamics of Jupiter's stratosphere.

SWI can be tuned to observe in parallel two spectral windows located in two spectral bands, 530-625 GHz (479-565 μm) and 1067-1275 GHz (235-281 μm), with one spatial pixel, and a suite of high resolution spectrometers (up to 10^7 resolving power) and continuum channels. These two windows in the sub-millimetre open the possibility to target key neutral and ion species (CH_4, H_2O, HCN, CO, CS, CH_3C_2H, etc.) as well as their isotopologues relevant for Jupiter chemistry (see Figure 20). The main limitation of the instrument concerns spatial resolution with a 1 mrad beam at best (i.e. 1000 km from about 15 R_J) which will not enable limb scanning. Despite more limited spatial resolution compared to other remote sensing instruments aboard JUICE, SWI will nonetheless get vertically-resolved information on temperature and composition from observations of the pressure broadened lineshapes. The high sensitivity ensured by the low receiver temperatures coupled with the highest resolution spectrometers, i.e. the Chirp Transform Spectrometers (CTS), which will have 1 GHz

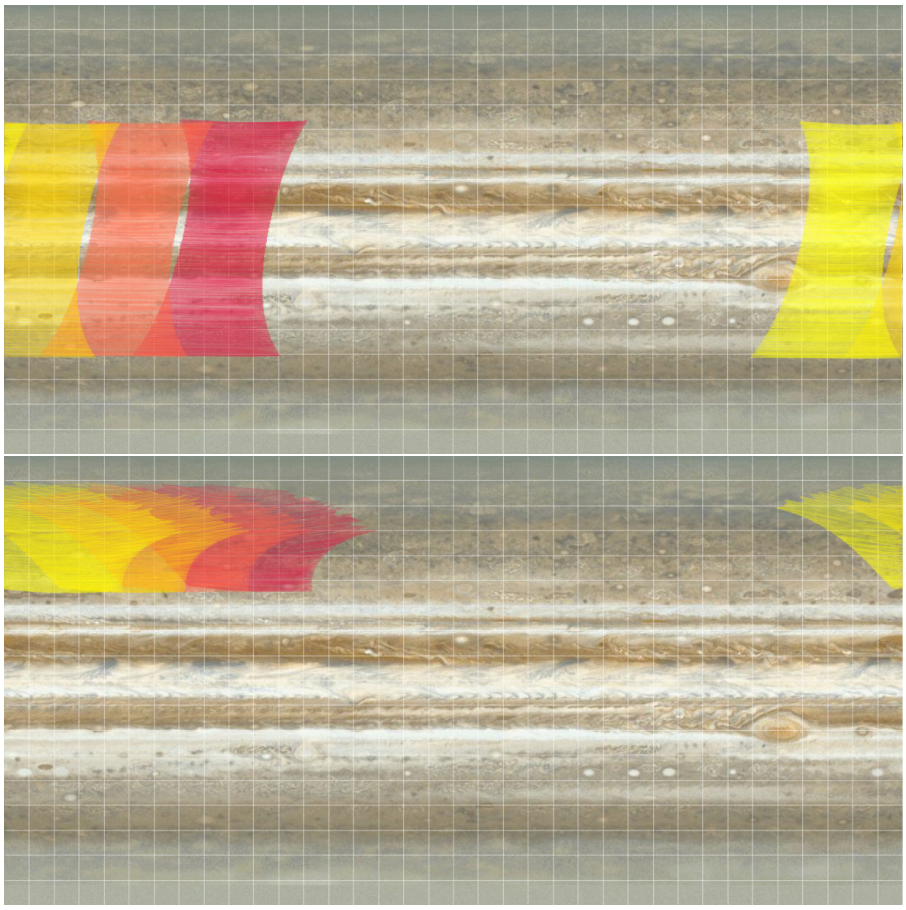

Fig. 18 (Top) Expected coverage of Jupiter's disk by MAJIS on 2032-Sep-24, near perijove #12. Different colours present the coverage of four cubes acquired at time intervals of 1h10m. (Bottom) Expected coverage of Jupiter's auroras by MAJIS on 2032-Sep-25, a few hours after perijove #12. Different colours present the coverage of four cubes acquired at time intervals of 46m.

bandwidth and 10000 channels of 100 kHz, will indeed result in very high S/N observations of the true lineshapes in few minute integrations. Observing in the two bands in parallel with the high spectral resolution of the CTS and the high sensitivity of the receivers will enable the simultaneous and independent retrieval of the vertical profiles of temperature (with CH_4 lines around 1256 GHz), abundance of the species observed in the 600 GHz band, and wind speeds (from the combination of the two lineshapes), from the upper troposphere to the upper stratosphere. SWI will thus improve over previous sub-millimetre observatories like IRAM-30m, ISO, Odin and Herschel for the characterization of the chemistry and general circulation of Jupiter's stratosphere (Moreno et al. 2003; Lellouch et al. 2002; Cavalié et al. 2008, 2012, 2013; Benmahi et al. 2020).

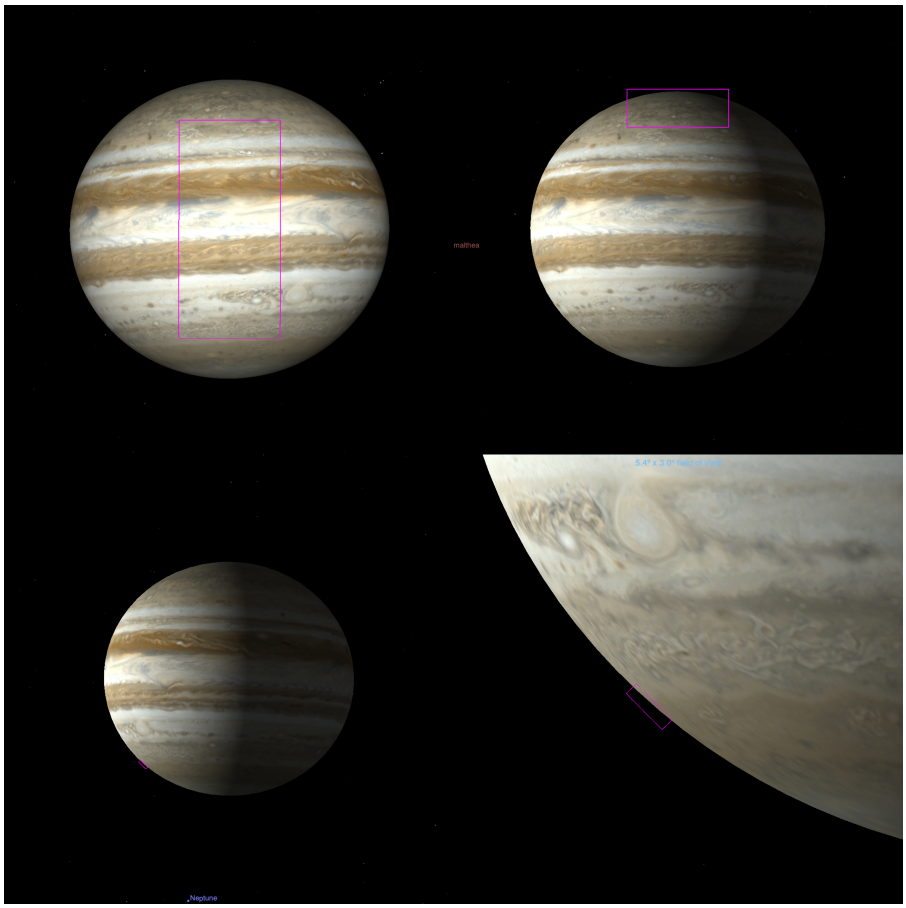

Fig. 19 Example fields-of-view of MAJIS for different observing modes. Each panel presents an individual cube from the set of several that are acquired in close temporal sequence: (top left) A cube from a MAJIS_JUP_DISK_SCAN set; acquisition starts on 2032-Sep-24 at 19:29 UTC, corresponding to the red cube of Fig. 18 (top). (top right) A cube from a MAJIS_JUP_AURORA_SCAN set; acquisition starts on 2032-Sep-25 at 06:51 UTC, corresponding to the red cube of Fig. 18 (bottom). (bottom left) A cube from a MAJIS_JUP_LIMB_SCAN set; acquisition starts on 2032-Sep-25 at 15:24 UTC. (bottom right) Detail of the same MAJIS_JUP_LIMB_SCAN cube.

Unlike other instruments, SWI will take advantage of its own pointing mechanism that will enable scanning up to $\pm 72^\circ$ along-track and $\pm 4.3^\circ$ cross-track away from the attitude of the JUICE spacecraft. This pointing capability has $\sim 30''$ and $\sim 9''$ steps along-track and cross-track, respectively, with $30''$ accuracy. This mechanism will serve several operational goals. SWI will be able to (i) map the whole Jovian disk from any distance $>15\,R_J$, (ii) compensate for spacecraft motions when performing scans for other remote sensing instruments to ensure a stable pointing, and (iii) reach any Galilean moon from the equatorial orbit on a daily basis to monitor their emissions and constrain the source of their atmospheres (Tosi et al. in prep.).

The main Jupiter science goals of SWI concern its stratospheric circulation and chemistry. Constraining the general circulation of Jupiter's stratosphere (e.g. Medvedev et al. 2013; Guerlet et al. 2020b) requires measuring temperature and winds simultaneously and continuously at all latitudes, longitudes and altitudes. This can only be rarely achieved from the ground (Benmahi et al. 2021). The duration of the Jupiter tour will provide SWI with the possibility to build a full 4-dimensional view of Jupiter's stratospheric composition and dynamics, from its QQO-dominated equatorial region to the auroral latitudes, while ALMA can only provide irregularly-spaced snapshots (e.g., Cavalié et al. 2021, 2022). A focus will be put on equatorial latitudes to constrain what maintains the QQO (Leovy et al. 1991b; Orton et al. 1991b; Li and Read 2000; Cosentino et al. 2017b; Giles et al. 2020a; Benmahi et al. 2021), and on the auroral regions to understand what controls its chemistry and dynamics (Sinclair et al. 2017b,a, 2018a, 2019; Cavalié et al. 2021, 2022). Composition maps will help to constrain the stratospheric photochemistry of Jupiter (Moses et al. 2005b; Hue et al. 2018b) and spectral scans will be performed in various regions to serendipitously search for new species and isotopologues. SWI will also detect and quantify sources of exogenic species other than SL9, like the Galilean moons, rings and torii (Hartogh et al. 2011; Cavalié et al. 2019), interplanetary dust (Moses and Poppe 2017), and comet/asteroid impacts. The latter seem to occur regularly in giant planet atmospheres (Bézard et al. 2002; Cavalié et al. 2010, 2014; Lellouch et al. 2005; Moreno et al. 2017; Hueso et al. 2010, 2013, 2018a; Orton et al. 2011).

4.3.2 SWI Operations

These goals will be achieved from the following observation products: regular 2D wind maps from 10 μbar to 400 mbar with 3° latitudinal resolution; global thermal structure also from 10 μbar to 400 mbar with 3° latitudinal resolution and 20° longitudinal resolution; vertical distribution of a variety of species, tracing atmospheric transport from SL9-derived species distributions; isotopic composition; and search for new species. The observation strategy adopted by SWI mostly depends on the distance to Jupiter (see Figure 21). When JUICE is closer than 25 R_J, limb stares and limb rasters will be prioritised to map temperatures (from CH_4), abundances and wind speeds with the required latitudinal resolution. Observations from these distances will be complemented by zonal scans to look for thermal waves, 2D maps and meridional scans to measure the latitudinal distributions of high priority species (H_2O, HCN, CO). These observations will be clustered around perijoves in the early phases of the tour and during Phase 5. At intermediate distances (between 25 R_J and 35 R_J), SWI will measure the latitudinal distributions of lower priority species (CS, CH_3C_2H, isotopologues) with 5° latitudinal resolution and look for new species using limb stares, limb rasters and 2D maps. At distances beyond 35 R_J, SWI will monitor line emissions at lower spatial resolutions from the equatorial region to the auroras, and perform calibration observations, using 2D maps, 5-point crosses and nadir stares.

4.4 JANUS

4.4.1 JANUS Description

The JUICE optical camera, JANUS (Jovis, Amorum ac Natorum Undique Scrutator, Palumbo et al. in prep.) is a multi-filter camera system with a CMOS detector and thirteen filters spanning the near-UV (340 nm) to the near-IR (1080 nm). JANUS addresses a number of the scientific investigations in Section 2 and Table 1. JANUS will investigate the dynamics of the weather layer by providing high-resolution observations of the atmosphere from the cloud layer to the upper hazes in multiple wavelengths. Repeated observations will be used to characterise the atmospheric dynamics and circulation [JA.1] including the role of atmospheric waves at multiple scales [JA.3]. Observations in multiple wavelength will be used to investigate the vertical cloud structure [JC.1] and the coupling of different clouds with the dynamics [JC.2]. Dayside and night-side observations of convective regions will be used to study the role of moist convection in meteorology [JB.4]. Auroral processes imaged at night [JA.4] will also constitute an important dataset to understand the auroral structure and the impact of auroral processes in forming high altitude aerosol layers in the polar regions. JANUS observations will consist in the combination of mappings of the planet taking advantage of the planet rotation, and high-resolution observations of different targets separated by different time-scales.

The field-of-view of the detector covers a rectangular area over the sky of $1.29^\circ \times 1.72^\circ$, with the largest size of the detector oriented parallel to Jupiter's equator with the nominal spacecraft attitude during Jupiter observations. The detector has 1504×1200 pixels with a pixel IFoV of 15 μrad that allows images with a 15 km/pix from a target distance of 10^6 km. Images with a Signal to Noise Ratio (SNR) larger than 100 are achievable in most operational conditions foreseen during the Jupiter investigation, with dayside integration times of 1 s or less even in the filters sensitive to strong methane absorption bands. JANUS observations of the nightside of the planet will be obtained with larger exposure times below an upper operational limit of 112 s.

Table 2 provides details about the filters. Each of these filters have spectral transmission curves that are almost rectangular-shaped. The instrument spectral response is also determined by the optical elements and detector spectral response, with a steep decrease at low and high range edges. JANUS filters can be compared with filters from previous missions in Table 3.

Table 2 JANUS filters

Position	Filter id.	Central wavelength / Bandpass [nm]	Note
F1	PAN	650/500	Panchromatic (clear) – monochromatic imaging
F2	BLUE	450/60	Blue – aerosol colours
F3	GREEN	540/60	Green, background for Na – aerosol colours
F4	RED	646/60	Red, background for Hα – aerosol colours
F5	CMT medium	750/20	Continuum for medium Jovian Methane band
F6	Na	590/10	Sodium D-lines in exospheres
F7	MT strong	889/20	Strong Jovian Methane band
F8	CMT strong	940/20	Continuum for strong Jovian Methane band
F9	MT medium	727/10	Medium Jovian Methane band
F10	Violet	380/80	UV slope
F11	NIR 1	910/80	Cloud structure
F12	NIR 2	1015/130	Cloud structure
F13	Hα	656/10	Hα-line for aurorae and lightning

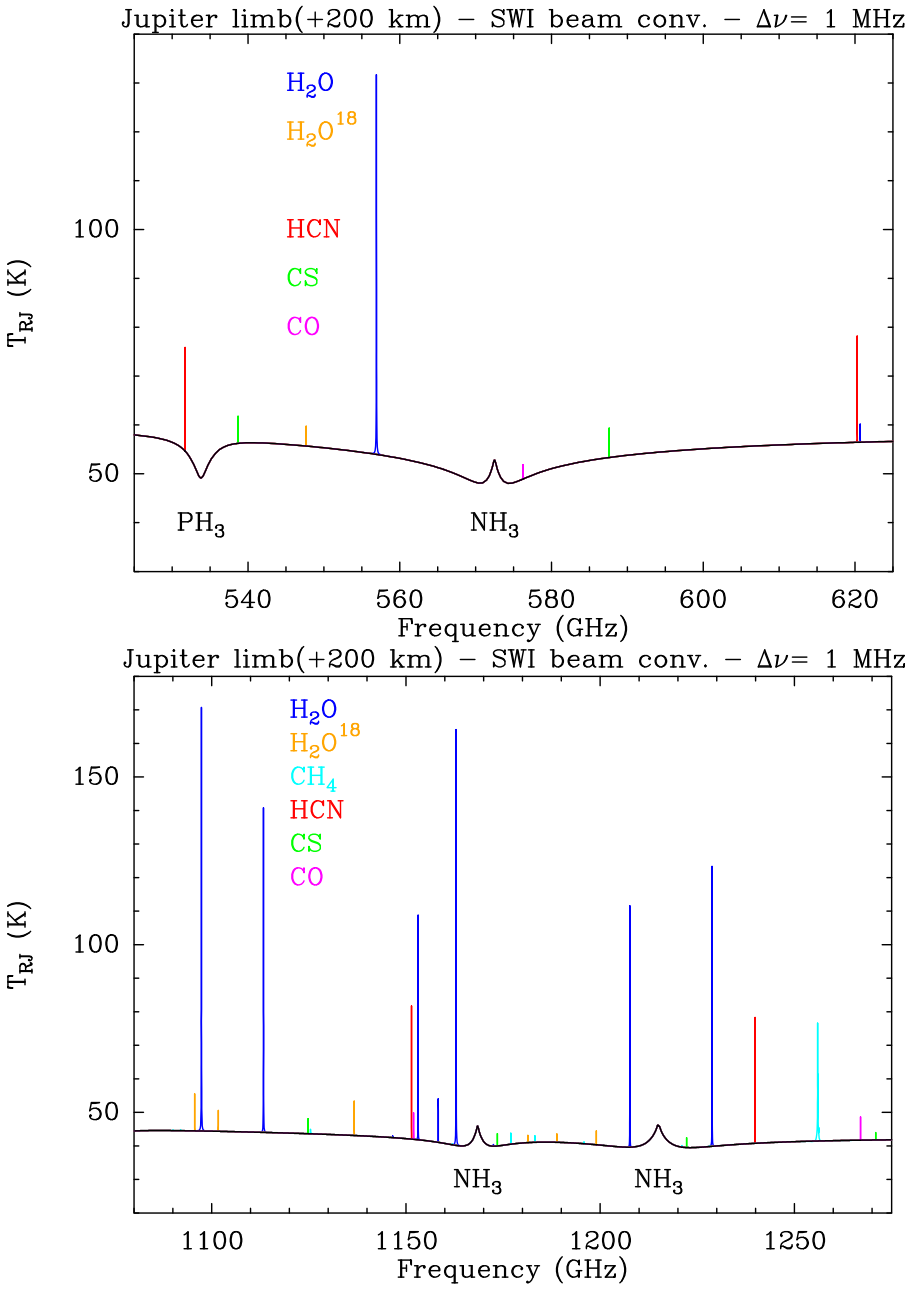

Fig. 20 Jupiter limb spectra in the 600 GHz (top) and 1200 GHz (bottom) bands probed by SWI, with the main observable molecular lines. Spectra are computed at the limb for a tangential height of 200 km above the 1-bar level and are convolved by the instrument beam and to a spectral resolution of 1 MHz.

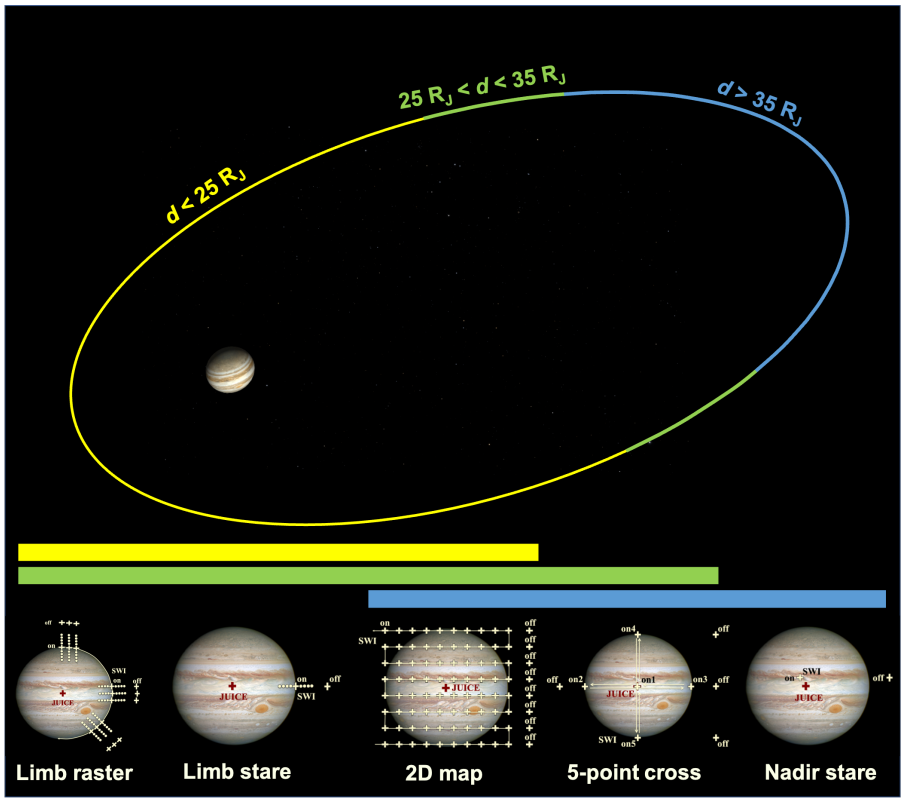

Fig. 21 Five main observations modes used by SWI for Jupiter atmospheric investigations. Their use mainly depends on the distance to the planet, as depicted by the color code: yellow, green and blue for modes to be used when JUICE is at distance $d < 25R_J$, $25R_J < d < 35R_J$, and $d > 35R_J$, respectively. The along-track and cross-track mechanisms of the instrument enable pointing independently from the spacecraft to build various patterns (stares, crosses, scans, and maps). The 2D map mode can be set such that meridional or zonal scans are performed. The limb stares and rasters use a limb-finding procedure at each latitude in which the continuum is recorded over several tens of positions from nadir to sky to reconstruct *a posteriori* the pointing of the long integration for accurate rotation removal in wind measurements.

Table 3 Comparison of JANUS filters with those on previous missions

Wavelength centres [nm]	Galileo SSI (a)	Voyager		Cassini ISS		New Horizon		Juno JunoCam (f)	JUICE JANUS
		NAC (b)	WAC (b)	NAC (c)	WAC (c)	RALPH (d)	LORRI (e)		
Clear	611 (440)	497 (360)	470 (290)	611	635	687 (575)	600 (500)	-	650 (500)
UV	-	-	-	258	-	-	-	-	n.a.
UV	-	-	-	298	-	-	-	-	n.a.
UV	-	346	-	338	-	-	-	-	n.a.
Violet	404	416	426	-	420	-	-	-	380 (80)
Blue (2)	-	-	-	440	-	-	-	-	-
Blue	-	479	476	451	460	475	-	Bayer Pattern blue	450 (60)
Methane	-	-	541	-	-	-	-	-	-
Green	559	566	560	568	567	-	-	Bayer Pattern green	540 (60)
Sodium-D	-	-	589	-	-	-	-	-	590 (10)
Orange	-	591	605	-	-	-	-	-	-
Methane	-	-	618	619	-	-	-	-	-
Continuum 2-lobed	-	-	-	603, 635	-	-	-	-	-
Red	671	-	-	650	648	620	-	Bayer Pattern red	646 (60)
H-alpha	-	-	-	656	656	-	-	-	656 (10)
Methane	734	-	-	727	728	-	-	-	727 (10)
Continuum / NIR	756	-	-	750	752	-	-	-	750 (20)
NIR (broad)	-	-	-	752	742	-	-	-	-
NIR (broad)	-	-	-	862	853	880	-	-	-
Methane	887	-	-	889	890	885	-	-	889 (20)
Near Infrared	-	-	-	930	918	-	-	-	910 (80)
Continuum	-	-	-	938	939	-	-	-	940 (20)
Near Infrared	986 -	-	1002	1001	-	-	-	1015 (130)	
NIR (broad)	-	-	-	-	1028	-	-	-	-

Notes: Bandwith is given in parentheses for the clear filter (ISS polarization filters and two-filter bandpasses not considered). (a) (Belton et al. 1992), (b) (Smith et al. 1977), (c) (Porco et al. 2004), (d) (Reuter et al. 2008), (e) (Cheng et al. 2008b), (f) (Hansen et al. 2017b).

4.4.2 JANUS Operations

Figure 22 shows sketches of some of the operational models of JANUS. JANUS will provide the highest spatial resolution observations over the planet with the capability to map the planet as it rotates and image specific features at very high spatial resolution ($\sim$10 km/pix). To map the planet JANUS will perform vertical scans of Jupiter (Figure 22a) in which different frames will cover different latitudinal ranges and different longitudes will be sampled as the planet rotates over its 10-hour rotation period. These maps will be obtained at low and intermediate phase angles ($<90^{\circ}$) over the illuminated side of Jupiter and will attain spatial resolutions of about 15–30 km/pix. The different opportunities in the orbital tour to obtain full maps of the planet separated by one Jovian rotation (10hr) will result in several determinations of the mean zonal winds and their variability over the course of the orbital tour. These wind fields will have a noise level of less than 1 m/s and will be used to answer fundamental question on the energy inputs of the jets and cloud systems and how is the interaction between the eddies and zonal winds (e.g., Salyk et al. 2006), and on the meridional transport on belts and zones (Duer et al. 2021) at different moments during the mission. Higher resolution observations of particular features will unveil the internal wind field of vortices, cyclonic regions, and convective storms (Figure 6).

Close to the planet, JANUS will observe specific regions at spatial resolutions down to 10 km/pix including the limbs (Figure 22b). Repeated observations of the same regions obtained after a given amount of time will be used to infer dynamics by examining cloud motions on time-scales of 0.5, 2.0 and 10.0 hr tracking specific features of interest like the Great Red Spot and other regions. Specific observations of the polar regions from sub-spacecraft latitudes of about $\pm 30^{\circ}$will be obtained to investigate long-term changes of the polar atmosphere since the Juno observations (Adriani et al. 2018b).

In addition, by using a combination of filters sensitive to color and cloud altitude via different atmospheric absorption bands, JANUS image will investigate the particle size and optical properties of the clouds, hazes and aerosols, investigating the complex and poorly determined relations between colour distribution and atmospheric dynamics in Jupiter. By observing the limbs at high spatial resolutions over a variety of phase angles over different latitudes JANUS will further investigate the elevated hazes at levels close to the stratopause and higher.

Nightside observations will map the spatial distribution of lightning (Figure 22c) to complement and extend the results from previous missions (Little et al. 1999; Dyudina et al. 2004; Baines et al. 2007; Becker et al. 2020b). Observations of lightning at high spatial resolution will be used to investigate lightning spot sizes to constrain the depth of the lightning source. Dayside observations of the same areas observed on the nightside with time differences of a few hours will also give information about the intensity, depth and vertical transport associated to moist convective storms. Nightside observations of the polar region (Figure 22c) will also investigate the emissions of the aurora and its vertical structure.

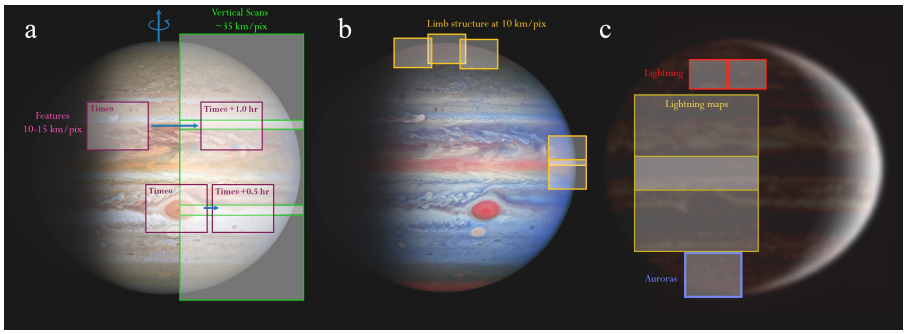

Fig. 22 Sketch of different JANUS frames over the planet covering different topics. (a) Dayside observations obtaining vertical scans of the planet as it rotates (green frames), or images of specific features obtained at high spatial resolution with small time differences (purple frames) will be used for dynamics. (b) Limb observations at different wavelengths will complement observations at a variety of phase angles to determine the vertical cloud structure and directly observe haze systems over the limb. (c) Night side observations at high phase angles will map lightning (dark yellow) at moderate resolution but high-resolution images of latitudes with convective activity will also be obtained at high-resolution (red). Auroras observations will also be possible at different spatial and temporal resolutions (blue). These observations will be spread over different phases of the mission.

4.5 3GM

4.5.1 3GM Description

The 3GM (Gravity & Geophysics of Jupiter and Galilean Moons, Iess et al. in prep.) is the experiment onboard the JUICE mission responsible for the radio science. This instrument consists of two separate and independently operated units incorporated in the Telemetry Tracking and Command subsystem of the spacecraft: a Ka band Transponder (KaT) and an Ultra Stable Oscillator (USO). The KaT will enable two-way range and Doppler measurements with very high accuracy at Ka band (34.5-32.2 GHz), measuring the gravity fields of Europa, Ganymede and Callisto (Cappuccio et al. 2022). Juno measured the gravity field of Jupiter to high accuracy (Iess et al. 2018), enabling the determination of the zonal wind depth (Kaspi et al. 2018). This was made possible by Juno's close proximity to Jupiter's cloud tops (a few thousand kilometres altitude). However, JUICE will orbit Jupiter with a proximity of hundreds of thousands of kilometres, rendering Juno-like gravity measurements of Jupiter's deep interior impracticable. However, the USO will enable radio occultations of Jupiter's atmosphere by providing a highly stable frequency reference for the transmitted signal, establishing the possibility of one-way downlink radio occultation experiments. Together with X and Ka band transponders, providing various communication links, the USO will be used to perform radio science to retrieve the structure and composition of the neutral atmosphere and ionosphere of both Jupiter and its moons.

These occultations and bistatic radar radio science experiments permit the retrieval of vertical profiles of density, pressure, temperature and composition in the Jovian neutral atmosphere and electron/ion densities in the Jovian Ionosphere. The

wide temporal and spatial variability of the experiments will also enable the study of vertically-propagating waves influencing the heating in the thermosphere, and monitor this variability with time and latitude.

The main principle of radio occultation measurements is the transmission of an electromagnetic signal in the radio spectrum (X and Ka band) between two separated stations (the JUICE spacecraft and an Earth-based ground-station), thereby passing through the atmosphere or ionosphere of a solar system object (Jupiter or its moons). Electromagnetic signals crossing an optical medium experience refraction, which can have two distinct effects on the signal. The first is the increase in the phase speed of the signal as the wave propagates in a neutral medium and the decrease in the phase speed of the signal while propagating in an ionised medium. The second is the bending of the signal towards regions of higher index of refraction, instead of traveling in a straight line from transmission to reception. These effects on the signal result in frequency shifts (Doppler shifts) with respect to a signal that would be traveling in vacuum. This refraction is exploited and studied in radio occultation experiments in order to retrieve the atmospheric properties of planetary atmospheres in the form of profiles varying with depth and latitude (e.g., Lindal et al. 1981, Schinder et al. 2015).

The orbit of JUICE will enable the widespread distribution of these vertical profiles, guaranteeing good spatial coverage. The vertical temperature profiles will be improved by the instrumental accuracy of the USO that will allow a resolution of about 0.1 K over 1 km. The vertical resolution of occultations is also characterised by the Fresnel scale, some 6 km in the stratosphere, and a few hundred meters in the troposphere (due to refractive defocusing), from the distance of Ganymede. In addition, the attenuation of the signal can be used to deduce the absorptivity of ammonia, since radio occultations (at X band) are expected to be able to probe down to approximately the cloud level at the $\pm$700 mbar level, whereupon NH_3 absorption fully attenuates the signal.

4.5.2 3GM Operations

All predicted JUICE radio occultation opportunities of Jupiter are portrayed for the period of July 2032 to January 2036, separated into the different phases of the mission (Figure 23). The latest scenario of an April 2023 launch campaign (Crema 5.0b23) allows for around 80 radio occultations of the gas giant. The orbit of JUICE allows for not only a large number of radio occultations over the timeframe of the mission, but also for a broad latitudinal coverage. This will enable a better three-dimensional mapping of the upper atmosphere of Jupiter than has been previously possible. Figure 23 shows the wide distribution of the radio occultation possibilities over Jovian latitude (upper) and longitude (lower). Jupiter's northern hemisphere has significantly more coverage due to the timing of the JUICE mission, providing the chance for occultations at approximately the same latitude twice. Equatorial latitudes will only be observable with occultations during Phase 4 (the inclined phase). Since the southern hemisphere has fewer opportunities, and all during Phase 3 (the Europa flybys), the portrayed radio occultations are important to include in the science activity plan. Note that future changes in the tour of JUICE can affect the frequency and possibilities of the radio occultation experiments, especially in the southern hemisphere.

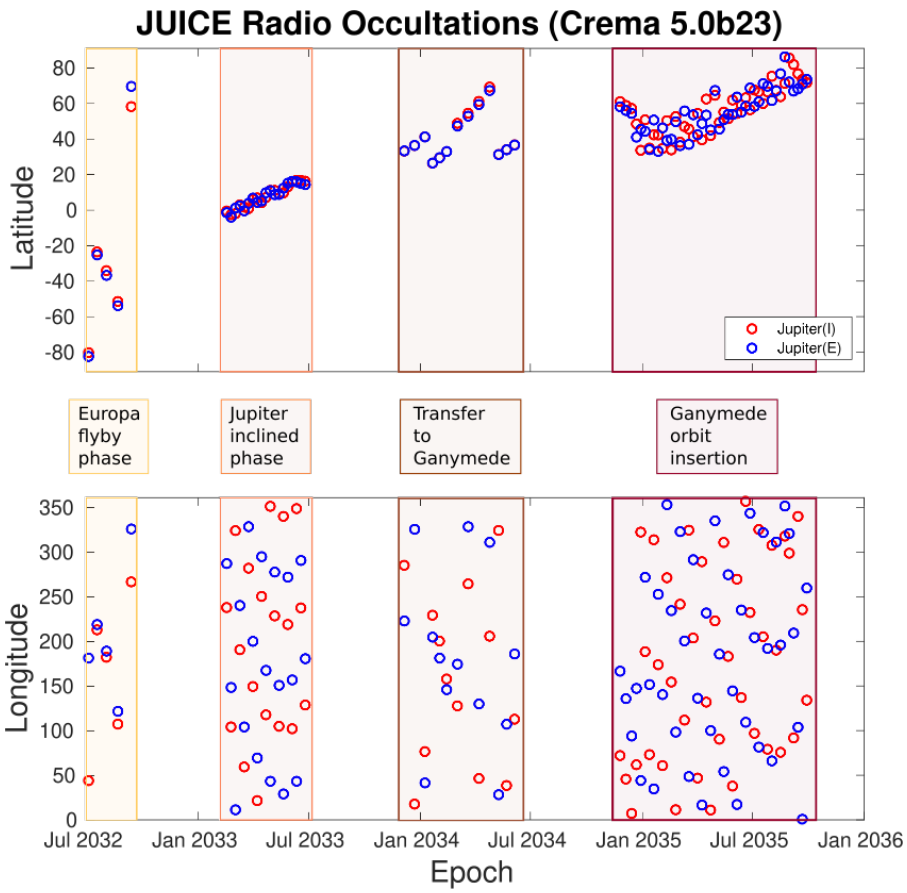

Fig. 23 JUICE radio occultation opportunities of Jupiter based on Crema 5.0b23, for both latitudinal coverage (top) and longitudinal coverage (bottom) for Phases 3 through 6 of the mission. Note the large numbers of occultations while JUICE is in orbit around Ganymede during Phase 6.

The USO on board of JUICE provides a highly stable frequency reference for the transmitted signal in X and Ka bands, leading to the possibility for one-way radio occultation analysis. In one-way mode, the pointing of the spacecraft will be adjusted continuously to the direction that allows the signal transmitted by the spacecraft to be bent in a way that it will be traveling toward the receiving station after traversing Jupiter's atmosphere. The analysis of radio occultations of oblate planetary objects is performed in a different way than for spherically symmetrical ones, due to the fact that the signal in the oblate case refracts three-dimensionally. The ray-tracing method used for the analysis of Jupiter follows Schinder et al. (2015). This method uses a numerical integration of the equations (Eikonal Equations) describing subsequent optical rays across a barotropic layered atmosphere.

A few radio occultation experiments of Jupiter have been performed in the past, and can provide benchmarks and constrain more finely the composition of the atmosphere. A series of radio occultations experiments of Jupiter were performed by the

Voyager 1 and 2 missions (Lindal et al. 1981; Gupta et al. 2022), with a similar configuration to the JUICE mission. Both Voyager spacecrafts carried a USO on board, which was used to provide a very stable frequency reference for the pure tones in the S and X frequency bands, so that the analysis could be performed in one-way mode.

The analysis of $\sim$ 20 upcoming radio occultations by the Juno spacecraft during its extended mission (2023-2025), covering both northern and southern hemispheres, will provide the most recent data for comparison to the JUICE radio science. Juno occultations will be performed in two-way mode since no USO is present on board Juno. In a two-way mode, the highly stable frequency reference is not on the spacecraft but at a transmitting station on the Earth.

4.6 RPWI

4.6.1 RPWI Description

The JUICE Radio & Plasma Wave Investigation (RPWI) instrument package and science objectives are described in detail in Wahlund et al. (in prep.) Here we briefly focus on the parts relevant for the Jupiter science goals. The RPWI instrument package will measure the electric- and magnetic-field vectors, as well as thermal plasma properties in a wide frequency range and with high temporal/spatial resolution. The electric field is measured from DC up to 1.4 MHz by a set of four Langmuir probes. A search coil magnetometer will measure the magnetic field in the frequency range 0.1-20 kHz, complementing the higher frequency wave components of the J-MAG measurements. Onboard analysis of these measurements, combined with the RPWI electric components, will be used to obtain the polarization and propagation properties of electromagnetic waves in this frequency range.

Broadband measurements of all these wave field components will be especially useful for analysis of electromagnetic signals emitted from electric discharges in the Jovian atmosphere and waves in different propagation modes linked to Jovian aurora. The near DC electric field measurements, together with the J-MAG magnetic field measurements, will enable us to continuously give values of the $\boldsymbol{E} \times \boldsymbol{B}$ convection (i.e., wherever JUICE is traversing in the Jovian system). These convection electric fields are mapped, along magnetic field flux tubes, down to Jupiter's atmosphere and ionosphere, there giving rise to electrodynamic momentum and energy exchange primarily within the Jovian thermosphere and ionosphere. Along these flux tubes energy and momentum is also transported by Alfvén wave activity, readily monitored by RPWI determining their Poynting flux and dispersive properties. This is especially important on magnetic footprints corresponding to the Jovian auroral regions and the flux tubes connecting to the larger icy moons (Callisto, Ganymede, and Europa). Jovian radio waves are monitored by a special antenna system operating from 80 kHz to 45 MHz. In addition, the RPWI sensors monitor thermal plasma and μm-sized dust properties wherever they operate.

More specifically, the RPWI will contribute to Jupiter science goals in the following ways:

- Map the thermal plasma and the electrodynamic (convection) interaction processes along Jovian magnetic footprint fluxtubes corresponding to the icy moons and the Jovian auroral regions.
- Characterise Alfvén waves, whistler mode waves, plasma waves in the Jovian magnetosphere of importance for the energy and momentum flux down to the Jovian ionosphere/thermosphere.
- Characterise radio and whistler wave emissions from lightning at Jupiter.
- Determination of the general dynamic state of the Jovian magnetosphere through monitoring of the Jovian radio emission activity.

4.6.2 RPWI Operations

The RPWI sensors will nominally be continuously operating together with J-MAG. The convection electric field (and $\boldsymbol{E} \times \boldsymbol{B}$), thermal plasma properties, and Jovian plasma and radio wave activity will therefore always be available, with limited impact on the remote sensing plan during the perijove windows in Section 3. Certain periods will require 'burst-mode data' to enable detailed studies near the large icy moons or magnetosphere boundaries, e.g., characterizing the icy moons ionospheres or icy thickness, the icy moons interaction with the Jovian magnetosphere, the energy and momentum processes related to the magnetospheric footprints to Jupiter, etc. Multidimensional electromagnetic signals from electrical discharges in the Jovian atmosphere will be also captured during the dedicated burst mode periods. The RPWI operations will implement a so-called selective downlink where the RPWI instrument almost always does burst mode measurements, while the telemetry allocation determines how much data RPWI can download at a specific time during a period of a few weeks.

4.7 PRIDE

The Planetary Radio Interferometry and Doppler Experiment (PRIDE) experiment will conduct radio occultation observations, alongside 3GM, using radio telescopes from the European VLBI network (EVN) as receivers in a one-way mode using X- and Ka- bands. In this setup, the PRIDE telescopes would perform shadow tracking of the spacecraft during the occultation (e.g., Bocanegra-Bahamón et al. 2019). The radio signal would be recorded as it gets refracted by Jupiter's ionosphere and atmosphere in a wideband open-loop configuration, which allows capturing its high dynamic range. The PRIDE experiment has access through the EVN to tens of radio telescopes in Europe, Asia, South Africa and Australia, including large antennas such as the 65-m Tianma, 64-m Sardinia and 100-m Effelsberg. The use of many antennas, and of large antennas in particular in radio occultation measurements, especially for those geometries with limited SNR (Bocanegra-Bahamón et al. 2018)), would improve the quality of the atmospheric data retrieved and allow sounding deeper in the atmosphere than with antennas of smaller collecting area. This is particularly important in the retrievals of NH_3 and PH_3 abundances (in terms of associated uncertainties and penetration depth) from radio occultation measurements, which would lead to an

improved characterisation of NH_3 condensation physics and PH_3 photochemical destruction processes in Jupiter's atmosphere.

5 Synergistic Science at Jupiter

The previous sections described the JUICE scientific objectives (Section 1), the requirements on the Jupiter tour and its segmentation (Section 3), and the capabilities of the payload for Jupiter science (Section 4). In this Section we provide a subset of examples of how the different instruments might work together synergistically to explore equatorial dynamics, moist convection and lightning, stratospheric chemistry, auroral activity, and vertical wave structures, e.g. by taking advantage from the complementary vertical coverage of the various remote sensing instruments as shown in Fig. 24.

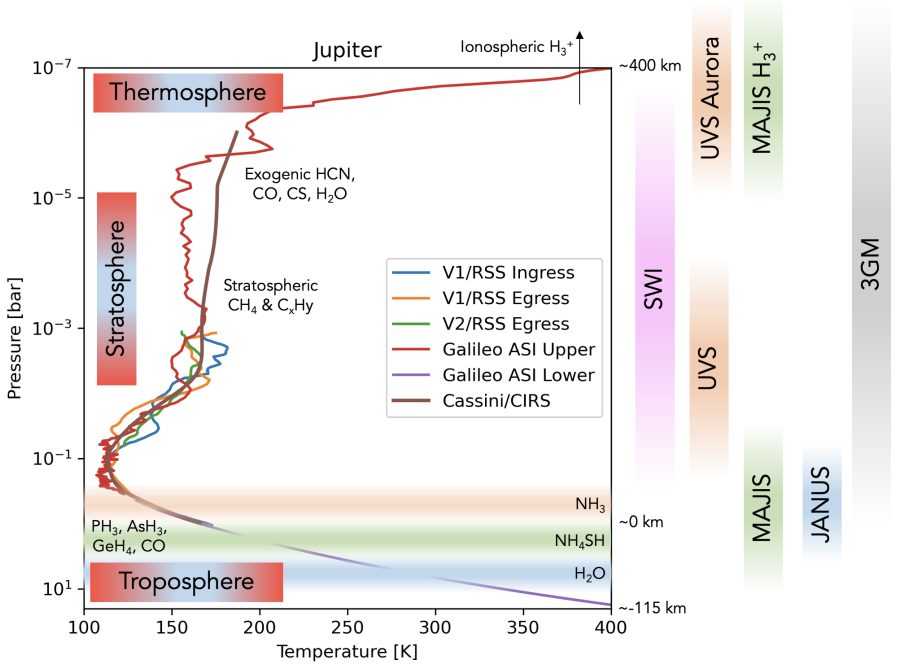

Fig. 24 Synergistic observations are possible due to the overlapping vertical sensitivity of each instrument in nadir sounding, compared to Jupiter's thermal structure from Voyager radio occultations (Gupta et al. 2022), the Galileo Probe Atmospheric Structure Instrument (Seiff et al. 1998), and an average of Cassini/CIRS temperature retrievals (Fletcher et al. 2016). Key atmospheric regions, species, and aerosols are labelled where they can be studied via spectroscopy. At higher altitudes, *in-situ* instruments (J-MAG, RPWI, PEP) will contribute to characterise the energy and dynamics of the thermosphere (and ionosphere).

5.1 Jupiter's Equatorial Circulation and Meteorology

Jupiter's Equatorial Zone (EZ) and neighbouring belts display a plethora of dynamic activity: from evidence of moist convection and lightning in the belts, to waves, variable winds, large vortices, and a Hadley-like circulation pattern generating extreme contrasts in volatiles (e.g., NH_3 de Pater et al. 2016; Li et al. 2017), temperatures and disequilibrium species (e.g., Fletcher et al. 2009) between the EZ, NEB and SEB. The sole *in situ* measurement of a giant planet comes from Galileo Probe observations in a region between the NEB and EZ (Atkinson et al. 1998; Wong et al. 2004), and it remains unclear how representative these measurements were of the planetary bulk. Tropospheric dynamics provide the spectrum of waves responsible for Jupiter's equatorial stratospheric oscillation (Leovy et al. 1991a), which subsequently influences the temperatures, winds and composition of the stratosphere. All of these processes vary over timescales from hours to months, but systematic multi-wavelength studies have proven challenging.

JUICE observations are designed to address the need for atmospheric monitoring, both from the perijove windows to the monitoring opportunities throughout Phases 2, 3 and 5. MAJIS spectral maps of reflected sunlight and thermal emission to map aerosols and gaseous composition will be interspersed with JANUS dayside cloud tracking for tropospheric winds and dynamics, UVS scans for aerosols and stratospheric composition, SWI zonal scans to determine the stratospheric temperature structure, and SWI limb observations to derive the vertical winds associated with the QQO. UVS, MAJIS and SWI (via the 572 GHz line) all have sensitivity to Jovian NH_3, enabling reconstruction of the gaseous distribution above the condensation clouds to study its temporal variability. Radio occultations during Phase 4 will provide the vertical $T(p)$ and NH_3 absorption for comparison with remote sensing measurements, and RPWI will be able to search for evidence of lightning activity (see below).

5.2 Moist Convection and Lightning

As described in Section 2.1.3, mapping of lightning activity provides a powerful probe of Jupiter's meteorology within the water-cloud regions. UVS may detect transient luminous events (Giles et al. 2020b) that could be associated with lightning; JANUS will use nightside imaging to search for optical flashes (and dayside imaging to find their storm counterparts) using a similar approach to Galileo (Gierasch et al. 2000) and Juno (Becker et al. 2020a). MAJIS observations of evolving storm plumes could constrain their changing optical depth from bright fresh plumes to darker ovals, following similar techniques for Cassini at Saturn (Sromovsky et al. 2018). Lightning whistler measurements will also be performed by the RPWI search coil magnetometer and the Langmuir probes used as electric antennas. Based on the received signals in a range from 10 Hz to 20 kHz the LF (low frequency) receiver will produce snapshots a few seconds long, producing spectra of high temporal resolution from which the whistler dispersion can be measured. Measurement of sferics or Jovian dispersed pulses from lightning by RPWI might also be possible using the three RWI anten-

nas and its corresponding HF (high frequency) receiver in the frequency range above 80 kHz, where each sweep will take a few seconds. Such a receiver mode at high frequencies would work for the detection of Saturn lightning, but previous attempts to use similar frequency-sweeping receivers on a spacecraft at Jupiter have so far failed to detect any Jovian sferics. Similarly, the RPWI LP receiver can use the Langmuir probes in the electric field mode from DC to 1.5 MHz to produce electric field spectra with low time resolution. Taken together, these techniques will build a statistical picture of lightning phenomena on Jupiter, relating lightning detection to discrete regions of features.

5.3 Stratospheric Chemistry

As described in Section 2.3.2, the vertical and meridional distributions of Jupiter's stratospheric hydrocarbons remain poorly understood. The high latitude distributions of C_2 species was first observed during the Cassini flyby, with C_2H_2 and C_2H_6 showing opposite behaviours as a function of latitude (Nixon et al. 2007a). Longitudinally resolved observations of the auroral regions unveiled and even more complex situation, with a high degree of variability in all three dimensions for the main C_2 species (Sinclair et al. 2018a) and for more complex hydrocarbons (Sinclair et al. 2019). Some binary or multi star systems have both UV bright and near-infrared bright stars collocated on the sky. Leveraging this group of unique targets, UVS and MAJIS will be able to perform simultaneous occultation observations. These synchronous observations will provide a high fidelity measurement of the thermal and chemical structure structure from the lower thermosphere to the troposphere. JANUS would contribute with contextual astrometry observations. All these observations would be complemented by SWI limb observations of the stratospheric thermal structure from CH_4 observations at 1256 GHz and the vertical profile of CH_3C_2H. These combined observations of the temperature and hydrocarbon distributions would help to constrain photochemical and transport models of Jupiter's stratosphere (Moses et al. 2005b; Hue et al. 2018b), alongside SWI measurements of the spatial distributions of long-lived H_2O, CO, HCN and CS deposited by the SL9 comet impact in 1994 and diffusing with latitude and depth ever since (Moreno et al. 2003; Griffith et al. 2004; Lellouch et al. 2002, 2006; Cavalié et al. 2013, 2022).

5.4 Auroral Morphology, Chemistry and Dynamics

Multi-wavelength simultaneous monitoring of the auroral emissions from the UV to the submillimeter will enable better understanding the variability, energetics, and dynamics of the auroras. UVS will perform regular meridional scans of the auroras to monitor the morphology of the auroras. The produced brightness and color ratio maps will make use of CH_4, C_2H_6 and C_2H_2 distributions retrieved from UV stellar occultation experiments (see Fig. 16) to capture the flux and energy of the precipitating auroral particles, giving a measure of the auroral energy deposited into the polar region. MAJIS maps of H_3^+ emission give insight into the cooling due to radiation to

space of some of the auroral heating via H_3^+ emissions (Gérard et al. 2023). Thermospheric temperatures and H_3^+ densities can be inferred from the H_3^+ emissions, while the upper stratospheric and lower thermospheric temperatures can be captured by SWI observations of CH_4 and HCN lines, revealing how auroral processes contribute to heating and cooling of the neutral atmosphere. JANUS observations of visible-light emissions will provide context for the auroral morphology and vertical structure of the auroral curtain (Vasavada et al. 1999). RPWI will detect electromagnetic waves of various modes linked to auroral phenomena in a broad frequency range, such as Alfvén waves, whistler mode waves, and free space mode radio waves. Multicomponent measurements of fluctuating electric and magnetic fields will be used to characterise the wave polarization and propagation properties, including their Poynting flux.

Compositional contrasts between the auroral ovals and their surroundings will be studied with UVS, MAJIS and SWI, and SWI will provide upper stratospheric wind measurements to assess whether auroral winds measured from the ionosphere (Rego et al. 1999; Stallard et al. 2001, 2003; Johnson et al. 2017) down to the stratosphere (Cavalié et al. 2021) play an active role in favouring auroral chemistry interior of the main ovals by confining photochemical products in a region rich in energetic magnetospheric electrons. UVS and SWI will also look in the moon auroral footprints for exogenic species possibly transported from the Io (and Europa) torus to Jupiter's atmosphere. For instance, UVS is sensitive to SO_2 and SWI can look for SO and SO_2 lines. These measurements, in combination with MAJIS H_3^+ emission detection from the moon footprints, will also try to solve the puzzling structure of the near footprint tail (Mura et al. 2018).

5.5 Occultations and Waves

The spatial distribution of radio occultation opportunities was described in Section 4.5 and shown in Figure 23. These will probe both the electron density of the ionosphere and the temperature structure of the neutral atmosphere with a high vertical resolution, at a variety of latitudes and local times. Once the occultation is complete and JUICE has rotated back to Jupiter, remote sensing instruments will be able to provide contextual measurements for the same locations: for example, MAJIS observations of aerosols and NH_3, SWI measurements of temperatures and winds; and JANUS and UVS observations of any layering observed in the aerosol field on the Jovian limb. Independently of the radio occultations, stellar occultations observed by UVS, MAJIS and JANUS will be coordinated to ensure multi-spectral context for any vertical variability. This would allow vertically-propagating waves observed during the radio/stellar occultations to be tied to thermal, aerosol, and chemical layering observed on the planetary limb, and its variability with time.

6 JUICE Science in Context

6.1 Complementary Earth-Based Observations

JUICE will be orbiting the Jupiter system for the first half of the 2030s, exploring the atmosphere and auroras from vantage points that can only be achieved from an orbiting spacecraft. It will be joined by NASA's Europa Clipper mission, dedicated to the exploration of Europa but carrying exciting additional capabilities for Jupiter science. However, just as with numerous previous planetary missions (including Cassini and Juno), Earth-based observatories, both professional and amateur, will be able to provide significant spatial, temporal, and spectral support for these missions. In terms of **spatial context,** imaging and spectroscopy from ground- and space-based telescopes provide global, moderate-resolution views of Jupiter to supplement the close-in high-resolution views of the spacecraft, aiding in registration of observations and providing broader context (e.g., by characterising environmental conditions across a broad belt or zone to support JUICE observations of an embedded thunderstorm).

Given limitations on system resources (e.g., data volume), competition between scientific disciplines, and the finite duration of the Jupiter tour, Earth-based monitoring can also provide **temporal context.** As storms, vortices, and the planetary bands evolve and shift over timescales ranging from days to years, ground-based records can be used to track meteorological features. Lucky-imaging techniques employed by amateur astronomers (Mousis et al. 2014) produce high-quality Jupiter imaging on a near nightly basis. By stacking only the sharpest frames, observers can reduce the blurring effects of atmospheric seeing to create excellent images, which are then shared with the community via repositories such as the Planetary Virtual Observatory (PVOL, Hueso et al. 2018b) and the Association of Lunar and Planetary Observers (ALPO-Japan[2]). Discrete storm features are tracked from night to night to reconstruct zonal winds, wave patterns, and drift of active domains. During Juno's prime mission, such drift charts proved essential for targeting JunoCam visible-light images. Asteroid and cometary impacts caught by amateur imaging (Hueso et al. 2010, 2013, 2018a) can also provide opportunities for JUICE to observe impact-driven alterations of atmospheric composition and temperature. With advances expected in amateur capabilities in the coming decade, and machine-learning approaches to tracking atmospheric features, such long-term atmospheric monitoring will help to connect the Jovian phenomena of the 2030s to the record of observations spanning back decades (Rogers 1995). Furthermore, ground-based infrared (e.g., 3-4 μm H_3^+) observations and space-based UV (e.g., HST) observations can track the fluctuating auroral emissions over short timescales to complement the JUICE observations.

But perhaps the most important contribution from Earth-based observations is access to wider wavelength ranges to provide **spectral context**, at potentially higher spectral resolutions, than is possible from the JUICE spacecraft. For example, JUICE does not have instrumentation spanning Jupiter X-ray emission (e.g., Dunn et al. 2017; Yao et al. 2021), so cannot access the hard X-ray bremsstrahlung emission, pulsed/flared soft X-ray emissions, and the dim flickering aurora observed by the

[2] http://alpo-j.sakura.ne.jp/indexE.htm

likes of Chandra and XMM Newton. These facilities (or their successors) should be able to observe Jupiter in tandem with JUICE to connect the X-ray emission to the remote sensing discussed in Section 4. There is also a significant infrared gap in JUICE's capabilities, between the long-wave cutoff of MAJIS at 5.5 μm, and the 250 μm channel of SWI. This spans the mid- and far-infrared spectrum previously studied by Cassini/CIRS (Flasar et al. 2004), which provides a means of mapping tropospheric and stratospheric temperatures via a host of absorption and emission features, respectively. The MIRI instrument on JWST, which is expected to be operating well into the 2030s, provides spectroscopic mapping in the 5-11 μm range without saturation, but the fields of view are too small (3-7" in size) to view the entirety of Jupiter without complex mosaicking (Norwood et al. 2016). Thus the only imaging capabilities for the mid- and far-infrared are likely to come from ground-based telescopes with 3- and 8-m diameter primary mirrors, which will hopefully still be available to the planetary community in the 2030s (at the time of writing, only a small number of aging mid-infrared instruments are still available).

At even longer wavelengths, JUICE observations could be supported in the millimetre, centimetre, and metre ranges by facilities like ALMA (Cavalié et al. 2021), the next-generation Very Large Array (ngVLA, de Pater et al. 2018), and the Square Kilometre Array (SKA, Butler et al. 2004). In the continuum bands, these facilities are sensitive to temperatures, ammonia, and possibly PH_3 at depths below the cloud-forming region described in Section 2. Joint campaigns between JUICE and these ground-based observatories could help connect Jupiter's dynamic weather layer to what is happening at great depth. At decimeter to decameter wavelengths, Jupiter is one of the most prominent celestial radio sources. LOFAR has revealed the first low frequency resolved images of the radiation belts of Jupiter (Girard et al. 2016); the long wavelength range makes the observations sensitive to the lower energy end of the Jovian radiation belt electrons. Io-induced and non-Io decametric emission have also been observed (Turner et al. 2019). LOFAR's unprecedented long baselines and spectra-temporal resolution also provide the opportunity to image the dynamics of charge bunches causing Jovian decametric emission and test physical models of the associated plasma instabilities (Zarka 2004). Jupiter is also likely to become an object of studies with prospective spaceborne radio telescopes at wavelengths longer than 20-m at the hitherto unreachable (to ground-based radio telescopes) ultra-low frequency part of the electromagnetic spectrum (Bentum et al. 2020).

JUICE operations in the 2030s will be in an era of major new facilities for astronomy. The European Extremely Large Telescope (ELT), a 39-m diameter observatory based in the Atacama desert, will provide high-resolution observations in the visible, near-infrared, and mid-infrared out to approximately 14 μm. The primary science targets for the first-light instruments require small fields of view, creating a substantial mosaicking challenge for the large disc of Jupiter (but excellent for mapping the Galilean satellites), but could nevertheless observe atmospheric phenomena at the same time as JUICE. The Vera C. Rubin Observatory, previously known as the Large Synoptic Survey Telescope (LSST), will begin operating in the 2020s, increasing the catalogue of small objects throughout the solar system. Within that extensive new survey, potential objects on collision courses with the Jovian system could be identified early, and then JUICE observations adjusted to investigate the aftermath. The JUICE

tour will therefore retain some flexibility in planning, to take advantage of potentially unique and unforeseen opportunities during the mission, as highlighted in Section 3.

6.2 JUICE and Exoplanets

Finally, the JUICE mission will be operating in an era when our exploration of extrasolar planets moves from a phase of detection into an era of spectroscopic characterisation, via techniques such as transit spectroscopy and direct imaging. The discovery of the first hot Jupiter exoplanet (Mayor and Queloz 1995) fundamentally modified our vision of the Solar System planets. Firstly, planetary formation models have been challenged by the discovery of the Jupiter-mass planets closer to their star than Mercury, with the introduction of migration processes as a natural step following planet formation (Morbidelli 2020). Secondly, the mass distribution of the ∼5000 exoplanets discovered to date exhibits a very different pattern than that in the Solar System, with a peak in the mass range of 5–10 Earth masses, corresponding to the "intermediate planets", mini-Neptunes or super-Earths, which are not found in our Solar System.

As JUICE will study Jupiter's origins in the 2030s, it will help to place the characterisation of exoplanets into a wider perspective, attempting to answer the question of whether Jupiter is a more or less *typical giant planet* in composition and structure, or a more rare and special product of our Solar System. Conversely, the growing census of exo-planetary system architectures may also lead to broader understanding of how Jupiter's formation and migration shaped the structure of our own Solar System. The climate, meteorology, energetics and variability of Jupiter explored by JUICE will serve as the archetype for hydrogen-dominated giant planets and Brown Dwarfs.

ESA's ARIEL mission, to be launched in 2029 (Tinetti et al. 2018), is expected to be contemporaneous to JUICE. ARIEL is devoted to a statistical study of the composition of ∼1000 exoplanets from warm super-Earths to hot Jupiters. Interaction between the science teams of these two missions could therefore improve the science return of both, by addressing astrophysical questions about planetary origins and environments in a much broader context.

7 Summary

The exploration of Jupiter as an archetype for giant planets, both in our Solar system and beyond, has been one of the two primary scientific objectives of ESA's JUICE mission since its original inception. Since that time, NASA's Juno mission has revealed a wealth of new insights into the interior, atmosphere, and magnetosphere of the gas giant, prompting us to revisit the JUICE scientific requirements in this article. Section 2 reviewed the current status of Jupiter exploration, from the dynamic weather layer with its belts, zones, vortices, and convective storms; to the chemistry and circulation of the middle atmosphere; the global composition as a window onto planetary origins; and the energetics and circulation of the ionosphere, thermosphere, and auroras. JUICE will explore how these different layers are interconnected and

coupled, both to the circulations of the deep interior, and to the processes at work in Jupiter's magnetosphere. These themes are used to justify the JUICE Jupiter science requirements in Table 1.

Section 3 then described how the 3.5-year Jupiter tour, with its equatorial and inclined phases bringing JUICE within 700,000 km of Jupiter at the closest perijoves, provides the observational opportunities needed to achieve the science goals. JUICE's long-term monitoring of atmospheric and auroral phenomena, its global perspective from a variety of phase angles (dayside to nightside), and its near-equatorial vantage point all complement Juno's close-in regional views of Jupiter from its highly-inclined orbit, its 40-to-50-day separation of perijoves, and its near-terminator (90° phase angle) viewing geometry. The high-inclination phase enables excellent spatial and temporal coverage of Jupiter's polar atmosphere and auroras, some 5-10 years after the Juno mission.

Section 4 then described the subset of instruments that are needed to achieve closure with respect to the JUICE science requirements: namely the remote sensing instruments (JANUS, MAJIS, UVS and SWI), radio occultations (3GM) and radio and plasma wave measurements (RPWI). These instruments offer flexible opportunities and modes, working within the spacecraft resource envelope of power and data volume, and can operate both independently and synergistically (Section 5 to explore phenomena across a broad spectral range. UVS covers the 50-204 nm range of the far-UV (similar to the 68-210 nm range of Juno/UVS); JANUS provides multi-wavelength imaging from 340 to 1080 nm (complementing the R, G, B and CH_4 bands on Juno/JunoCam); and MAJIS provides visible and near-infrared spectroscopy from 0.49 to 5.56 μm (extending the 2.0-5.0 μm coverage of Juno/JIRAM). SWI provides a unique capability to access the temperatures, winds, and composition high in Jupiter's stratosphere, using sub-millimetre spectroscopy in two channels, 530-625 GHz (479-565 μm) and 1080-1275 GHz (235-277 μm). JUICE does not have capabilities in the mid-infrared (5.5-30 μm), nor in the microwave ($>$ 1 cm, like Juno/MWR) or X-ray. JUICE observations will therefore be supported by ground- and space-based observatories (including JWST) wherever possible (Section 6). Finally, 3GM radio occultations will provide electron and neutral temperature profiles at a range of latitudes, longitudes, and local times, complementing those being acquired by Juno during its extended mission.

JUICE launched in April 2023, and the scientific questions will no doubt evolve as JUICE cruises towards Jupiter in the 2020s, informed by discoveries made by Juno, by ground- and space-based observatories, by theoretical modelling, by laboratory investigations, and by the ongoing characterisation of giant exoplanets. Most importantly, Jupiter has the ability to surprise us, with unforeseen connections, unexpected events, and new puzzles. The JUICE spacecraft, scientific payload, and orbital tour have been designed to maximise our capability to explore the unexpected, and to provide our best four-dimensional characterisation of this archetypal giant planet.

Acknowledgements We wish to express our gratitude to the teams of scientists, engineers, and mission planners that have made JUICE a reality, far beyond those scientists listed here as co-authors. Without them, the scientific potential expressed in this article would remain unrealised. L.N. Fletcher is a JUICE Interdisciplinary Scientist supported by a European Research Council Consolidator Grant (under

the European Union's Horizon 2020 research and innovation programme, grant agreement No 723890) at the University of Leicester. T. Cavalié acknowledges support from CNES and the Programme National de Planétologie (PNP) of CNRS/INSU. Fletcher and Cavalié have jointly chaired the 'JUICE Jupiter Working Group' since 2015. D. Grassi, P. Palumbo, G. Piccioni, F. Altieri and A. Mura were supported by Italian Space Agency "Accordo ASI-INAF n. 2018-25-HH.0, Attività scientifiche per JUICE fase C/D". R. Hueso and A. Sánchez-Lavega were supported by grant PID2019-109467GB-I00 funded by MCIN/AEI/10.13039/501100011033/ and Grupos Gobierno Vasco IT- 1742-22. L. M. Lara was supported by project PGC2018-099425-B-I00 (MCI/AEI/FEDER, UE). Y. Kaspi, E. Galanti and M. Smirnova were supported by the Israeli Space Agency. T. K. Greathouse, P. M. Molyneux, G.R. Gladstone and K. D. Retherford acknowledge NASA funding supporting the UVS team for ESA's JUICE mission. M. Galand was supported by the UK Space Agency [grant number ST/W001071/1]. The JUICE/RPWI efforts are supported by the Swedish National Space Agency (SNSA). I. Kolmasova and O. Santolik were supported from the Czech contribution to the ESA PRODEX programme and from the MŠMT grant LUAUS23152. P. G. J. Irwin acknowledges the support of the UK Science and Technology Facilities Council (ST/S000461/1). A. Coustenis was supported by the Centre National d'Études Spatiales (CNES) in France. G. H. Jones acknowledges the support of the UK Science and Technology Facilities Council, as well as to the International Space Science Institute, ISSI, Bern, for support as a Visiting Scientist.

References

N. Achilleos, S. Miller, J. Tennyson, A.D. Aylward, I. Mueller-Wodarg, D. Rees, JIM: A time-dependent, three-dimensional model of Jupiter's thermosphere and ionosphere. Journal of Geophysical Research **103**(E9), 20089–20112 (1998). doi:10.1029/98JE00947

R.K. Achterberg, B.J. Conrath, P.J. Gierasch, Cassini CIRS retrievals of Ammonia in Jupiter's Upper Troposphere. Icarus **182**, 169–180 (2006). doi:10.1016/j.icarus.2005.12.020

A. Adriani, A. Mura, M.L. Moriconi, B.M. Dinelli, F. Fabiano, F. Altieri, G. Sindoni, S.J. Bolton, J.E.P. Connerney, S.K. Atreya, F. Bagenal, J.-C.M.C. Gérard, G. Filacchione, F. Tosi, A. Migliorini, D. Grassi, G. Piccioni, R. Noschese, A. Cicchetti, G.R. Gladstone, C. Hansen, W.S. Kurth, S.M. Levin, B.H. Mauk, D.J. McComas, A. Olivieri, D. Turrini, S. Stefani, M. Amoroso, Preliminary JIRAM results from Juno polar observations: 2. Analysis of the Jupiter southern H_3^+ emissions and comparison with the north aurora. Geophys. Res. Lett. **44**(10), 4633–4640 (2017). doi:10.1002/2017GL072905

A. Adriani, M.L. Moriconi, F. Altieri, G. Sindoni, D. Grassi, L.N. Fletcher, H. Melin, A. Mura, A.P. Ingersoll, S.K. Atreya, F. Tosi, A. Cicchetti, R. Noschese, J.I. Lunine, G.S. Orton, C. Plainaki, R. Sordini, A. Olivieri, S. Bolton, J.E.P. Connerney, S. Levin, Characterization of mesoscale waves in Jupiter's NEB by Jupiter InfraRed Auroral Mapper onboard Juno. in preparation (2018a)

A. Adriani, A. Mura, G. Orton, C. Hansen, F. Altieri, M.L. Moriconi, J. Rogers, G. Eichstädt, T. Momary, A.P. Ingersoll, G. Filacchione, G. Sindoni, F. Tabataba-Vakili, B.M. Dinelli, F. Fabiano, S.J. Bolton, J.E.P. Connerney, S.K. Atreya, J.I. Lunine, F. Tosi, A. Migliorini, D. Grassi, G. Piccioni, R. Noschese, A. Cicchetti, C. Plainaki, A. Olivieri, M.E. O'Neill, D. Turrini, S. Stefani, R. Sordini, M. Amoroso, Clusters of cyclones encircling Jupiter's poles. Nature **555**(7695), 216–219 (2018b). doi:10.1038/nature25491

F. Allegrini, B. Mauk, G. Clark, G.R. Gladstone, V. Hue, W.S. Kurth, F. Bagenal, S. Bolton, B. Bonfond, J.E.P. Connerney, R.W. Ebert, T. Greathouse, M. Imai, S. Levin, P. Louarn, D.J. McComas, J. Saur, J.R. Szalay, P.W. Valek, R.J. Wilson, Energy Flux and Characteristic Energy of Electrons Over Jupiter's Main Auroral Emission. Journal of Geophysical Research (Space Physics) **125**(4), 27693 (2020). doi:10.1029/2019JA027693

M. Allison, Planetary waves in Jupiter's equatorial atmosphere. Icarus **83**, 282–307 (1990). doi:10.1016/0019-1035(90)90069-L

C.M. Anderson, N. Biver, G.L. Bjoraker, T. Cavalié, G. Chin, M.A. DiSanti, P. Hartogh, A. Tielens, C.K. Walker, Solar System Science with the Orbiting Astronomical Satellite Investigating Stellar Systems (OASIS) Observatory. Space Sci. Rev. **218**(5), 43 (2022). doi:10.1007/s11214-022-00911-5

A. Anguiano-Arteaga, S. Pérez-Hoyos, A. Sánchez-Lavega, J.F. Sanz-Requena, P.G.J. Irwin, Vertical Distribution of Aerosols and Hazes Over Jupiter's Great Red Spot and Its Surroundings in 2016 From HST/WFC3 Imaging. Journal of Geophysical Research (Planets) **126**(11), 06996 (2021). doi:10.1029/2021JE006996

A. Antuñano, L.N. Fletcher, G.S. Orton, H. Melin, J.H. Rogers, J. Harrington, P.T. Donnelly, N. Rowe-Gurney, J.S.D. Blake, Infrared Characterization of Jupiter's Equatorial Disturbance Cycle. Geophys. Res. Lett. **45**, 10 (2018). doi:10.1029/2018GL080382

A. Antuñano, L.N. Fletcher, G.S. Orton, H. Melin, S. Milan, J. Rogers, T. Greathouse, J. Harrington, P.T. Donnelly, R. Giles, Jupiter's Atmospheric Variability from Long-term Ground-based Observations at 5 μm. Astronomical Journal **158**(3), 130 (2019). doi:10.3847/1538-3881/ab2cd6

A. Antuñano, R.G. Cosentino, L.N. Fletcher, A.A. Simon, T.K. Greathouse, G.S. Orton, Fluctuations in Jupiter's equatorial stratospheric oscillation. Nature Astronomy **5**, 71–77 (2021). doi:10.1038/s41550-020-1165-5

J. Arregi, J.F. Rojas, A. Sánchez-Lavega, A. Morgado, Phase dispersion relation of the 5-micron hot spot wave from a long-term study of Jupiter in the visible. Journal of Geophysical Research (Planets) **111**, 9010 (2006). doi:10.1029/2005JE002653

J. Arregi, J.F. Rojas, R. Hueso, A. Sánchez-Lavega, Gravity waves in Jupiter's equatorial clouds observed by the Galileo orbiter. Icarus **202**, 358–360 (2009). doi:10.1016/j.icarus.2009.03.028

D.H. Atkinson, J.B. Pollack, A. Seiff, The Galileo probe Doppler wind experiment: Measurement of the deep zonal winds on Jupiter. J. Geophys. Res. **103**, 22911–22928 (1998). doi:10.1029/98JE00060

S.K. Atreya, M.H. Wong, T.C. Owen, P.R. Mahaffy, H.B. Niemann, I. de Pater, P. Drossart, T. Encrenaz, A comparison of the atmospheres of Jupiter and Saturn: deep atmospheric composition, cloud structure, vertical mixing, and origin. Plan. & Space Sci. **47**, 1243–1262 (1999)

S.K. Atreya, P.R. Mahaffy, H.B. Niemann, M.H. Wong, T.C. Owen, Composition and origin of the atmosphere of Jupiter-an update, and implications for the extrasolar giant planets. Plan. & Space Sci. **51**, 105–112 (2003). doi:10.1016/S0032-0633(02)00144-7

K.H. Baines, A.A. Simon-Miller, G.S. Orton, H.A. Weaver, A. Lunsford, T.W. Momary, J. Spencer, A.F. Cheng, D.C. Reuter, D.E. Jennings, G.R. Gladstone, J. Moore, S.A. Stern, L.A. Young, H. Throop, P. Yanamandra-Fisher, B.M. Fisher, J. Hora, M.E. Ressler, Polar Lightning and Decadal-Scale Cloud Variability on Jupiter. Science **318**, 226–228 (2007). doi:10.1126/science.1147912

K.H. Baines, L.A. Sromovsky, R.W. Carlson, T.W. Momary, P.M. Fry, The visual spectrum of Jupiter's Great Red Spot accurately modeled with aerosols produced by photolyzed ammonia reacting with acetylene. Icarus **330**, 217–229 (2019). doi:10.1016/j.icarus.2019.04.008

K.H. Baines, R.W. Carlson, L.W. Kamp, Fresh Ammonia Ice Clouds in Jupiter I. Spectroscopic Identification, Spatial Distribution, and Dynamical Implications. Icarus **159**(1), 74–94 (2002)

A. Barcilon, P. Gierasch, A Moist, Hadley Cell Model for Jupiter's Cloud Bands. Journal of Atmospheric Sciences **27**, 550–560 (1970). doi:10.1175/1520-0469(1970)027¡0550:AMHCMF¿2.0.CO;2

N. Barrado-Izagirre, A. Sánchez-Lavega, S. Pérez-Hoyos, R. Hueso, Jupiter's polar clouds and waves from Cassini and HST images: 1993 2006. Icarus **194**, 173–185 (2008a). doi:10.1016/j.icarus.2007.08.025

N. Barrado-Izagirre, A. Sánchez-Lavega, S. Pérez-Hoyos, R. Hueso, Jupiter's polar clouds and waves from Cassini and HST images: 1993 2006. Icarus **194**(1), 173–185 (2008b). doi:10.1016/j.icarus.2007.08.025

H.N. Becker, J.W. Alexander, S.K. Atreya, S.J. Bolton, M.J. Brennan, S.T. Brown, A. Guillaume, T. Guillot, A.P. Ingersoll, S.M. Levin, J.I. Lunine, Y.S. Aglyamov, P.G. Steffes, Small lightning flashes from shallow electrical storms on Jupiter. Nature **584**(7819), 55–58 (2020a). doi:10.1038/s41586-020-2532-1

H.N. Becker, J.W. Alexander, S.K. Atreya, S.J. Bolton, M.J. Brennan, S.T. Brown, A. Guillaume, T. Guillot, A.P. Ingersoll, S.M. Levin, J.I. Lunine, Y.S. Aglyamov, P.G. Steffes, Small lightning flashes from shallow electrical storms on Jupiter. Nature **584**(7819), 55–58 (2020b). doi:10.1038/s41586-020-2532-1

M.J.S. Belton, K.P. Klaasen, M.C. Clary, J.L. Anderson, C.D. Anger, M.H. Carr, C.R. Chapman, M.E. Davies, R. Greeley, D. Anderson, L.K. Bolef, T.E. Townsend, R. Greenberg, I. Head James W., G. Neukum, C.B. Pilcher, J. Veverka, P.J. Gierasch, F.P. Fanale, A.P. Ingersoll, H. Masursky, D. Morrison, J.B. Pollack, The Galileo Solid-State Imaging experiment. Space Sci. Rev. **60**(1-4), 413–455 (1992). doi:10.1007/BF00216864

B. Benmahi, T. Cavalié, M. Dobrijevic, N. Biver, K. Bermudez-Diaz, A. Sandqvist, E. Lellouch, R. Moreno, T. Fouchet, V. Hue, P. Hartogh, F. Billebaud, A. Lecacheux, Å. Hjalmarson, U. Frisk, M. Olberg, Odin Team, Monitoring of the evolution of H_2O vapor in the stratosphere of Jupiter over an 18-yr period with the Odin space telescope. Astron. Astrophys. **641**, 140 (2020). doi:10.1051/0004-6361/202038188

B. Benmahi, T. Cavalié, T.K. Greathouse, V. Hue, R. Giles, S. Guerlet, A. Spiga, R. Cosentino, Mapping the zonal winds of Jupiter's stratospheric equatorial oscillation. Astron. Astrophys. **652**, 125 (2021).

doi:10.1051/0004-6361/202141523
B. Benmahi, T. Cavalié, T. Fouchet, R. Moreno, E. Lellouch, D. Bardet, S. Guerlet, V. Hue, A. Spiga, First absolute wind measurements in Saturn's stratosphere from ALMA observations. Astron. Astrophys. **666**, 117 (2022). doi:10.1051/0004-6361/202244200
M.J. Bentum, M.K. Verma, R.T. Rajan, A.J. Boonstra, C.J.M. Verhoeven, E.K.A. Gill, A.J. van der Veen, H. Falcke, M.K. Wolt, B. Monna, S. Engelen, J. Rotteveel, L.I. Gurvits, A roadmap towards a space-based radio telescope for ultra-low frequency radio astronomy. Advances in Space Research **65**(2), 856–867 (2020). doi:10.1016/j.asr.2019.09.007
B. Bézard, E. Lellouch, D. Strobel, J.-P. Maillard, P. Drossart, Carbon Monoxide on Jupiter: Evidence for Both Internal and External Sources. Icarus **159**, 95–111 (2002). doi:10.1006/icar.2002.6917
D. Bhattacharyya, J.T. Clarke, J. Montgomery, B. Bonfond, J.-C. Gérard, D. Grodent, Evidence for Auroral Emissions From Callisto's Footprint in HST UV Images. Journal of Geophysical Research (Space Physics) **123**(1), 364–373 (2018). doi:10.1002/2017JA024791
G.L. Bjoraker, M.H. Wong, I. de Pater, T. Hewagama, M. Ádámkovics, G.S. Orton, The Gas Composition and Deep Cloud Structure of Jupiter's Great Red Spot. Astron. J. **156**(3), 101 (2018). doi:10.3847/1538-3881/aad186
M. Blanc, R. Greeley, Science of the Joint ESA-NASA Europa Jupiter System Mission (EJSM), in *EGU General Assembly Conference Abstracts*. EGU General Assembly Conference Abstracts, 2010, p. 13347
M. Blanc, Y. Alibert, N. André, S. Atreya, R. Beebe, W. Benz, S.J. Bolton, A. Coradini, A. Coustenis, V. Dehant, M. Dougherty, P. Drossart, M. Fujimoto, O. Grasset, L. Gurvits, P. Hartogh, H. Hussmann, Y. Kasaba, M. Kivelson, K. Khurana, N. Krupp, P. Louarn, J. Lunine, M. McGrath, D. Mimoun, O. Mousis, J. Oberst, T. Okada, R. Pappalardo, O. Prieto-Ballesteros, D. Prieur, P. Regnier, M. Roos-Serote, S. Sasaki, G. Schubert, C. Sotin, T. Spilker, Y. Takahashi, T. Takashima, F. Tosi, D. Turrini, T. van Hoolst, L. Zelenyi, LAPLACE: A mission to Europa and the Jupiter System for ESA's Cosmic Vision Programme. Experimental Astronomy **23**(3), 849–892 (2009). doi:10.1007/s10686-008-9127-4
T.M. Bocanegra-Bahamón, G. Molera Calvés, L.I. Gurvits, D.A. Duev, S.V. Pogrebenko, G. Cimò, D. Dirkx, P. Rosenblatt, Planetary Radio Interferometry and Doppler Experiment (PRIDE) technique: A test case of the Mars Express Phobos Flyby. II. Doppler tracking: Formulation of observed and computed values, and noise budget. Astron. Astrophys. **609**, 59 (2018). doi:10.1051/0004-6361/201731524
T.M. Bocanegra-Bahamón, G. Molera Calvés, L.I. Gurvits, G. Cimò, D. Dirkx, D.A. Duev, S.V. Pogrebenko, P. Rosenblatt, S. Limaye, L. Cui, P. Li, T. Kondo, M. Sekido, A.G. Mikhailov, M.A. Kharinov, A.V. Ipatov, W. Wang, W. Zheng, M. Ma, J.E.J. Lovell, J.N. McCallum, Venus Express radio occultation observed by PRIDE. Astron. Astrophys. **624**, 59 (2019). doi:10.1051/0004-6361/201833160
S.J. Bolton, A. Adriani, V. Adumitroaie, M. Allison, J. Anderson, S. Atreya, J. Bloxham, S. Brown, J.E.P. Connerney, E. DeJong, W. Folkner, D. Gautier, D. Grassi, S. Gulkis, T. Guillot, C. Hansen, W.B. Hubbard, L. Iess, A. Ingersoll, M. Janssen, J. Jorgensen, Y. Kaspi, S.M. Levin, C. Li, J. Lunine, Y. Miguel, A. Mura, G. Orton, T. Owen, M. Ravine, E. Smith, P. Steffes, E. Stone, D. Stevenson, R. Thorne, J. Waite, D. Durante, R.W. Ebert, T.K. Greathouse, V. Hue, M. Parisi, J.R. Szalay, R. Wilson, Jupiter's interior and deep atmosphere: The initial pole-to-pole passes with the Juno spacecraft. Science **356**, 821–825 (2017). doi:10.1126/science.aal2108
S.J. Bolton, S.M. Levin, T. Guillot, C. Li, Y. Kaspi, G. Orton, M.H. Wong, F. Oyafuso, M. Allison, J. Arballo, S. Atreya, H.N. Becker, J. Bloxham, S.T. Brown, L.N. Fletcher, E. Galanti, S. Gulkis, M. Janssen, A. Ingersoll, J.L. Lunine, S. Misra, P. Steffes, D. Stevenson, J.H. Waite, R.K. Yadav, Z. Zhang, Microwave observations reveal the deep extent and structure of Jupiter's atmospheric vortices. Science **374**(6570), 968–972 (2021). doi:10.1126/science.abf1015
B. Bonfond, G.R. Gladstone, D. Grodent, T.K. Greathouse, M.H. Versteeg, V. Hue, M.W. Davis, M.F. Vogt, J.-C. Gérard, A. Radioti, S. Bolton, S.M. Levin, J.E.P. Connerney, B.H. Mauk, P. Valek, A. Adriani, W.S. Kurth, Morphology of the UV aurorae Jupiter during Juno's first perijove observations. Geophys. Res. Lett. **44**(10), 4463–4471 (2017). doi:10.1002/2017GL073114
B. Bonfond, Z.H. Yao, G.R. Gladstone, D. Grodent, J.-C. Gérard, J. Matar, B. Palmaerts, T.K. Greathouse, V. Hue, M.H. Versteeg, J.A. Kammer, R.S. Giles, C. Tao, M.F. Vogt, A. Mura, A. Adriani, B.H. Mauk, W.S. Kurth, S.J. Bolton, Are Dawn Storms Jupiter's Auroral Substorms? AGU Advances **2**(1), 00275 (2021a). doi:10.1029/2020AV000275
B. Bonfond, Z.H. Yao, G.R. Gladstone, D. Grodent, J.-C. Gérard, J. Matar, B. Palmaerts, T.K. Greathouse,

V. Hue, M.H. Versteeg, J.A. Kammer, R.S. Giles, C. Tao, M.F. Vogt, A. Mura, A. Adriani, B.H. Mauk, W.S. Kurth, S.J. Bolton, Are Dawn Storms Jupiter's Auroral Substorms? AGU Advances **2**(1), 00275 (2021b). doi:10.1029/2020AV000275

W.J. Borucki, M.A. Williams, Lightning in the Jovian water cloud. J. Geophys. Res. **91**, 9893–9903 (1986). doi:10.1029/JD091iD09p09893

W.J. Borucki, C.P. McKay, D. Jebens, H.S. Lakkaraju, C.T. Vanajakshi, Spectral Irradiance Measurements of Simulated Lightning in Planetary Atmospheres. Icarus **123**(2), 336–344 (1996). doi:10.1006/icar.1996.0162

Boutonnet et al., JUICE Trajectory Design. Space Science Reviews (in prep.)

A.S. Braude, P.G.J. Irwin, G.S. Orton, L.N. Fletcher, Colour and tropospheric cloud structure of Jupiter from MUSE/VLT: Retrieving a universal chromophore. Icarus **338**, 113589 (2020). doi:10.1016/j.icarus.2019.113589

S. Brown, M. Janssen, V. Adumitroaie, S. Atreya, S. Bolton, S. Gulkis, A. Ingersoll, S. Levin, C. Li, L. Li, J. Lunine, S. Misra, G. Orton, P. Steffes, F. Tabataba-Vakili, I. Kolmašová, M. Imai, O. Santolík, W. Kurth, G. Hospodarsky, D. Gurnett, J. Connerney, Prevalent lightning sferics at 600 megahertz near Jupiter's poles. Nature **558**, 87–90 (2018). doi:10.1038/s41586-018-0156-5

B.J. Butler, D.B. Campbell, I. de Pater, D.E. Gary, Solar system science with SKA. New Astron. Rev. **48**(11-12), 1511–1535 (2004). doi:10.1016/j.newar.2004.09.031

H. Cao, D.J. Stevenson, Zonal flow magnetic field interaction in the semi-conducting region of giant planets. Icarus **296**, 59–72 (2017). doi:10.1016/j.icarus.2017.05.015

P. Cappuccio, M. Di Benedetto, D. Durante, L. Iess, Callisto and Europa Gravity Measurements from JUICE 3GM Experiment Simulation. Plan. Sci. J. **3**(8), 199 (2022). doi:10.3847/PSJ/ac83c4

T. Cavalié, J. Lunine, O. Mousis, A subsolar oxygen abundance or a raditaive region revealed by thermochemical modeling. Nat. Astron. **accepted** (2023). doi:10.1038/s41550-023-01928-8

T. Cavalié, F. Billebaud, N. Biver, M. Dobrijevic, E. Lellouch, J. Brillet, A. Lecacheux, Å. Hjalmarson, A. Sandqvist, U. Frisk, M. Olberg, E.A. Bergin, The Odin Team, Observation of water vapor in the stratosphere of Jupiter with the Odin space telescope. Planet. Space Sci. **56**, 1573–1584 (2008). doi:10.1016/j.pss.2008.04.013

T. Cavalié, P. Hartogh, F. Billebaud, M. Dobrijevic, T. Fouchet, E. Lellouch, T. Encrenaz, J. Brillet, G.H. Moriarty-Schieven, A cometary origin for CO in the stratosphere of Saturn? Astron. Astrophys. **510**, 88 (2010)

T. Cavalié, N. Biver, P. Hartogh, M. Dobrijevic, F. Billebaud, E. Lellouch, A. Sandqvist, J. Brillet, A. Lecacheux, Å. Hjalmarson, U. Frisk, M. Olberg, Odin Team, Odin space telescope monitoring of water vapor in the stratosphere of Jupiter. Planet. Space Sci. **61**, 3–14 (2012). doi:10.1016/j.pss.2011.04.001

T. Cavalié, H. Feuchtgruber, E. Lellouch, M. de Val-Borro, C. Jarchow, R. Moreno, P. Hartogh, G. Orton, T.K. Greathouse, F. Billebaud, M. Dobrijevic, L.M. Lara, A. González, H. Sagawa, Spatial distribution of water in the stratosphere of Jupiter from Herschel HIFI and PACS observations. Astron. Astrophys. **553**, 21 (2013). doi:10.1051/0004-6361/201220797

T. Cavalié, R. Moreno, E. Lellouch, P. Hartogh, O. Venot, G.S. Orton, C. Jarchow, T. Encrenaz, F. Selsis, F. Hersant, L.N. Fletcher, The first submillimeter observation of CO in the stratosphere of Uranus. Astron. Astrophys. **562**, 33 (2014). doi:10.1051/0004-6361/201322297

T. Cavalié, V. Hue, P. Hartogh, R. Moreno, E. Lellouch, H. Feuchtgruber, C. Jarchow, T. Cassidy, L.N. Fletcher, F. Billebaud, M. Dobrijevic, L. Rezac, G.S. Orton, M. Rengel, T. Fouchet, S. Guerlet, Herschel map of Saturn's stratospheric water, delivered by the plumes of Enceladus. Astron. Astrophys. **630**, 87 (2019). doi:10.1051/0004-6361/201935954

T. Cavalié, B. Benmahi, V. Hue, R. Moreno, E. Lellouch, T. Fouchet, P. Hartogh, L. Rezac, T.K. Greathouse, G.R. Gladstone, J.A. Sinclair, M. Dobrijevic, F. Billebaud, C. Jarchow, First direct measurement of auroral and equatorial jets in the stratosphere of Jupiter. Astron. Astrophys **647**, 8 (2021). doi:10.1051/0004-6361/202140330

T. Cavalié, L. Rezac, R. Moreno, E. Lellouch, T. Fouchet, B. Benmahi, T.K. Greathouse, J.A. Sinclair, V. Hue, P. Hartogh, M. Dobrijevic, N. Carrasco, Z. Perrin, Evidence for auroral influence on Jupiter's stratospheric composition revealed by ALMA. Nat. Astron. **submitted** (2022)

A.F. Cheng, A.A. Simon-Miller, H.A. Weaver, K.H. Baines, G.S. Orton, P.A. Yanamandra-Fisher, O. Mousis, E. Pantin, L. Vanzi, L.N. Fletcher, J.R. Spencer, S.A. Stern, J.T. Clarke, M.J. Mutchler, K.S. Noll, Changing Characteristics of Jupiter's Little Red Spot. Astronomical Journal **135**, 2446–2452 (2008a). doi:10.1088/0004-6256/135/6/2446

A.F. Cheng, H.A. Weaver, S.J. Conard, M.F. Morgan, O. Barnouin-Jha, J.D. Boldt, K.A. Cooper, E.H. Dar-

lington, M.P. Grey, J.R. Hayes, K.E. Kosakowski, T. Magee, E. Rossano, D. Sampath, C. Schlemm, H.W. Taylor, Long-Range Reconnaissance Imager on New Horizons. Space Sci. Rev. **140**(1-4), 189–215 (2008b). doi:10.1007/s11214-007-9271-6

D.S. Choi, A.P. Showman, A.R. Vasavada, A.A. Simon-Miller, Meteorology of Jupiter's equatorial hot spots and plumes from Cassini. Icarus **223**, 832–843 (2013). doi:10.1016/j.icarus.2013.02.001

U.R. Christensen, J. Wicht, W. Dietrich, Mechanisms for Limiting the Depth of Zonal Winds in the Gas Giant Planets. Astrophys. J. **890**(1), 61 (2020). doi:10.3847/1538-4357/ab698c

J.T. Clarke, D. Grodent, S.W.H. Cowley, E.J. Bunce, P. Zarka, J.E.P. Connerney, T. Satoh, In Jupiter. The Planet, Satellites and Magnetosphere, in *Jupiter's Aurora*, 2004, pp. 79–104

J.T. Clarke, J. Nichols, J.-C. Gérard, D. Grodent, K.C. Hansen, W. Kurth, G.R. Gladstone, J. Duval, S. Wannawichian, E. Bunce, S.W.H. Cowley, F. Crary, M. Dougherty, L. Lamy, D. Mitchell, W. Pryor, K. Retherford, T. Stallard, B. Zieger, P. Zarka, B. Cecconi, Response of Jupiter's and Saturn's auroral activity to the solar wind. Journal of Geophysical Research (Space Physics) **114**(A5), 05210 (2009). doi:10.1029/2008JA013694

J.E.P. Connerney, Magnetic connection for Saturn's rings and atmosphere. Geophys. Res. Lett. **13**(8), 773–776 (1986). doi:10.1029/GL013i008p00773

B.J. Conrath, J.A. Pirraglia, Thermal structure of Saturn from Voyager infrared measurements - Implications for atmospheric dynamics. Icarus **53**, 286–292 (1983). doi:10.1016/0019-1035(83)90148-3

R.G. Cosentino, B. Butler, R.J. Sault, R. Morales-Juberías, A.A. Simon, I. de Pater, Atmospheric waves and dynamics beneath Jupiter's clouds from radio wavelength observations. Icarus, in press (2017a). doi:http://dx.doi.org/10.1016/j.icarus.2017.01.006

R.G. Cosentino, R. Morales-Juberías, T. Greathouse, G. Orton, P. Johnson, L.N. Fletcher, A. Simon, New Observations and Modeling of Jupiter's Quasi-Quadrennial Oscillation. J. Geophys. Res. **122**(12), 2719–2744 (2017b). doi:10.1002/2017JE005342

S.W.H. Cowley, E.J. Bunce, Origin of the main auroral oval in Jupiter's coupled magnetosphere-ionosphere system. Plan. & Space Sci. **49**(10-11), 1067–1088 (2001). doi:10.1016/S0032-0633(00)00167-7

E.K. Dahl, N.J. Chanover, G.S. Orton, K.H. Baines, J.A. Sinclair, D.G. Voelz, E.A. Wijerathna, P.D. Strycker, P.G.J. Irwin, Vertical Structure and Color of Jovian Latitudinal Cloud Bands during the Juno Era. Plan. Sci. J. **2**(1), 16 (2021). doi:10.3847/PSJ/abd400

M.W. Davis, G.R. Gladstone, R.S. Giles, T.K. Greathouse, P.M. Molyneux, U. Raut, K.D. Retherford, S. Baldor, M.H. Versteeg, M. Freeman, K. Persson, S.C. Persyn, Ground calibration results of the JUICE ultraviolet spectrograph, in *Society of Photo-Optical Instrumentation Engineers (SPIE) Conference Series*. Society of Photo-Optical Instrumentation Engineers (SPIE) Conference Series, vol. 11444, 2020, p. 1144404. doi:10.1117/12.2562986

I. de Pater, R.J. Sault, B. Butler, D. DeBoer, M.H. Wong, Peering through Jupiter's clouds with radio spectral imaging. Science **352**, 1198–1201 (2016). doi:10.1126/science.aaf2210

I. de Pater, B. Butler, R.J. Sault, A. Moullet, C. Moeckel, J. Tollefson, K. de Kleer, M. Gurwell, S. Milam, Potential for Solar System Science with the ngVLA. Science with a Next Generation Very Large Array **517**, 49 (2018)

I. de Pater, R.J. Sault, C. Moeckel, A. Moullet, M.H. Wong, C. Goullaud, D. DeBoer, B.J. Butler, G. Bjoraker, M. Ádámkovics, R. Cosentino, P.T. Donnelly, L.N. Fletcher, Y. Kasaba, G.S. Orton, J.H. Rogers, J.A. Sinclair, E. Villard, First ALMA Millimeter-wavelength Maps of Jupiter, with a Multiwavelength Study of Convection. Astronomical Journal **158**(4), 139 (2019a). doi:10.3847/1538-3881/ab3643

I. de Pater, R.J. Sault, M.H. Wong, L.N. Fletcher, D. DeBoer, B. Butler, Jupiter's ammonia distribution derived from VLA maps at 3-37 GHz. Icarus **322**, 168–191 (2019b). doi:10.1016/j.icarus.2018.11.024

Denk et al., Io and the Minor Moons from JUICE. Space Science Reviews (in prep.)

B.M. Dinelli, F. Fabiano, A. Adriani, F. Altieri, M.L. Moriconi, A. Mura, G. Sindoni, G. Filacchione, F. Tosi, A. Migliorini, D. Grassi, G. Piccioni, R. Noschese, A. Cicchetti, S.J. Bolton, J.E.P. Connerney, S.K. Atreya, F. Bagenal, G.R. Gladstone, C.J. Hansen, W.S. Kurth, S.M. Levin, B.H. Mauk, D.J. McComas, J.-C. Gèrard, D. Turrini, S. Stefani, M. Amoroso, A. Olivieri, Preliminary JIRAM results from Juno polar observations: 1. Methodology and analysis applied to the Jovian northern polar region. Geophys. Res. Lett. **44**(10), 4625–4632 (2017). doi:10.1002/2017GL072929

T.E. Dowling, Saturn's Longitude: Rise of the Second Branch of Shear-Stability Theory and Fall of the First. International Journal of Modern Physics D **23**(4), 1430006–86 (2014). doi:10.1142/S0218271814300067

P. Drossart, J.-P. Maillard, J. Caldwell, S.J. Kim, J.K.G. Watson, W.A. Majewski, J. Tennyson, S. Miller, S.K. Atreya, J.T. Clarke, J.H. Waite, R. Wagener, Detection of H_3^+ on Jupiter. Nature **340**(6234),

539–541 (1989). doi:10.1038/340539a0

K. Duer, N. Gavriel, E. Galanti, Y. Kaspi, L.N. Fletcher, T. Guillot, S.J. Bolton, S.M. Levin, S.K. Atreya, D. Grassi, A.P. Ingersoll, C. Li, L. Li, J.I. Lunine, G.S. Orton, F.A. Oyafuso, J.H. Waite, Evidence for Multiple Ferrel-Like Cells on Jupiter. Geophys. Res. Lett. **48**(23), 95651 (2021). doi:10.1029/2021GL095651

W.R. Dunn, G. Branduardi-Raymont, L.C. Ray, C.M. Jackman, R.P. Kraft, R.F. Elsner, I.J. Rae, Z. Yao, M.F. Vogt, G.H. Jones, G.R. Gladstone, G.S. Orton, J.A. Sinclair, P.G. Ford, G.A. Graham, R. Caro-Carretero, A.J. Coates, The independent pulsations of Jupiter's northern and southern X-ray auroras. Nature Astronomy **1**, 758–764 (2017). doi:10.1038/s41550-017-0262-6

U.A. Dyudina, A.D. Del Genio, A.P. Ingersoll, C.C. Porco, R.A. West, A.R. Vasavada, J.M. Barbara, Lightning on Jupiter observed in the H_α line by the Cassini imaging science subsystem. Icarus **172**(1), 24–36 (2004). doi:10.1016/j.icarus.2004.07.014

U.A. Dyudina, A.P. Ingersoll, S.P. Ewald, C.C. Porco, G. Fischer, Y. Yair, Saturn's visible lightning, its radio emissions, and the structure of the 2009-2011 lightning storms. Icarus **226**, 1020–1037 (2013). doi:10.1016/j.icarus.2013.07.013

R.W. Ebert, F. Allegrini, F. Bagenal, S.J. Bolton, J.E.P. Connerney, G. Clark, G.A. DiBraccio, D.J. Gershman, W.S. Kurth, S. Levin, P. Louarn, B.H. Mauk, D.J. McComas, M. Reno, J.R. Szalay, M.F. Thomsen, P. Valek, S. Weidner, R.J. Wilson, Accelerated flows at Jupiter's magnetopause: Evidence for magnetic reconnection along the dawn flank. Geophys. Res. Lett. **44**(10), 4401–4409 (2017). doi:10.1002/2016GL072187

S.G. Edgington, S.K. Atreya, L.M. Trafton, J.J. Caldwell, R.F. Beebe, A.A. Simon, R.A. West, C. Barnet, On the Latitude Variation of Ammonia, Acetylene, and Phosphine Altitude Profiles on Jupiter from HST Faint Object Spectrograph Observations. Icarus **133**, 192–209 (1998). doi:10.1006/icar.1998.5925

S.G. Edgington, S.K. Atreya, L.M. Trafton, J.J. Caldwell, R.F. Beebe, A.A. Simon, R.A. West, Ammonia and Eddy Mixing Variations in the Upper Troposphere of Jupiter from HST Faint Object Spectrograph Observations. Icarus **142**, 342–356 (1999). doi:10.1006/icar.1999.6228

T. Encrenaz, ISO observations of the giant planets and Titan: what have we learnt? Planet. Space Sci. **51**(2), 89–103 (2003). doi:10.1016/S0032-0633(02)00145-9

H. Feuchtgruber, E. Lellouch, T. de Graauw, B. Bezard, T. Encrenaz, M. Griffin, External supply of oxygen to the atmospheres of giant planets. Nature **389**, 159–162 (1997)

F.M. Flasar, V.G. Kunde, R.K. Achterberg, B.J. Conrath, A.A. Simon-Miller, C.A. Nixon, P.J. Gierasch, P.N. Romani, B. Bézard, P. Irwin, G.L. Bjoraker, J.C. Brasunas, D.E. Jennings, J.C. Pearl, M.D. Smith, G.S. Orton, L.J. Spilker, R. Carlson, S.B. Calcutt, P.L. Read, F.W. Taylor, P. Parrish, A. Barucci, R. Courtin, A. Coustenis, D. Gautier, E. Lellouch, A. Marten, R. Prangé, Y. Biraud, T. Fouchet, C. Ferrari, T.C. Owen, M.M. Abbas, R.E. Samuelson, F. Raulin, P. Ade, C.J. Césarsky, K.U. Grossman, A. Coradini, An intense stratospheric jet on Jupiter. Nature **427**, 132–135 (2004)

L.N. Fletcher, Cycles of activity in the Jovian atmosphere. Geophys. Res. Lett. **44**, 4725–4729 (2017). doi:10.1002/2017GL073806

L.N. Fletcher, G.S. Orton, N.A. Teanby, P.G.J. Irwin, Phosphine on Jupiter and Saturn from Cassini/CIRS. Icarus **202**, 543–564 (2009). doi:10.1016/j.icarus.2009.03.023

L.N. Fletcher, G.S. Orton, O. Mousis, P. Yanamandra-Fisher, P.D. Parrish, P.G.J. Irwin, B.M. Fisher, L. Vanzi, T. Fujiyoshi, T. Fuse, A.A. Simon-Miller, E. Edkins, T.L. Hayward, J. De Buizer, Thermal structure and composition of Jupiter's Great Red Spot from high-resolution thermal imaging. Icarus **208**, 306–328 (2010). doi:10.1016/j.icarus.2010.01.005

L.N. Fletcher, K.H. Baines, T.W. Momary, A.P. Showman, P.G.J. Irwin, G.S. Orton, M. Roos-Serote, C. Merlet, Saturn's tropospheric composition and clouds from Cassini/VIMS 4.6-5.1 μm nightside spectroscopy. Icarus **214**, 510–533 (2011). doi:10.1016/j.icarus.2011.06.006

L.N. Fletcher, T.K. Greathouse, G.S. Orton, J.A. Sinclair, R.S. Giles, P.G.J. Irwin, T. Encrenaz, Mid-infrared mapping of Jupiter's temperatures, aerosol opacity and chemical distributions with IRTF/TEXES. Icarus **278**, 128–161 (2016). doi:10.1016/j.icarus.2016.06.008

L.N. Fletcher, G.S. Orton, J.A. Sinclair, P. Donnelly, H. Melin, J.H. Rogers, T.K. Greathouse, Y. Kasaba, T. Fujiyoshi, T.M. Sato, J. Fernandes, P.G.J. Irwin, R.S. Giles, A.A. Simon, M.H. Wong, M. Vedovato, Jupiter's North Equatorial Belt expansion and thermal wave activity ahead of Juno's arrival. Geophys. Res. Lett. **44**, 7140–7148 (2017a). doi:10.1002/2017GL073383

L.N. Fletcher, I. de Pater, W.T. Reach, M. Wong, G.S. Orton, P.G.J. Irwin, R.D. Gehrz, Jupiter's para-H_2 distribution from SOFIA/FORCAST and Voyager/IRIS 17-37 μm spectroscopy. Icarus **286**, 223–240 (2017b). doi:10.1016/j.icarus.2016.10.002

L.N. Fletcher, G.S. Orton, J.H. Rogers, R.S. Giles, A.V. Payne, P.G.J. Irwin, M. Vedovato, Moist convection and the 2010-2011 revival of Jupiter's South Equatorial Belt. Icarus **286**, 94–117 (2017c). doi:10.1016/j.icarus.2017.01.001

L.N. Fletcher, H. Melin, A. Adriani, A.A. Simon, A. Sanchez-Lavega, P.T. Donnelly, A. Antuñano, G.S. Orton, R. Hueso, M.L. Moriconi, F. Altieri, G. Sindoni, Jupiter's Mesoscale Waves Observed at 5 μm by Ground-Based Observations and Juno JIRAM. ApJ, submitted (2018)

L.N. Fletcher, F.A. Oyafuso, M. Allison, A. Ingersoll, L. Li, Y. Kaspi, E. Galanti, M.H. Wong, G.S. Orton, K. Duer, Z. Zhang, C. Li, T. Guillot, S.M. Levin, S. Bolton, Jupiter's Temperate Belt/Zone Contrasts Revealed at Depth by Juno Microwave Observations. Journal of Geophysical Research (Planets) **126**(10), 06858 (2021). doi:10.1029/2021JE006858

L.N. Fletcher, Y. Kaspi, T. Guillot, A.P. Showman, How Well Do We Understand the Belt/Zone Circulation of Giant Planet Atmospheres? Space Science Reviews **216**(2), 30 (2020). doi:10.1007/s11214-019-0631-9

A.J. Friedson, New Observations and Modelling of a QBO-Like Oscillation in Jupiter's Stratosphere. Icarus **137**, 34–55 (1999). doi:10.1006/icar.1998.6038

A.J. Friedson, A.-S. Wong, Y.L. Yung, Models for polar haze formation in Jupiter's stratosphere. Icarus **158**, 389–400 (2002a)

A.J. Friedson, A.-S. Wong, Y.L. Yung, Models for Polar Haze Formation in Jupiter's Stratosphere. Icarus **158**(2), 389–400 (2002b). doi:10.1006/icar.2002.6885

E. García-Melendo, A. Sánchez-Lavega, A Study of the Stability of Jovian Zonal Winds from HST Images: 1995-2000. Icarus **152**, 316–330 (2001). doi:10.1006/icar.2001.6646

N. Gavriel, Y. Kaspi, The number and location of Jupiter's circumpolar cyclones explained by vorticity dynamics. Nature Geoscience **14**(8), 559–563 (2021). doi:10.1038/s41561-021-00781-6

J.-C. Gérard, A. Mura, B. Bonfond, G.R. Gladstone, A. Adriani, V. Hue, B.M. Dinelli, T.K. Greathouse, D. Grodent, F. Altieri, M.L. Moriconi, A. Radioti, J.E.P. Connerney, S.J. Bolton, S.M. Levin, Concurrent ultraviolet and infrared observations of the north Jovian aurora during Juno's first perijove. Icarus **312**, 145–156 (2018). doi:10.1016/j.icarus.2018.04.020

J.-C. Gérard, L. Gkouvelis, B. Bonfond, G.R. Gladstone, A. Mura, A. Adriani, D. Grodent, V. Hue, T.K. Greathouse, $H_3{}^+$ cooling in the jovian aurora: Juno remote sensing observations and modeling. Icarus **389**, 115261 (2023). doi:10.1016/j.icarus.2022.115261

P.J. Gierasch, J.A. Magalhaes, B.J. Conrath, Zonal mean properties of Jupiter's upper troposphere from Voyager infrared observations. Icarus **67**, 456–483 (1986). doi:10.1016/0019-1035(86)90125-9

P.J. Gierasch, A.P. Ingersoll, D. Banfield, S.P. Ewald, P. Helfenstein, A. Simon-Miller, A. Vasavada, H.H. Breneman, D.A. Senske, Galileo Imaging Team, Observation of moist convection in Jupiter's atmosphere. Nature **403**, 628–630 (2000). doi:10.1038/35001017

R.S. Giles, L.N. Fletcher, P.G.J. Irwin, Latitudinal variability in Jupiter's tropospheric disequilibrium species: GeH_4, AsH_3 and PH_3. Icarus **289**, 254–269 (2017). doi:10.1016/j.icarus.2016.10.023

R.S. Giles, T.K. Greathouse, R.G. Cosentino, G.S. Orton, J.H. Lacy, Vertically-resolved observations of Jupiter's quasi-quadrennial oscillation from 2012 to 2019. Icarus **350**, 113905 (2020a). doi:10.1016/j.icarus.2020.113905

R.S. Giles, T.K. Greathouse, B. Bonfond, G.R. Gladstone, J.A. Kammer, V. Hue, D.C. Grodent, J.-C. Gérard, M.H. Versteeg, M.H. Wong, S.J. Bolton, J.E.P. Connerney, S.M. Levin, Possible Transient Luminous Events Observed in Jupiter's Upper Atmosphere. Journal of Geophysical Research (Planets) **125**(11), 06659 (2020b). doi:10.1029/2020JE006659

R.S. Giles, T.K. Greathouse, J.A. Kammer, G.R. Gladstone, B. Bonfond, V. Hue, D.C. Grodent, J.-C. Gérard, M.H. Versteeg, S.J. Bolton, J.E.P. Connerney, S.M. Levin, Detection of a Bolide in Jupiter's Atmosphere With Juno UVS. Geophys. Res. Lett. **48**(5), 91797 (2021a). doi:10.1029/2020GL091797

R.S. Giles, T.K. Greathouse, V. Hue, G.R. Gladstone, H. Melin, L.N. Fletcher, P.G.J. Irwin, J.A. Kammer, M.H. Versteeg, B. Bonfond, D.C. Grodent, S.J. Bolton, S.M. Levin, Meridional Variations of C_2H_2 in Jupiter's Stratosphere From Juno UVS Observations. Journal of Geophysical Research (Planets) **126**(8), 06928 (2021b). doi:10.1029/2021JE006928

R.S. Giles, V. Hue, T.K. Greathouse, G.R. Gladstone, J.A. Kammer, M.H. Versteeg, B. Bonfond, D.C. Grodent, J.-C. Gérard, J.A. Sinclair, S.J. Bolton, S.M. Levin, Enhanced C_2H_2 Absorption Within Jupiter's Southern Auroral Oval From Juno UVS Observations. Journal of Geophysical Research (Planets) **128**(2), 2022–007610 (2023). doi:10.1029/2022JE007610

J.N. Girard, P. Zarka, C. Tasse, S. Hess, I. de Pater, D. Santos-Costa, Q. Nenon, A. Sicard, S. Bourdarie, J. Anderson, A. Asgekar, M.E. Bell, I. van Bemmel, M.J. Bentum, G. Bernardi, P. Best, A. Bonafede, F. Breitling, R.P. Breton, J.W. Broderick, W.N. Brouw, M. Brüggen, B. Ciardi, S. Corbel, A. Corstanje,

F. de Gasperin, E. de Geus, A. Deller, S. Duscha, J. Eislöffel, H. Falcke, W. Frieswijk, M.A. Garrett, J. Grießmeier, A.W. Gunst, J.W.T. Hessels, M. Hoeft, J. Hörandel, M. Iacobelli, E. Juette, V.I. Kondratiev, M. Kuniyoshi, G. Kuper, J. van Leeuwen, M. Loose, P. Maat, G. Mann, S. Markoff, R. McFadden, D. McKay-Bukowski, J. Moldon, H. Munk, A. Nelles, M.J. Norden, E. Orru, H. Paas, M. Pandey-Pommier, R. Pizzo, A.G. Polatidis, W. Reich, H. Röttgering, A. Rowlinson, D. Schwarz, O. Smirnov, M. Steinmetz, J. Swinbank, M. Tagger, S. Thoudam, M.C. Toribio, R. Vermeulen, C. Vocks, R.J. van Weeren, R.A.M.J. Wijers, O. Wucknitz, Imaging Jupiter's radiation belts down to 127 MHz with LOFAR. Astron. Astrophys. **587**, 3 (2016). doi:10.1051/0004-6361/201527518

G.R. Gladstone, Y.L. Yung, An analysis of the reflection spectrum of Jupiter from 1500 A to 1740 A. Astrophys. J. **266**, 415–424 (1983). doi:10.1086/160789

Gladstone et al., The UVS Instrument for JUICE. Space Science Reviews (in prep.)

O. Grasset, M.K. Dougherty, A. Coustenis, E.J. Bunce, C. Erd, D. Titov, M. Blanc, A. Coates, P. Drossart, L.N. Fletcher, H. Hussmann, R. Jaumann, N. Krupp, J.-P. Lebreton, O. Prieto-Ballesteros, P. Tortora, F. Tosi, T. Van Hoolst, JUpiter ICy moons Explorer (JUICE): An ESA mission to orbit Ganymede and to characterise the Jupiter system. Planet. Space Sci. **78**, 1–21 (2013). doi:10.1016/j.pss.2012.12.002

D. Grassi, A. Adriani, M.L. Moriconi, N.I. Ignatiev, E. D'Aversa, F. Colosimo, A. Negrão, L. Brower, B.M. Dinelli, A. Coradini, G. Piccioni, Jupiter's hot spots: Quantitative assessment of the retrieval capabilities of future IR spectro-imagers. Plan. & Space Sci. **58**(10), 1265–1278 (2010). doi:10.1016/j.pss.2010.05.003

D. Grassi, A. Adriani, A. Mura, B.M. Dinelli, G. Sindoni, D. Turrini, G. Filacchione, A. Migliorini, M.L. Moriconi, F. Tosi, R. Noschese, A. Cicchetti, F. Altieri, F. Fabiano, G. Piccioni, S. Stefani, S. Atreya, J. Lunine, G. Orton, A. Ingersoll, S. Bolton, S. Levin, J. Connerney, A. Olivieri, M. Amoroso, Preliminary results on the composition of Jupiter's troposphere in hot spot regions from the JIRAM/Juno instrument. Geophys. Res. Lett. **44**, 4615–4624 (2017). doi:10.1002/2017GL072841

D. Grassi, A. Adriani, A. Mura, S.K. Atreya, L.N. Fletcher, J.I. Lunine, G.S. Orton, S. Bolton, C. Plainaki, G. Sindoni, F. Altieri, A. Cicchetti, B.M. Dinelli, G. Filacchione, A. Migliorini, M.L. Moriconi, R. Noschese, A. Olivieri, G. Piccioni, R. Sordini, S. Stefani, F. Tosi, D. Turrini, On the Spatial Distribution of Minor Species in Jupiter's Troposphere as Inferred From Juno JIRAM Data. Journal of Geophysical Research (Planets) **125**(4), 06206 (2020). doi:10.1029/2019JE006206

D. Grassi, A. Mura, G. Sindoni, A. Adriani, S.K. Atreya, G. Filacchione, L.N. Fletcher, J.I. Lunine, M.L. Moriconi, R. Noschese, G.S. Orton, C. Plainaki, R. Sordini, F. Tosi, D. Turrini, A. Olivieri, G. Eichstädt, C.J. Hansen, H. Melin, F. Altieri, A. Cicchetti, B.M. Dinelli, A. Migliorini, G. Piccioni, S. Stefani, S.J. Bolton, On the clouds and ammonia in Jupiter's upper troposphere from Juno JIRAM reflectivity observations. Mon. Not. R. Astron. Soc. **503**(4), 4892–4907 (2021). doi:10.1093/mnras/stab740

T. Greathouse, J. Moses, L. Fletcher, G. Orton, S. Guerlet, Seasonal Temperature Variations in Saturn's Stratosphere: Radiative Seasonal Model vs. Observations., in *EGU General Assembly Conference Abstracts*. EGU General Assembly Conference Abstracts, vol. 12, 2010, p. 4806

T. Greathouse, R. Gladstone, M. Versteeg, V. Hue, J. Kammer, R. Giles, M. Davis, S. Bolton, S. Levin, J. Connerney, J.-C. Gérard, D. Grodent, B. Bonfond, E. Bunce, M.F. Vogt, Local Time Dependence of Jupiter's Polar Auroral Emissions Observed by Juno UVS. Journal of Geophysical Research (Planets) **126**(12), 06954 (2021). doi:10.1029/2021JE006954

C.A. Griffith, B. Bézard, T. Greathouse, E. Lellouch, J. Lacy, D. Kelly, M.J. Richter, Meridional transport of HCN from SL9 impacts on Jupiter. Icarus **170**, 58–69 (2004). doi:10.1016/j.icarus.2004.02.006

D. Grodent, J.T. Clarke, J.H. Waite, S.W.H. Cowley, J.-C. GéRard, J. Kim, Jupiter's polar auroral emissions. Journal of Geophysical Research (Space Physics) **108**(A10), 1366 (2003). doi:10.1029/2003JA010017

D. Grodent, A Brief Review of Ultraviolet Auroral Emissions on Giant Planets. Space Science Reviews **187**(1-4), 23–50 (2015). doi:10.1007/s11214-014-0052-8

D. Grodent, B. Bonfond, J.-C. GéRard, A. Radioti, J. Gustin, J.T. Clarke, J. Nichols, J.E.P. Connerney, Auroral evidence of a localized magnetic anomaly in Jupiter's northern hemisphere. Journal of Geophysical Research (Space Physics) **113**(A9), 09201 (2008). doi:10.1029/2008JA013185

S. Guerlet, A. Spiga, H. Delattre, T. Fouchet, Radiative-equilibrium model of Jupiter's atmosphere and application to estimating stratospheric circulations. Icarus **351**, 113935 (2020a). doi:10.1016/j.icarus.2020.113935

S. Guerlet, A. Spiga, H. Delattre, T. Fouchet, Radiative-equilibrium model of Jupiter's atmosphere and application to estimating stratospheric circulations. Icarus **351**, 113935 (2020b). doi:10.1016/j.icarus.2020.113935

T. Guillot, Condensation of Methane, Ammonia, and Water and the Inhibition of Convection in Giant Planets. Science **269**, 1697–1699 (1995). doi:10.1126/science.7569896

T. Guillot, Y. Miguel, B. Militzer, W.B. Hubbard, Y. Kaspi, E. Galanti, H. Cao, R. Helled, S.M. Wahl, L. Iess, W.M. Folkner, D.J. Stevenson, J.I. Lunine, D.R. Reese, A. Biekman, M. Parisi, D. Durante, J.E.P. Connerney, S.M. Levin, S.J. Bolton, A suppression of differential rotation in Jupiter's deep interior. Nature **555**, 227–230 (2018). doi:10.1038/nature25775

T. Guillot, D.J. Stevenson, W.B. Hubbard, D. Saumon, The Interior of Jupiter, ed. by F. Bagenal, T.E. Dowling, W.B. McKinnon, vol. 1 (Jupiter. The Planet, Satellites and Magnetosphere, 2004), pp. 35–57

T. Guillot, D.J. Stevenson, S.K. Atreya, S.J. Bolton, H.N. Becker, Storms and the Depletion of Ammonia in Jupiter: I. Microphysics of "Mushballs". Journal of Geophysical Research (Planets) **125**(8), 06403 (2020a). doi:10.1029/2020JE006403

T. Guillot, C. Li, S.J. Bolton, S.T. Brown, A.P. Ingersoll, M.A. Janssen, S.M. Levin, J.I. Lunine, G.S. Orton, P.G. Steffes, D.J. Stevenson, Storms and the Depletion of Ammonia in Jupiter: II. Explaining the Juno Observations. Journal of Geophysical Research (Planets) **125**(8), 06404 (2020b). doi:10.1029/2020JE006404

P. Gupta, S.K. Atreya, P.G. Steffes, L.N. Fletcher, T. Guillot, M.D. Allison, S.J. Bolton, R. Helled, S. Levin, C. Li, J.I. Lunine, Y. Miguel, G.S. Orton, J. Hunter Waite, P. Withers, Jupiter's Temperature Structure: A Reassessment of the Voyager Radio Occultation Measurements. Plan. Sci. J. **3**(7), 159 (2022). doi:10.3847/PSJ/ac6956

D.A. Gurnett, R.R. Shaw, R.R. Anderson, W.S. Kurth, F.L. Scarf, Whistlers observed by Voyager 1: Detection of lightning on Jupiter. Geophys. Res. Lett. **6**(6), 511–514 (1979). doi:10.1029/GL006i006p00511

Gurvits et al., The PRIDE experiment for JUICE. Space Science Reviews (in prep.)

H.B. Hammel, M.H. Wong, J.T. Clarke, I. de Pater, L.N. Fletcher, R. Hueso, K. Noll, G.S. Orton, S. Pérez-Hoyos, A. Sánchez-Lavega, A.A. Simon-Miller, P.A. Yanamandra-Fisher, Jupiter after the 2009 Impact: Hubble Space Telescope Imaging of the Impact-generated Debris and its Temporal Evolution. ApJ **715**(2), 150–154 (2010)

C.J. Hansen, M.A. Caplinger, A. Ingersoll, M.A. Ravine, E. Jensen, S. Bolton, G. Orton, Junocam: Juno's Outreach Camera. Space Science Reviews **213**(1-4), 475–506 (2017a). doi:10.1007/s11214-014-0079-x

C.J. Hansen, M.A. Caplinger, A. Ingersoll, M.A. Ravine, E. Jensen, S. Bolton, G. Orton, Junocam: Juno's Outreach Camera. Space Sci. Rev. **213**(1-4), 475–506 (2017b). doi:10.1007/s11214-014-0079-x

J. Harrington, I. de Pater, S.H. Brecht, D. Deming, V. Meadows, K. Zahnle, P.D. Nicholson, Lessons from Shoemaker-Levy 9 about Jupiter and planetary impacts (Cambridge Planetary Science. Cambridge Univ. Press, New York, ???, 2004), pp. 159–184. Chap. 8

P. Hartogh, E. Lellouch, R. Moreno, D. Bockelée-Morvan, N. Biver, T. Cassidy, M. Rengel, C. Jarchow, T. Cavalié, J. Crovisier, F.P. Helmich, M. Kidger, Direct detection of the Enceladus water torus with Herschel. Astron. Astrophys. **532**, 2 (2011). doi:10.1051/0004-6361/201117377

Hartogh et al., The SWI Instrument for JUICE. Space Science Reviews (in prep.)

J.R. Holton, *An Introduction to Dynamic Meteorology* (Academic press, ???, 2004). ISBN 0123540151

V. Hue, F. Hersant, T. Cavalié, M. Dobrijevic, J.A. Sinclair, Photochemistry, mixing and transport in Jupiter's stratosphere constrained by Cassini. Icarus **307**, 106–123 (2018a). doi:10.1016/j.icarus.2018.02.018

V. Hue, F. Hersant, T. Cavalié, M. Dobrijevic, J.A. Sinclair, Photochemistry, mixing and transport in Jupiter's stratosphere constrained by Cassini. Icarus **307**, 106–123 (2018b). doi:10.1016/j.icarus.2018.02.018

R. Hueso, A. Sánchez-Lavega, T. Guillot, A model for large-scale convective storms in Jupiter. Journal of Geophysical Research (Planets) **107**, 5–1 (2002). doi:10.1029/2001JE001839

R. Hueso, A. Wesley, C. Go, S. Pérez-Hoyos, M.H. Wong, L.N. Fletcher, A. Sánchez-Lavega, M.B.E. Boslough, I. de Pater, G.S. Orton, A.A. Simon-Miller, S.G. Djorgovski, M.L. Edwards, H.B. Hammel, J.T. Clarke, K.S. Noll, P.A. Yanamandra-Fisher, First Earth-based Detection of a Superbolide on Jupiter. Astrophys. J. Lett. **721**(2), 129–133 (2010). doi:10.1088/2041-8205/721/2/L129

R. Hueso, S. Pérez-Hoyos, A. Sánchez-Lavega, A. Wesley, G. Hall, C. Go, M. Tachikawa, K. Aoki, M. Ichimaru, J.W.T. Pond, D.G. Korycansky, C. Palotai, G. Chappell, N. Rebeli, J. Harrington, M. Delcroix, M. Wong, I. de Pater, L.N. Fletcher, H. Hammel, G.S. Orton, I. Tabe, J. Watanabe, J.C. Moreno, Impact flux on Jupiter: From superbolides to large-scale collisions. Astron. Astrophys. **560**, 55 (2013). doi:10.1051/0004-6361/201322216

R. Hueso, A. Sánchez-Lavega, P. Iñurrigarro, J.F. Rojas, S. Pérez-Hoyos, I. Mendikoa, J.M. Gómez-Forrellad, C. Go, D. Peach, F. Colas, M. Vedovato, Jupiter cloud morphology and zonal winds from ground-based observations before and during Juno's first perijove. Geophys. Res. Lett. **44**, 4669–4678 (2017). doi:10.1002/2017GL073444

R. Hueso, M. Delcroix, A. Sánchez-Lavega, S. Pedranghelu, G. Kernbauer, J. McKeon, A. Fleckstein, A. Wesley, J.M. Gómez-Forrellad, J.F. Rojas, J. Juaristi, Small impacts on the giant planet Jupiter. Astron. Astrophys. **617**, 68 (2018a). doi:10.1051/0004-6361/201832689

R. Hueso, J. Juaristi, J. Legarreta, A. Sánchez-Lavega, J.F. Rojas, S. Erard, B. Cecconi, P. Le Sidaner, The Planetary Virtual Observatory and Laboratory (PVOL) and its integration into the Virtual European Solar and Planetary Access (VESPA). Plan. & Space Sci. **150**, 22–35 (2018b). doi:10.1016/j.pss.2017.03.014

R. Hueso, P. Iñurrigarro, A. Sánchez-Lavega, C.R. Foster, J.H. Rogers, G.S. Orton, C. Hansen, G. Eichstädt, I. Ordonez-Etxeberria, J.F. Rojas, S.R. Brueshaber, J.F. Sanz-Requena, S. Pérez-Hoyos, M.H. Wong, T.W. Momary, B. Jónsson, A. Antuñano, K.H. Baines, E.K. Dahl, S. Mizumoto, C. Go, A. Anguiano-Arteaga, Convective storms in closed cyclones in Jupiter's South Temperate Belt: (I) observations. Icarus **380**, 114994 (2022). doi:10.1016/j.icarus.2022.114994

L. Iess, W.M. Folkner, D. Durante, M. Parisi, Y. Kaspi, E. Galanti, T. Guillot, W.B. Hubbard, D.J. Stevenson, J.D. Anderson, D.R. Buccino, L.G. Casajus, A. Milani, R. Park, P. Racioppa, D. Serra, P. Tortora, M. Zannoni, H. Cao, R. Helled, J.I. Lunine, Y. Miguel, B. Militzer, S. Wahl, J.E.P. Connerney, S.M. Levin, S.J. Bolton, Measurement of Jupiter's asymmetric gravity field. Nature **555**(7695), 220–222 (2018). doi:10.1038/nature25776

Iess et al., The 3GM Instrument for JUICE. Space Science Reviews (in prep.)

M. Imai, I. Kolmašová, W.S. Kurth, O. Santolík, G.B. Hospodarsky, D.A. Gurnett, S.T. Brown, S.J. Bolton, J.E.P. Connerney, S.M. Levin, Evidence for low density holes in Jupiter's ionosphere. Nature Communications **10**, 2751 (2019). doi:10.1038/s41467-019-10708-w

A.P. Ingersoll, G.P. J., B. D., A.R. Vasavada, Galileo Imaging Team, Moist convection as an energy source for the large-scale motions in Jupiter's atmosphere. Nature **403**, 630–632 (2000). doi:10.1038/35001021

A.P. Ingersoll, T.E. Dowling, P.J. Gierasch, G.S. Orton, P.L. Read, A. Sánchez-Lavega, A.P. Showman, A.A. Simon-Miller, A.R. Vasavada, Dynamics of Jupiter's atmosphere, ed. by F. Bagenal, T.E. Dowling, W.B. McKinnon (Jupiter. The Planet, Satellites and Magnetosphere, 2004), pp. 105–128

A.P. Ingersoll, V. Adumitroaie, M.D. Allison, S. Atreya, A.A. Bellotti, S.J. Bolton, S.T. Brown, S. Gulkis, M.A. Janssen, S.M. Levin, C. Li, L. Li, J.I. Lunine, G.S. Orton, F.A. Oyafuso, P.G. Steffes, Implications of the ammonia distribution on Jupiter from 1 to 100 bars as measured by the Juno microwave radiometer. Geophys. Res. Lett. **44**, 7676–7685 (2017). doi:10.1002/2017GL074277

P.G.J. Irwin, A.L. Weir, S.E. Smith, F.W. Taylor, A.L. Lambert, S.B. Calcutt, P.J. Cameron-Smith, R.W. Carlson, K. Baines, G.S. Orton, P. Drossart, T. Encrenaz, M. Roos-Serote, Cloud structure and atmospheric composition of Jupiter retrieved from Galileo near-infrared mapping spectrometer real-time spectra. J. Geophys. Res. **103**(12), 23001–23022 (1998). doi:10.1029/98JE00948

R.E. Johnson, T.S. Stallard, H. Melin, J.D. Nichols, S.W.H. Cowley, Jupiter's polar ionospheric flows: High resolution mapping of spectral intensity and line-of-sight velocity of H_3^+ ions. J. Geophys. Res. **122**(7), 7599–7618 (2017). doi:10.1002/2017JA024176

E. Karkoschka, Spectrophotometry of the Jovian Planets and Titan at 300- to 1000-nm Wavelength: The Methane Spectrum. Icarus **111**(1), 174–192 (1994). doi:10.1006/icar.1994.1139

Y. Kaspi, E. Galanti, W.B. Hubbard, D.J. Stevenson, S.J. Bolton, L. Iess, T. Guillot, J. Bloxham, J.E.P. Connerney, H. Cao, D. Durante, W.M. Folkner, R. Helled, A.P. Ingersoll, S.M. Levin, J.I. Lunine, Y. Miguel, B. Militzer, M. Parisi, S.M. Wahl, Jupiter's atmospheric jet streams extend thousands of kilometres deep. Nature **555**, 223–226 (2018). doi:10.1038/nature25793

Y. Kaspi, E. Galanti, A.P. Showman, D.J. Stevenson, T. Guillot, L. Iess, S.J. Bolton, Comparison of the Deep Atmospheric Dynamics of Jupiter and Saturn in Light of the Juno and Cassini Gravity Measurements. Space Sci. Rev. **216**(5), 84 (2020). doi:10.1007/s11214-020-00705-7

J.A. Kaye, D.F. Strobel, Phosphine photochemistry in the atmosphere of Saturn. Icarus **59**, 314–335 (1984). doi:10.1016/0019-1035(84)90105-2

I. Kolmašová, M. Imai, O. Santolík, W.S. Kurth, G.B. Hospodarsky, D.A. Gurnett, J.E.P. Connerney, S.J. Bolton, Discovery of rapid whistlers close to Jupiter implying lightning rates similar to those on Earth. Nature Astronomy **2**, 544–548 (2018). doi:10.1038/s41550-018-0442-z

T.T. Koskinen, B.R. Sandel, R.V. Yelle, D.F. Strobel, I.C.F. Müller-Wodarg, J.T. Erwin, Saturn's variable thermosphere from Cassini/UVIS occultations. Icarus **260**, 174–189 (2015).

doi:10.1016/j.icarus.2015.07.008
W.S. Kurth, B.D. Strayer, D.A. Gurnett, F.L. Scarf, A summary of whistlers observed by Voyager 1 at Jupiter. Icarus **61**(3), 497–507 (1985). doi:10.1016/0019-1035(85)90138-1
W.S. Kurth, B.H. Mauk, S.S. Elliott, D.A. Gurnett, G.B. Hospodarsky, O. Santolik, J.E.P. Connerney, P. Valek, F. Allegrini, G.R. Gladstone, S.J. Bolton, S.M. Levin, Whistler Mode Waves Associated With Broadband Auroral Electron Precipitation at Jupiter. Geophys. Res. Lett. **45**(18), 9372–9379 (2018). doi:10.1029/2018GL078566
A.L. Laraia, A.P. Ingersoll, M.A. Janssen, S. Gulkis, F. Oyafuso, M. Allison, Analysis of Saturn's thermal emission at 2.2-cm wavelength: Spatial distribution of ammonia vapor. Icarus **226**, 641–654 (2013). doi:10.1016/j.icarus.2013.06.017
J. Leconte, F. Selsis, F. Hersant, T. Guillot, Condensation-inhibited convection in hydrogen-rich atmospheres . Stability against double-diffusive processes and thermal profiles for Jupiter, Saturn, Uranus, and Neptune. Astron. Astrophys. **598**, 98 (2017). doi:10.1051/0004-6361/201629140
E. Lellouch, R. Moreno, G. Paubert, A dual origin for Neptune's carbon monoxide? Astron. Astrophys. **430**, 37–40 (2005). doi:10.1051/0004-6361:200400127
E. Lellouch, G. Paubert, R. Moreno, M.C. Festou, B. Bézard, D. Bockelée-Morvan, P. Colom, J. Crovisier, T. Encrenaz, D. Gautier, A. Marten, D. Despois, D.F. Strobel, A. Sievers, Chemical and thermal response of Jupiter's atmosphere following the impact of comet Shoemaker-Levy 9. Nature **373**, 592–595 (1995a). doi:10.1038/373592a0
E. Lellouch, G. Paubert, R. Moreno, M.C. Festou, B. Bezard, D. Bockelee-Morvan, P. Colom, J. Crovisier, T. Encrenaz, D. Gautier, A. Marten, D. Despois, D.F. Strobel, A. Sievers, The collision of Comet P/Shoemaker-Levy 9 with Jupiter: Detection and monitoring of CO, CS and OCS. Highlights of Astronomy **10**, 648 (1995b)
E. Lellouch, B. Bézard, T. Fouchet, H. Feuchtgruber, T. Encrenaz, T. de Graauw, The deuterium abundance in Jupiter and Saturn from ISO-SWS observations. Astron. Astrophys. **370**, 610–622 (2001a). doi:10.1051/0004-6361:20010259
E. Lellouch, B. Bézard, T. Fouchet, H. Feuchtgruber, T. Encrenaz, T. de Graauw, The deuterium abundance in Jupiter and Saturn from ISO-SWS observations. Astron. Astrophys. **370**, 610–622 (2001b). doi:10.1051/0004-6361:20010259
E. Lellouch, B. Bézard, J.I. Moses, G.R. Davis, P. Drossart, H. Feuchtgruber, E.A. Bergin, R. Moreno, T. Encrenaz, The Origin of Water Vapor and Carbon Dioxide in Jupiter's Stratosphere. Icarus **159**, 112–131 (2002). doi:10.1006/icar.2002.6929
E. Lellouch, B. Bézard, D.F. Strobel, G.L. Bjoraker, F.M. Flasar, P.N. Romani, On the HCN and CO_2 abundance and distribution in Jupiter's stratosphere. Icarus **184**(2), 478–497 (2006). doi:10.1016/j.icarus.2006.05.018
D. Lemasquerier, G. Facchini, B. Favier, M. Le Bars, Remote determination of the shape of Jupiter's vortices from laboratory experiments. Nature Physics **16**(6), 695–700 (2020). doi:10.1038/s41567-020-0833-9
C.B. Leovy, A.J. Friedson, G.S. Orton, The quasiquadrennial oscillation of Jupiter's equatorial stratosphere. Nature **354**, 380–382 (1991a). doi:10.1038/354380a0
C.B. Leovy, A.J. Friedson, G.S. Orton, The quasiquadrennial oscillation of Jupiter's equatorial stratosphere. Nature **354**(6352), 380–382 (1991b). doi:10.1038/354380a0
J.S. Levine, D.R. Kraemer, W.R. Kuhn, Solar Radiation Incident on Mars and the Outer Planets: Latitudinal, Seasonal, and Atmospheric Effects. Icarus **31**(1), 136–145 (1977). doi:10.1016/0019-1035(77)90076-8
C. Li, A.P. Ingersoll, Moist convection in hydrogen atmospheres and the frequency of Saturn's giant storms. Nature Geoscience **8**, 398–403 (2015). doi:10.1038/ngeo2405
C. Li, A. Ingersoll, M. Janssen, S. Levin, S. Bolton, V. Adumitroaie, M. Allison, J. Arballo, A. Bellotti, S. Brown, S. Ewald, L. Jewell, S. Misra, G. Orton, F. Oyafuso, P. Steffes, R. Williamson, The distribution of ammonia on Jupiter from a preliminary inversion of Juno microwave radiometer data. Geophys. Res. Lett. **44**, 5317–5325 (2017). doi:10.1002/2017GL073159
C. Li, T. Le, X. Zhang, Y.L. Yung, A high-performance atmospheric radiation package: With applications to the radiative energy budgets of giant planets. J. Quant. Spectrosc. Radiat. Transfer **217**, 353–362 (2018). doi:10.1016/j.jqsrt.2018.06.002
C. Li, A. Ingersoll, S. Bolton, S. Levin, M. Janssen, S. Atreya, J. Lunine, P. Steffes, S. Brown, T. Guillot, M. Allison, J. Arballo, A. Bellotti, V. Adumitroaie, S. Gulkis, A. Hodges, L. Li, S. Misra, G. Orton, F. Oyafuso, D. Santos-Costa, H. Waite, Z. Zhang, The water abundance in Jupiter's equatorial zone. Nature Astronomy **4**, 609–616 (2020). doi:10.1038/s41550-020-1009-3

L. Li, R.K. Achterberg, B.J. Conrath, P.J. Gierasch, M.A. Smith, A.A. Simon-Miller, C.A. Nixon, G.S. Orton, F.M. Flasar, X. Jiang, K.H. Baines, R. Morales-Juberías, A.P. Ingersoll, A.R. Vasavada, A.D. Del Genio, R.A. West, S.P. Ewald, Strong Temporal Variation Over One Saturnian Year: From Voyager to Cassini. Scientific Reports **3** (2013). doi:10.1038/srep02410

X. Li, P.L. Read, A mechanistic model of the quasi-quadrennial oscillation in Jupiter's stratosphere. Planet. Space Sci. **48**(7-8), 637–669 (2000). doi:10.1016/S0032-0633(00)00033-7

G.F. Lindal, G.E. Wood, G.S. Levy, J.D. Anderson, D.N. Sweetnam, H.B. Hotz, B.J. Buckles, D.P. Holmes, P.E. Doms, V.R. Eshleman, G.L. Tyler, T.A. Croft, The atmosphere of Jupiter: an analysis of the Voyager radio occulation measurements. Journal of Geophysical Research **86**(A10), 8721–8727 (1981). doi:10.1029/JA086iA10p08721

B. Little, C.D. Anger, A.P. Ingersoll, A.R. Vasavada, D.A. Senske, H.H. Breneman, W.J. Borucki, The Galileo SSI Team, Galileo Images of Lightning on Jupiter. Icarus **142**, 306–323 (1999). doi:10.1006/icar.1999.6195

J.I. Lunine, A. Coradini, D. Gautier, T.C. Owen, G. Wuchterl, The origin of Jupiter, ed. by Bagenal, F., Dowling, T. E., & McKinnon, W. B. 2004, pp. 19–34

P.R. Mahaffy, H.B. Niemann, A. Alpert, S.K. Atreya, J. Demick, T.M. Donahue, D.N. Harpold, T.C. Owen, Noble gas abundance and isotope ratios in the atmosphere of Jupiter from the Galileo Probe Mass Spectrometer. J. Geophys. Res. **105**, 15061–15072 (2000). doi:10.1029/1999JE001224

Masters et al., Magnetosphere and plasma science with the Jupiter Icy Moons Explorer. Space Science Reviews (in prep.)

K.I. Matcheva, D.F. Strobel, F.M. Flasar, Interaction of Gravity Waves with Ionospheric Plasma: Implications for Jupiter's Ionosphere. Icarus **152**(2), 347–365 (2001). doi:10.1006/icar.2001.6631

B.H. Mauk, G. Clark, G.R. Gladstone, S. Kotsiaros, A. Adriani, F. Allegrini, F. Bagenal, S.J. Bolton, B. Bonfond, J.E.P. Connerney, R.W. Ebert, D.K. Haggerty, P. Kollmann, W.S. Kurth, S.M. Levin, C.P. Paranicas, A.M. Rymer, Energetic Particles and Acceleration Regions Over Jupiter's Polar Cap and Main Aurora: A Broad Overview. Journal of Geophysical Research (Space Physics) **125**(3), 27699 (2020). doi:10.1029/2019JA027699

M. Mayor, D. Queloz, A Jupiter-mass companion to a solar-type star. Nature **378**(6555), 355–359 (1995). doi:10.1038/378355a0

A.S. Medvedev, J. Sethunadh, P. Hartogh, From cold to warm gas giants: A three-dimensional atmospheric general circulation modeling. Icarus **225**(1), 228–235 (2013). doi:10.1016/j.icarus.2013.03.028

M. Meftah, L. Damé, D. Bolsée, A. Hauchecorne, N. Pereira, D. Sluse, G. Cessateur, A. Irbah, J. Bureau, M. Weber, K. Bramstedt, T. Hilbig, R. Thiéblemont, M. Marchand, F. Lefèvre, A. Sarkissian, S. Bekki, SOLAR-ISS: A new reference spectrum based on SOLAR/SOLSPEC observations. Astron. Astrophys. **611**, 1 (2018). doi:10.1051/0004-6361/201731316

H. Melin, L.N. Fletcher, P.T. Donnelly, T.K. Greathouse, J.H. Lacy, G.S. Orton, R.S. Giles, J.A. Sinclair, P.G.J. Irwin, Assessing the long-term variability of acetylene and ethane in the stratosphere of Jupiter. Icarus **305**, 301–313 (2018). doi:10.1016/j.icarus.2017.12.041

H. Melin, L.N. Fletcher, P.G.J. Irwin, S.G. Edgington, Jupiter in the Ultraviolet: Acetylene and Ethane Abundances in the Stratosphere of Jupiter from Cassini Observations between 0.15 and 0.19 μm. Astron. J. **159**(6), 291 (2020). doi:10.3847/1538-3881/ab91a6

A. Moirano, A. Mura, A. Adriani, V. Dols, B. Bonfond, J.H. Waite, V. Hue, J.R. Szalay, A.H. Sulaiman, B.M. Dinelli, F. Tosi, F. Altieri, A. Cicchetti, G. Filacchione, D. Grassi, A. Migliorini, M.L. Moriconi, R. Noschese, G. Piccioni, R. Sordini, D. Turrini, C. Plainaki, G. Sindoni, S. Massetti, R.L. Lysak, S.L. Ivanovski, S.J. Bolton, Morphology of the Auroral Tail of Io, Europa, and Ganymede From JIRAM L-Band Imager. Journal of Geophysical Research (Space Physics) **126**(9), 29450 (2021). doi:10.1029/2021JA029450

A. Morbidelli, Planet formation by pebble accretion in ringed disks. Astron. Astrophys. **638**, 1 (2020). doi:10.1051/0004-6361/202037983

R. Moreno, A. Marten, H.E. Matthews, Y. Biraud, Long-term evolution of CO, CS and HCN in Jupiter after the impacts of comet Shoemaker-Levy 9. Planet. Space Sci. **51**, 591–611 (2003)

R. Moreno, E. Lellouch, T. Cavalié, A. Moullet, Detection of CS in Neptune's atmosphere from ALMA observations. Astron. Astrophys. **608**, 5 (2017). doi:10.1051/0004-6361/201731472

M.L. Moriconi, A. Adriani, B.M. Dinelli, F. Fabiano, F. Altieri, F. Tosi, G. Filacchione, A. Migliorini, J.C. Gérard, A. Mura, D. Grassi, G. Sindoni, G. Piccioni, R. Noschese, A. Cicchetti, S.J. Bolton, J.E.P. Connerney, S.K. Atreya, F. Bagenal, G.R. Gladstone, C. Hansen, W.S. Kurth, S.M. Levin, B.H. Mauk, D.J. McComas, D. Turrini, S. Stefani, A. Olivieri, M. Amoroso, Preliminary JIRAM results from Juno polar observations: 3. Evidence of diffuse methane presence in the Jupiter auroral regions.

Geophys. Res. Lett. **44**(10), 4641–4648 (2017). doi:10.1002/2017GL073592

J.I. Moses, A.R. Poppe, Dust ablation on the giant planets: Consequences for stratospheric photochemistry. Icarus **297**, 33–58 (2017). doi:10.1016/j.icarus.2017.06.002

J.I. Moses, T. Fouchet, B. Bézard, G.R. Gladstone, E. Lellouch, H. Feuchtgruber, Photochemistry and diffusion in Jupiter's stratosphere: Constraints from ISO observations and comparisons with other giant planets. Journal of Geophysical Research (Planets) **110**, 08001 (2005a). doi:10.1029/2005JE002411

J.I. Moses, T. Fouchet, B. Bézard, G.R. Gladstone, E. Lellouch, H. Feuchtgruber, Photochemistry and diffusion in Jupiter's stratosphere: Constraints from ISO observations and comparisons with other giant planets. Journal of Geophysical Research (Planets) **110**, 08001 (2005b). doi:10.1029/2005JE002411

J.I. Moses, A.R. Poppe, Dust ablation on the giant planets: Consequences for stratospheric photochemistry. Icarus **297**, 33–58 (2017). doi:10.1016/j.icarus.2017.06.002

O. Mousis, R. Hueso, J.-P. Beaulieu, S. Bouley, B. Carry, F. Colas, A. Klotz, C. Pellier, J.-M. Petit, P. Rousselot, M. Ali-Dib, W. Beisker, M. Birlan, C. Buil, A. Delsanti, E. Frappa, H.B. Hammel, A.C. Levasseur-Regourd, G.S. Orton, A. Sánchez-Lavega, A. Santerne, P. Tanga, J. Vaubaillon, B. Zanda, D. Baratoux, T. Böhm, V. Boudon, A. Bouquet, L. Buzzi, J.-L. Dauvergne, A. Decock, M. Delcroix, P. Drossart, N. Esseiva, G. Fischer, L.N. Fletcher, S. Foglia, J.M. Gómez-Forrellad, J. Guarro-Fló, D. Herald, E. Jehin, F. Kugel, J.-P. Lebreton, J. Lecacheux, A. Leroy, L. Maquet, G. Masi, A. Maury, F. Meyer, S. Pérez-Hoyos, A.S. Rajpurohit, C. Rinner, J.H. Rogers, F. Roques, R.W. Schmude, B. Sicardy, B. Tregon, M. Vanhuysse, A. Wesley, T. Widemann, Instrumental methods for professional and amateur collaborations in planetary astronomy. Experimental Astronomy **38**, 91–191 (2014). doi:10.1007/s10686-014-9379-0

A. Mura, A. Adriani, F. Altieri, J.E.P. Connerney, S.J. Bolton, M.L. Moriconi, J.-C. Gérard, W.S. Kurth, B.M. Dinelli, F. Fabiano, F. Tosi, S.K. Atreya, F. Bagenal, G.R. Gladstone, C. Hansen, S.M. Levin, B.H. Mauk, D.J. McComas, G. Sindoni, G. Filacchione, A. Migliorini, D. Grassi, G. Piccioni, R. Noschese, A. Cicchetti, D. Turrini, S. Stefani, M. Amoroso, A. Olivieri, Infrared observations of Jovian aurora from Juno's first orbits: Main oval and satellite footprints. Geophys. Res. Lett. **44**(11), 5308–5316 (2017a). doi:10.1002/2017GL072954

A. Mura, A. Adriani, F. Altieri, J.E.P. Connerney, S.J. Bolton, M.L. Moriconi, J.-C. Gérard, W.S. Kurth, B.M. Dinelli, F. Fabiano, F. Tosi, S.K. Atreya, F. Bagenal, G.R. Gladstone, C. Hansen, S.M. Levin, B.H. Mauk, D.J. McComas, G. Sindoni, G. Filacchione, A. Migliorini, D. Grassi, G. Piccioni, R. Noschese, A. Cicchetti, D. Turrini, S. Stefani, M. Amoroso, A. Olivieri, Infrared observations of Jovian aurora from Juno's first orbits: Main oval and satellite footprints. Geophysical Research Letters **44**(11), 5308–5316 (2017b). doi:10.1002/2017GL072954

A. Mura, A. Adriani, J.E.P. Connerney, S. Bolton, F. Altieri, F. Bagenal, B. Bonfond, B.M. Dinelli, J.-C. Gérard, T. Greathouse, D. Grodent, S. Levin, B. Mauk, M.L. Moriconi, J. Saur, J.H. Waite, M. Amoroso, A. Cicchetti, F. Fabiano, G. Filacchione, D. Grassi, A. Migliorini, R. Noschese, A. Olivieri, G. Piccioni, C. Plainaki, G. Sindoni, R. Sordini, F. Tosi, D. Turrini, Juno observations of spot structures and a split tail in Io-induced aurorae on Jupiter. Science **361**(6404), 774–777 (2018). doi:10.1126/science.aat1450

A. Mura, P. Scarica, D. Grassi, A. Adriani, A. Bracco, G. Piccioni, G. Sindoni, M.L. Moriconi, C. Plainaki, A. Ingersoll, F. Altieri, A. Cicchetti, B.M. Dinelli, G. Filacchione, A. Migliorini, R. Noschese, R. Sordini, S. Stefani, F. Tosi, D. Turrini, Five Years of Observations of the Circumpolar Cyclones of Jupiter. Journal of Geophysical Research (Planets) **127**(9), 07241 (2022). doi:10.1029/2022JE007241

J.D. Nichols, J.T. Clarke, J.C. Gérard, D. Grodent, K.C. Hansen, Variation of different components of Jupiter's auroral emission. Journal of Geophysical Research (Space Physics) **114**(A6), 06210 (2009). doi:10.1029/2009JA014051

J.D. Nichols, S.V. Badman, F. Bagenal, S.J. Bolton, B. Bonfond, E.J. Bunce, J.T. Clarke, J.E.P. Connerney, S.W.H. Cowley, R.W. Ebert, M. Fujimoto, J.-C. Gérard, G.R. Gladstone, D. Grodent, T. Kimura, W.S. Kurth, B.H. Mauk, G. Murakami, D.J. McComas, G.S. Orton, A. Radioti, T.S. Stallard, C. Tao, P.W. Valek, R.J. Wilson, A. Yamazaki, I. Yoshikawa, Response of Jupiter's auroras to conditions in the interplanetary medium as measured by the Hubble Space Telescope and Juno. Geophys. Res. Lett. **44**(15), 7643–7652 (2017). doi:10.1002/2017GL073029

C.A. Nixon, R.K. Achterberg, B.J. Conrath, P.G.J. Irwin, N.A. Teanby, T. Fouchet, P.D. Parrish, P.N. Romani, M. Abbas, A. LeClair, D. Strobel, A.A. Simon-Miller, D.J. Jennings, F.M. Flasar, V.G. Kunde, Meridional variations of C_2H_2 and C_2H_6 in Jupiter's atmosphere from Cassini CIRS infrared spectra. Icarus **188**(1), 47–71 (2007a). doi:10.1016/j.icarus.2006.11.016

C.A. Nixon, R.K. Achterberg, B.J. Conrath, P.G.J. Irwin, N.A. Teanby, T. Fouchet, P.D. Parrish, P.N. Romani, M. Abbas, A. Leclair, D. Strobel, A.A. Simon-Miller, D.J. Jennings, F.M. Flasar, V.G. Kunde,

Meridional variations of C_2H_2 and C_2H_6 in Jupiter's atmosphere from Cassini CIRS infrared spectra. Icarus **188**, 47–71 (2007b). doi:10.1016/j.icarus.2006.11.016

C.A. Nixon, R.K. Achterberg, P.N. Romani, M. Allen, X. Zhang, N.A. Teanby, P.G.J. Irwin, F.M. Flasar, Abundances of Jupiter's trace hydrocarbons from Voyager and Cassini. Plan. & Space Sci. **58**, 1667–1680 (2010). doi:10.1016/j.pss.2010.05.008

J. Norwood, J. Moses, L.N. Fletcher, G. Orton, P.G.J. Irwin, S. Atreya, K. Rages, T. Cavalié, A. Sánchez-Lavega, R. Hueso, N. Chanover, Giant Planet Observations with the James Webb Space Telescope. PASP **128**(1), 018005 (2016). doi:10.1088/1538-3873/128/959/018005

J. O'Donoghue, L. Moore, T.S. Stallard, H. Melin, Heating of Jupiter's upper atmosphere above the Great Red Spot. Nature **536**(7615), 190–192 (2016). doi:10.1038/nature18940

J. O'Donoghue, L. Moore, T. Bhakyapaibul, H. Melin, T. Stallard, J.E.P. Connerney, C. Tao, Global upper-atmospheric heating on Jupiter by the polar aurorae. Nature **596**(7870), 54–57 (2021). doi:10.1038/s41586-021-03706-w

G.S. Orton, C. Hansen, A.P. Ingersoll, The First Close-Up Images of Jupiter's Polar Regions: Results from the Juno Mission JunoCam Instrument. Geophys. Res. Lett., submitted (2017)

G.S. Orton, A.J. Friedson, J. Caldwell, H.B. Hammel, K.H. Baines, J.T. Bergstralh, T.Z. Martin, M.E. Malcom, R.A. West, W.F. Golisch, D.M. Griep, C.D. Kaminski, A.T. Tokunaga, R. Baron, M. Shure, Thermal maps of Jupiter - Spatial organization and time dependence of stratospheric temperatures, 1980 to 1990. Science **252**, 537–542 (1991a)

G.S. Orton, A.J. Friedson, J. Caldwell, H.B. Hammel, K.H. Baines, J.T. Bergstralh, T.Z. Martin, M.E. Malcom, R.A. West, W.F. Golisch, D.M. Griep, C.D. Kaminski, A.T. Tokunaga, R. Baron, M. Shure, Thermal maps of Jupiter - Spatial organization and time dependence of stratospheric temperatures, 1980 to 1990. Science **252**(5005), 537–542 (1991b). doi:10.1126/science.252.5005.537

G.S. Orton, L.N. Fletcher, C.M. Lisse, P.W. Chodas, A. Cheng, P.A. Yanamandra-Fisher, K.H. Baines, B.M. Fisher, A. Wesley, S. Perez-Hoyos, I. de Pater, H.B. Hammel, M.L. Edwards, A.P. Ingersoll, O. Mousis, F. Marchis, W. Golisch, A. Sanchez-Lavega, A.A. Simon-Miller, R. Hueso, T.W. Momary, Z. Greene, N. Reshetnikov, E. Otto, G. Villar, S. Lai, M.H. Wong, The atmospheric influence, size and possible asteroidal nature of the July 2009 Jupiter impactor. Icarus **211**(1), 587–602 (2011). doi:10.1016/j.icarus.2010.10.010

G.S. Orton, F. Tabataba-Vakili, G. Eichstädt, J. Rogers, C.J. Hansen, T.W. Momary, A.P. Ingersoll, S. Brueshaber, M.H. Wong, A.A. Simon, L.N. Fletcher, M. Ravine, M. Caplinger, D. Smith, S.J. Bolton, S.M. Levin, J.A. Sinclair, C. Thepenier, H. Nicholson, A. Anthony, A Survey of Small-Scale Waves and Wave-Like Phenomena in Jupiter's Atmosphere Detected by JunoCam. Journal of Geophysical Research (Planets) **125**(7), 06369 (2020). doi:10.1029/2019JE006369

T. Owen, T. Encrenaz, Element Abundances and Isotope Ratios in the Giant Planets and Titan. Space Science Reviews **106**, 121–138 (2003)

F. Oyafuso, S. Levin, G. Orton, S.T. Brown, V. Adumitroaie, M. Janssen, M.H. Wong, L.N. Fletcher, P. Steffes, C. Li, S. Gulkis, S. Atreya, S. Misra, S. Bolton, Angular Dependence and Spatial Distribution of Jupiter's Centimeter-Wave Thermal Emission From Juno's Microwave Radiometer. Earth and Space Science **7**(11), 01254 (2020). doi:10.1029/2020EA001254

Palumbo et al., The JANUS Instrument for JUICE. Space Science Reviews (in prep.)

M. Parisi, Y. Kaspi, E. Galanti, D. Durante, S.J. Bolton, S.M. Levin, D.R. Buccino, L.N. Fletcher, W.M. Folkner, T. Guillot, R. Helled, L. Iess, C. Li, K. Oudrhiri, M.H. Wong, The depth of Jupiter's Great Red Spot constrained by Juno gravity overflights. Science **374**(6570), 964–968 (2021). doi:10.1126/science.abf1396

C.D. Parkinson, A.I.F. Stewart, A.S. Wong, Y.L. Yung, J.M. Ajello, Enhanced transport in the polar mesosphere of Jupiter: Evidence from Cassini UVIS helium 584 Å airglow. Journal of Geophysical Research (Planets) **111**(E2), 02002 (2006). doi:10.1029/2005JE002539

S. Pérez-Hoyos, A. Sánchez-Lavega, J.F. Sanz-Requena, N. Barrado-Izagirre, Ó. Carrión-González, A. Anguiano-Arteaga, P.G.J. Irwin, A.S. Braude, Color and aerosol changes in Jupiter after a North Temperate Belt disturbance. Icarus **352**, 114031 (2020). doi:10.1016/j.icarus.2020.114031

Z. Perrin, N. Carrasco, A. Chatain, L. Jovanovic, L. Vettier, N. Ruscassier, G. Cernogora, An atmospheric origin for hcn-derived polymers on titan. Processes **9**(6) (2021). doi:10.3390/pr9060965. https://www.mdpi.com/2227-9717/9/6/965

J.J. Perry, Y.H. Kim, J.L. Fox, H.S. Porter, Chemistry of the Jovian auroral ionosphere. J. Geophys. Res. **104**(E7), 16541–16566 (1999). doi:10.1029/1999JE900022

J.D.R. Pierel, C.A. Nixon, E. Lellouch, L.N. Fletcher, G.L. Bjoraker, R.K. Achterberg, B. Bézard, B.E. Hesman, P.G.J. Irwin, F.M. Flasar, D/H Ratios on Saturn and Jupiter from Cassini CIRS. Astron. J.

154(5), 178 (2017). doi:10.3847/1538-3881/aa899d

J.A. Pirraglia, B.J. Conrath, M.D. Allison, P.J. Gierasch, Thermal structure and dynamics of Saturn and Jupiter. Nature **292**(5825), 677–679 (1981). doi:10.1038/292677a0

C.C. Porco, R.A. West, A. McEwen, A.D. Del Genio, A.P. Ingersoll, P. Thomas, S. Squyres, L. Dones, C.D. Murray, T.V. Johnson, J.A. Burns, A. Brahic, G. Neukum, J. Veverka, J.M. Barbara, T. Denk, M. Evans, J.J. Ferrier, P. Geissler, P. Helfenstein, T. Roatsch, H. Throop, M. Tiscareno, A.R. Vasavada, Cassini Imaging of Jupiter's Atmosphere, Satellites, and Rings. Science **299**, 1541–1547 (2003). doi:10.1126/science.1079462

C.C. Porco, R.A. West, S. Squyres, A. McEwen, P. Thomas, C.D. Murray, A. Del Genio, A.P. Ingersoll, T.V. Johnson, G. Neukum, J. Veverka, L. Dones, A. Brahic, J.A. Burns, V. Haemmerle, B. Knowles, D. Dawson, T. Roatsch, K. Beurle, W. Owen, Cassini Imaging Science: Instrument Characteristics And Anticipated Scientific Investigations At Saturn. Space Sci. Rev. **115**(1-4), 363–497 (2004). doi:10.1007/s11214-004-1456-7

Poulet et al., The MAJIS Instrument for JUICE. Space Science Reviews (in prep.)

J.T. Rayner, M.C. Cushing, W.D. Vacca, The Infrared Telescope Facility (IRTF) Spectral Library: Cool Stars. ApJ Supplement **185**(2), 289–432 (2009). doi:10.1088/0067-0049/185/2/289

P.L. Read, P.J. Gierasch, B.J. Conrath, A. Simon-Miller, T. Fouchet, Y.H. Yamazaki, Mapping potential-vorticity dynamics on Jupiter. I: Zonal-mean circulation from Cassini and Voyager 1 data. Q. J. R. Meteorol. Soc. **132**, 1577–1603 (2006)

D. Rego, N. Achilleos, T. Stallard, S. Miller, R. Prangé, M. Dougherty, R.D. Joseph, Supersonic winds in Jupiter's aurorae. Nature **399**(6732), 121–124 (1999). doi:10.1038/20121

D.C. Reuter, S.A. Stern, J. Scherrer, D.E. Jennings, J.W. Baer, J. Hanley, L. Hardaway, A. Lunsford, S. McMuldroch, J. Moore, C. Olkin, R. Parizek, H. Reitsma, D. Sabatke, J. Spencer, J. Stone, H. Throop, J. van Cleve, G.E. Weigle, L.A. Young, Ralph: A Visible/Infrared Imager for the New Horizons Pluto/Kuiper Belt Mission. Space Sci. Rev. **140**(1-4), 129–154 (2008). doi:10.1007/s11214-008-9375-7

J.H. Rogers, *The Giant Planet Jupiter* (Cambridge University Press, ???, 1995)

H. Sagawa, P. Hartogh, E. Lellouch, H. Feuchtgruber, G. Orton, C. Jarchow, T. Cavalié, R. Moreno, T. de Graauw, HssO TEAM, Far Infrared Spectra of Jupiter Observed with PACS Onboard Herschel, in *AAS/Division for Planetary Sciences Meeting Abstracts #42*. AAS/Division for Planetary Sciences Meeting Abstracts, vol. 42, 2010, pp. 11–31

C. Salyk, A.P. Ingersoll, J. Lorre, A. Vasavada, A.D. Del Genio, Interaction between eddies and mean flow in Jupiter's atmosphere: Analysis of Cassini imaging data. Icarus **185**(2), 430–442 (2006)

A. Sánchez-Lavega, J.M. Gomez, The South Equatorial Belt of Jupiter, I: Its Life Cycle. Icarus **121**, 1–17 (1996). doi:10.1006/icar.1996.0067

A. Sánchez-Lavega, G.S. Orton, R. Morales, J. Lecacheux, F. Colas, B. Fisher, P. Fukumura-Sawada, W. Golisch, D. Griep, C. Kaminski, K. Baines, K. Rages, R. West, NOTE: The Merger of Two Giant Anticyclones in the Atmosphere of Jupiter. Icarus **149**, 491–495 (2001). doi:10.1006/icar.2000.6548

A. Sánchez-Lavega, A. Wesley, G. Orton, R. Hueso, S. Perez-Hoyos, L.N. Fletcher, P. Yanamandra-Fisher, J. Legarreta, I. de Pater, H. Hammel, A. Simon-Miller, J.M. Gomez-Forrellad, J.L. Ortiz, E. García-Melendo, R.C. Puetter, P. Chodas, The impact of a large object with Jupiter in July 2009. ApJ **715**(2), 155–159 (2010)

A. Sánchez-Lavega, E. García-Melendo, S. Pérez-Hoyos, R. Hueso, M.H. Wong, A. Simon, J.F. Sanz-Requena, A. Antuñano, N. Barrado-Izagirre, I. Garate-Lopez, J.F. Rojas, T. Del Río-Gaztelurrutia, J.M. Gómez-Forrellad, I. de Pater, L. Li, T. Barry, An enduring rapidly moving storm as a guide to Saturn's Equatorial jet's complex structure. Nature Communications **7**, 13262 (2016). doi:10.1038/ncomms13262

A. Sánchez-Lavega, R. Hueso, G. Eichstädt, G. Orton, J. Rogers, C.J. Hansen, T. Momary, F. Tabataba-Vakili, S. Bolton, The Rich Dynamics of Jupiter's Great Red Spot from JunoCam: Juno Images. Astron. J. **156**(4), 162 (2018). doi:10.3847/1538-3881/aada81

A. Sánchez-Lavega, A. Anguiano-Arteaga, P. Iñurrigarro, E. Garcia-Melendo, J. Legarreta, R. Hueso, J.F. Sanz-Requena, S. Pérez-Hoyos, I. Mendikoa, M. Soria, J.F. Rojas, M. Andrés-Carcasona, A. Prat-Gasull, I. Ordoñez-Extebarria, J.H. Rogers, C. Foster, S. Mizumoto, A. Casely, C.J. Hansen, G.S. Orton, T. Momary, G. Eichstädt, Jupiter's Great Red Spot: Strong Interactions With Incoming Anticyclones in 2019. Journal of Geophysical Research (Planets) **126**(4), 06686 (2021). doi:10.1029/2020JE006686

A. Sánchez-Lavega, R. Hueso, J. Ramón Acarreta, A system of circumpolar waves in Jupiter's stratosphere. Geophys. Res. Lett. **25**(21), 4043–4046 (1998). doi:10.1029/1998GL900059

A. Sánchez-Lavega, L.A.. Sromovsky, A.P. Showman, A.D. Del Genio, R.M.B. Young, R. Hueso, E. García-Melendo, Y. Kaspi, G.S.O. Orton, N. Barrado-Izagirre, et al., Gas Giants, ed. by B. Galperin, P.L.E. Read (Cambridge University Press, 2019), pp. 72–103. doi:10.1017/9781107358225.004

P.J. Schinder, F.M. Flasar, E.A. Marouf, R.G. French, A. Anabtawi, E. Barbinis, A.J. Kliore, A numerical technique for two-way radio occultations by oblate axisymmetric atmospheres with zonal winds. Radio Science **50**(7), 712–727 (2015). doi:10.1002/2015RS005690

Schmidt et al., Jupiter's Rings and Dust from JUICE. Space Science Reviews (in prep.)

G. Schubert, M.P. Hickey, R.L. Walterscheid, Heating of Jupiter's thermosphere by the dissipation of upward propagating acoustic waves. Icarus **163**(2), 398–413 (2003). doi:10.1016/S0019-1035(03)00078-2

A. Seiff, D.B. Kirk, T.C.D. Knight, R.E. Young, J.D. Mihalov, L.A. Young, F.S. Milos, G. Schubert, R.C. Blanchard, D. Atkinson, Thermal structure of Jupiter's atmosphere near the edge of a 5-μm hot spot in the north equatorial belt. J. Geophys. Res. **103**, 22857–22890 (1998). doi:10.1029/98JE01766

A.A. Simon, R. Hueso, P. Iñurrigarro, A. Sánchez-Lavega, R. Morales-Juberías, R. Cosentino, L.N. Fletcher, M.H. Wong, A.I. Hsu, I. de Pater, G.S. Orton, F. Colas, M. Delcroix, D. Peach, J.-M. Gómez-Forrellad, A New, Long-lived, Jupiter Mesoscale Wave Observed at Visible Wavelengths. Astron. J. **156**(2), 79 (2018a). doi:10.3847/1538-3881/aacaf5

A.A. Simon, F. Tabataba-Vakili, R. Cosentino, R.F. Beebe, M.H. Wong, G.S. Orton, Historical and Contemporary Trends in the Size, Drift, and Color of Jupiter's Great Red Spot. Astronomical Journal **155**(4), 151 (2018b). doi:10.3847/1538-3881/aaae01

A.A. Simon-Miller, B.J. Conrath, P.J. Gierasch, G.S. Orton, R.K. Achterberg, F.M. Flasar, B.M. Fisher, Jupiter's atmospheric temperatures: From Voyager IRIS to Cassini CIRS. Icarus **180**, 98–112 (2006). doi:10.1016/j.icarus.2005.07.019

J.A. Sinclair, G.S. Orton, T.K. Greathouse, L.N. Fletcher, C. Tao, G.R. Gladstone, A. Adriani, W. Dunn, J.I. Moses, V. Hue, P.G.J. Irwin, H. Melin, R.S. Giles, Independent evolution of stratospheric temperatures in Jupiter's northern and southern auroral regions from 2014 to 2016. Geophys. Res. Lett. **44**(11), 5345–5354 (2017a). doi:10.1002/2017GL073529

J.A. Sinclair, G.S. Orton, T.K. Greathouse, L.N. Fletcher, J.I. Moses, V. Hue, P.G.J. Irwin, Jupiter's auroral-related stratospheric heating and chemistry I: Analysis of Voyager-IRIS and Cassini-CIRS spectra. Icarus **292**, 182–207 (2017b). doi:10.1016/j.icarus.2016.12.033

J.A. Sinclair, G.S. Orton, T.K. Greathouse, L.N. Fletcher, J.I. Moses, V. Hue, P.G.J. Irwin, Jupiter's auroral-related stratospheric heating and chemistry II: Analysis of IRTF-TEXES spectra measured in December 2014. Icarus **300**, 305–326 (2018a). doi:10.1016/j.icarus.2017.09.016

J.A. Sinclair, G.S. Orton, T.K. Greathouse, L.N. Fletcher, J.I. Moses, V. Hue, P.G.J. Irwin, Jupiter's auroral-related stratospheric heating and chemistry II: Analysis of IRTF-TEXES spectra measured in December 2014. Icarus **300**, 305–326 (2018b). doi:10.1016/j.icarus.2017.09.016

J.A. Sinclair, J.I. Moses, V. Hue, T.K. Greathouse, G.S. Orton, L.N. Fletcher, P.G.J. Irwin, Jupiter's auroral-related stratospheric heating and chemistry III: Abundances of C_2H_4, CH_3C_2H, C_4H_2 and C_6H_6 from Voyager-IRIS and Cassini-CIRS. Icarus **328**, 176–193 (2019). doi:10.1016/j.icarus.2019.03.012

J.A. Sinclair, T.K. Greathouse, R.S. Giles, J. Lacy, J. Moses, V. Hue, D. Grodent, B. Bonfond, C. Tao, T. Cavalié, E. Dahl, G.S. Orton, L.N. Fletcher, P.G.J. Irwin, A high spatial and spectral resolution study of Jupiter's mid-infrared auroral emissions and their response to a solar wind compression. Plan. Sci. J., (2023)

B.A. Smith, G.A. Briggs, G.E. Danielson, A.F. Cook, M.E. Davies, G.E. Hunt, H. Masursky, L.A. Soderblom, T.C. Owen, C. Sagan, V.E. Suomi, Voyager Imaging Experiment. Space Sci. Rev. **21**(2), 103–127 (1977). doi:10.1007/BF00200847

L.A. Sromovsky, P.M. Fry, The source of 3-μm absorption in Jupiter's clouds: Reanalysis of ISO observations using new NH_3 absorption models. Icarus **210**, 211–229 (2010a). doi:10.1016/j.icarus.2010.06.040

L.A. Sromovsky, P.M. Fry, The source of widespread 3-μm absorption in Jupiter's clouds: Constraints from 2000 Cassini VIMS observations. Icarus **210**, 230–257 (2010b). doi:10.1016/j.icarus.2010.06.039

L.A. Sromovsky, P.M. Fry, Composition and structure of fresh ammonia clouds on Jupiter based on quantitative analysis of Galileo/NIMS and New Horizons/LEISA spectra. Icarus **307**, 347–370 (2018). doi:10.1016/j.icarus.2017.10.037

L.A. Sromovsky, K.H. Baines, P.M. Fry, Models of bright storm clouds and related dark ovals in Saturn's Storm Alley as constrained by 2008 Cassini/VIMS spectra. Icarus **302**, 360–385 (2018). doi:10.1016/j.icarus.2017.11.027

T.S. Stallard, S. Miller, S.W.H. Cowley, E.J. Bunce, Jupiter's polar ionospheric flows: Measured intensity

and velocity variations poleward of the main auroral oval. Geophys. Res. Lett. **30**(5), 1221 (2003). doi:10.1029/2002GL016031

T.S. Stallard, A.G. Burrell, H. Melin, L.N. Fletcher, S. Miller, L. Moore, J. O'Donoghue, J.E.P. Connerney, T. Satoh, R.E. Johnson, Identification of Jupiter's magnetic equator through H_3^+ ionospheric emission. Nature Astronomy **2**, 773–777 (2018). doi:10.1038/s41550-018-0523-z

T. Stallard, S. Miller, G. Millward, R.D. Joseph, On the Dynamics of the Jovian Ionosphere and Thermosphere. I. The Measurement of Ion Winds. Icarus **154**(2), 475–491 (2001). doi:10.1006/icar.2001.6681

K. Sugiyama, K. Nakajima, M. Odaka, K. Kuramoto, Y.-Y. Hayashi, Numerical simulations of Jupiter's moist convection layer: Structure and dynamics in statistically steady states. Icarus **229**, 71–91 (2014). doi:10.1016/j.icarus.2013.10.016

A.H. Sulaiman, G.B. Hospodarsky, S.S. Elliott, W.S. Kurth, D.A. Gurnett, M. Imai, F. Allegrini, B. Bonfond, G. Clark, J.E.P. Connerney, R.W. Ebert, D.J. Gershman, V. Hue, S. Janser, S. Kotsiaros, C. Paranicas, O. Santolík, J. Saur, J.R. Szalay, S.J. Bolton, Wave-Particle Interactions Associated With Io's Auroral Footprint: Evidence of Alfvén, Ion Cyclotron, and Whistler Modes. Geophys. Res. Lett. **47**(22), 88432 (2020). doi:10.1029/2020GL088432

A.H. Sulaiman, B.H. Mauk, J.R. Szalay, F. Allegrini, G. Clark, G.R. Gladstone, S. Kotsiaros, W.S. Kurth, F. Bagenal, B. Bonfond, J.E.P. Connerney, R.W. Ebert, S.S. Elliott, D.J. Gershman, G.B. Hospodarsky, V. Hue, R.L. Lysak, A. Masters, O. Santolík, J. Saur, S.J. Bolton, Jupiter's Low-Altitude Auroral Zones: Fields, Particles, Plasma Waves, and Density Depletions. Journal of Geophysical Research (Space Physics) **127**(8), 30334 (2022). doi:10.1029/2022JA030334

G. Tinetti, P. Drossart, P. Eccleston, P. Hartogh, A. Heske, J. Leconte, G. Micela, M. Ollivier, G. Pilbratt, L. Puig, D. Turrini, B. Vandenbussche, P. Wolkenberg, J.-P. Beaulieu, L.A. Buchave, M. Ferus, M. Griffin, M. Guedel, K. Justtanont, P.-O. Lagage, P. Machado, G. Malaguti, M. Min, H.U. Nørgaard-Nielsen, M. Rataj, T. Ray, I. Ribas, M. Swain, R. Szabo, S. Werner, J. Barstow, M. Burleigh, J. Cho, V. Coudé du Foresto, A. Coustenis, L. Decin, T. Encrenaz, M. Galand, M. Gillon, R. Helled, J.C. Morales, A. García Muñoz, A. Moneti, I. Pagano, E. Pascale, G. Piccioni, D. Pinfield, S. Sarkar, F. Selsis, J. Tennyson, A. Triaud, O. Venot, I. Waldmann, D. Waltham, G. Wright, J. Amiaux, J.-L. Auguères, M. Berthé, N. Bezawada, G. Bishop, N. Bowles, D. Coffey, J. Colomé, M. Crook, P.-E. Crouzet, V. Da Peppo, I.E. Sanz, M. Focardi, M. Frericks, T. Hunt, R. Kohley, K. Middleton, G. Morgante, R. Ottensamer, E. Pace, C. Pearson, R. Stamper, K. Symonds, M. Rengel, E. Renotte, P. Ade, L. Affer, C. Alard, N. Allard, F. Altieri, Y. André, C. Arena, I. Argyriou, A. Aylward, C. Baccani, G. Bakos, M. Banaszkiewicz, M. Barlow, V. Batista, G. Bellucci, S. Benatti, P. Bernardi, B. Bézard, M. Blecka, E. Bolmont, B. Bonfond, R. Bonito, A.S. Bonomo, J.R. Brucato, A.S. Brun, I. Bryson, W. Bujwan, S. Casewell, B. Charnay, C.C. Pestellini, G. Chen, A. Ciaravella, R. Claudi, R. Clédassou, M. Damasso, M. Damiano, C. Danielski, P. Deroo, A.M. Di Giorgio, C. Dominik, V. Doublier, S. Doyle, R. Doyon, B. Drummond, B. Duong, S. Eales, B. Edwards, M. Farina, E. Flaccomio, L. Fletcher, F. Forget, S. Fossey, M. Fränz, Y. Fujii, Á. García-Piquer, W. Gear, H. Geoffray, J.C. Gérard, L. Gesa, H. Gomez, R. Graczyk, C. Griffith, D. Grodent, M.G. Guarcello, J. Gustin, K. Hamano, P. Hargrave, Y. Hello, K. Heng, E. Herrero, A. Hornstrup, B. Hubert, S. Ida, M. Ikoma, N. Iro, P. Irwin, C. Jarchow, J. Jaubert, H. Jones, Q. Julien, S. Kameda, F. Kerschbaum, P. Kervella, T. Koskinen, M. Krijger, N. Krupp, M. Lafarga, F. Landini, E. Lellouch, G. Leto, A. Luntzer, T. Rank-Lüftinger, A. Maggio, J. Maldonado, J.-P. Maillard, U. Mall, J.-B. Marquette, S. Mathis, P. Maxted, T. Matsuo, A. Medvedev, Y. Miguel, V. Minier, G. Morello, A. Mura, N. Narita, V. Nascimbeni, N. Nguyen Tong, V. Noce, F. Oliva, E. Palle, P. Palmer, M. Pancrazzi, A. Papageorgiou, V. Parmentier, M. Perger, A. Petralia, S. Pezzuto, R. Pierrehumbert, I. Pillitteri, G. Piotto, G. Pisano, L. Prisinzano, A. Radioti, J.-M. Réess, L. Rezac, M. Rocchetto, A. Rosich, N. Sanna, A. Santerne, G. Savini, G. Scandariato, B. Sicardy, C. Sierra, G. Sindoni, K. Skup, I. Snellen, M. Sobiecki, L. Soret, A. Sozzetti, A. Stiepen, A. Strugarek, J. Taylor, W. Taylor, L. Terenzi, M. Tessenyi, A. Tsiaras, C. Tucker, D. Valencia, G. Vasisht, A. Vazan, F. Vilardell, S. Vinatier, S. Viti, R. Waters, P. Wawer, A. Wawrzaszek, A. Whitworth, Y.L. Yung, S.N. Yurchenko, M.R. Zapatero Osorio, R. Zellem, T. Zingales, F. Zwart, A chemical survey of exoplanets with ARIEL. Experimental Astronomy **46**(1), 135–209 (2018). doi:10.1007/s10686-018-9598-x

Tobie et al., Geophysical characterization of the interiors of Ganymede, Callisto and Europa by ESA's JUpiter ICy moons Explorer. Space Science Reviews (in prep.)

J. Tollefson, M.H. Wong, I.d. Pater, A.A. Simon, G.S. Orton, J.H. Rogers, S.K. Atreya, R.G. Cosentino, W. Januszewski, R. Morales-Juberías, P.S. Marcus, Changes in Jupiter's Zonal Wind Profile preceding and during the Juno mission. Icarus **296**, 163–178 (2017). doi:10.1016/j.icarus.2017.06.007

Tosi et al., Characterization of the surfaces and near-surface atmospheres of Ganymede, Europa and Cal-

listo by JUICE. Space Science Reviews (in prep.)
J.D. Turner, J.-M. Grießmeier, P. Zarka, I. Vasylieva, The search for radio emission from exoplanets using LOFAR beam-formed observations: Jupiter as an exoplanet. Astron. Astrophys. **624**, 40 (2019). doi:10.1051/0004-6361/201832848
A.R. Vasavada, A.P. Showman, Jovian atmospheric dynamics: an update after Galileo and Cassini. Reports on Progress in Physics **68**, 1935–1996 (2005). doi:10.1088/0034-4885/68/8/R06
A.R. Vasavada, A.H. Bouchez, A.P. Ingersoll, B. Little, C.D. Anger, Galileo SSI Team, Jupiter's visible aurora and Io footprint. Journal of Geophysical Research **104**(E11), 27133–27142 (1999). doi:10.1029/1999JE001055
J. Venturini, R. Helled, Jupiter's heavy-element enrichment expected from formation models. Astron. Astrophys. **634**, 31 (2020). doi:10.1051/0004-6361/201936591
J. Vervack R. J., B.R. Sandel, G.R. Gladstone, J.C. McConnell, C.D. Parkinson, Jupiter's He 584 Å Dayglow: New Results. Icarus **114**(1), 163–173 (1995). doi:10.1006/icar.1995.1051
C. Visscher, J.I. Moses, S.A. Saslow, The deep water abundance on Jupiter: New constraints from thermochemical kinetics and diffusion modeling. Icarus **209**, 602–615 (2010). doi:10.1016/j.icarus.2010.03.029
S.M. Wahl, W.B. Hubbard, B. Militzer, T. Guillot, Y. Miguel, N. Movshovitz, Y. Kaspi, R. Helled, D. Reese, E. Galanti, S. Levin, J.E. Connerney, S.J. Bolton, Comparing Jupiter interior structure models to Juno gravity measurements and the role of a dilute core. Geophys. Res. Lett. **44**(10), 4649–4659 (2017). doi:10.1002/2017GL073160
Wahlund et al., The RPWI Instrument for JUICE. Space Science Reviews (in prep.)
S.J. Weidenschilling, J.S. Lewis, Atmospheric and cloud structures of the jovian planets. Icarus **20**, 465–476 (1973)
J.L. Weiland, N. Odegard, R.S. Hill, E. Wollack, G. Hinshaw, M.R. Greason, N. Jarosik, L. Page, C.L. Bennett, J. Dunkley, B. Gold, M. Halpern, A. Kogut, E. Komatsu, D. Larson, M. Limon, S.S. Meyer, M.R. Nolta, K.M. Smith, D.N. Spergel, G.S. Tucker, E.L. Wright, Seven-year Wilkinson Microwave Anisotropy Probe (WMAP) Observations: Planets and Celestial Calibration Sources. Astrophys. J. Suppl. **192**(2), 19 (2011). doi:10.1088/0067-0049/192/2/19
R. West, K. Baines, A. Friedson, D. Banfield, B. Ragent, F. Taylor, In Jupiter. The Planet, Satellites and Magnetosphere, in *Jovian Clouds and Hazes*, 2004, pp. 79–104
Witasse et al., JUICE Mission Overview. Space Science Reviews (in prep.)
A.-S. Wong, Y.L. Yung, A.J. Friedson, Benzene and Haze Formation in the Polar Atmosphere of Jupiter. Geophys. Res. Lett. **30**(8), 1447 (2003). doi:10.1029/2002GL016661
A.-S. Wong, A.Y.T. Lee, Y.L. Yung, J.M. Ajello, Jupiter: Aerosol Chemistry in the Polar Atmosphere. Astrophys. J. Lett. **534**(2), 215–217 (2000). doi:10.1086/312675
M.H. Wong, G.L. Bjoraker, C. Goullaud, A.W. Stephens, S.H. Luszcz-Cook, S.K. Atreya, I. de Pater, S.T. Brown, Deep clouds on jupiter. Remote Sensing **15**, 702 (2023). doi:10.3390/rs15030702
M.H. Wong, P.R. Mahaffy, S.K. Atreya, H.B. Niemann, T.C. Owen, Updated Galileo probe mass spectrometer measurements of carbon, oxygen, nitrogen, and sulfur on Jupiter. Icarus **171**(1), 153–170 (2004)
M.H. Wong, A.A. Simon, J.W. Tollefson, I. de Pater, M.N. Barnett, A.I. Hsu, A.W. Stephens, G.S. Orton, S.W. Fleming, C. Goullaud, W. Januszewski, A. Roman, G.L. Bjoraker, S.K. Atreya, A. Adriani, L.N. Fletcher, High-resolution UV/Optical/IR Imaging of Jupiter in 2016-2019. ApJ Supplement **247**(2), 58 (2020). doi:10.3847/1538-4365/ab775f
Y. Yair, Z. Levin, S. Tzivion, Model interpretation of Jovian lightning activity and the Galileo Probe results. Journal of Geophysical Research **103**(D12), 14157–14166 (1998). doi:10.1029/98JD00310
Z. Yao, W.R. Dunn, E.E. Woodfield, G. Clark, B.H. Mauk, R.W. Ebert, D. Grodent, B. Bonfond, D. Pan, I.J. Rae, B. Ni, R. Guo, G. Branduardi-Raymont, A.D. Wibisono, P. Rodriguez, S. Kotsiaros, J.-U. Ness, F. Allegrini, W.S. Kurth, G.R. Gladstone, R. Kraft, A.H. Sulaiman, H. Manners, R.T. Desai, S.J. Bolton, Revealing the source of jupiter's x-ray auroral flares. Science Advances **7**(28), 0851 (2021)
J.N. Yates, N. Achilleos, P. Guio, Response of the Jovian thermosphere to a transient 'pulse' in solar wind pressure. Planet. Space Sci. **91**, 27–44 (2014). doi:10.1016/j.pss.2013.11.009
J.N. Yates, L.C. Ray, N. Achilleos, O. Witasse, N. Altobelli, Magnetosphere-Ionosphere-Thermosphere Coupling at Jupiter Using a Three-Dimensional Atmospheric General Circulation Model. Journal of Geophysical Research (Space Physics) **125**(1), 26792 (2020). doi:10.1029/2019JA026792
R.V. Yelle, S. Miller, Jupiter's thermosphere and ionosphere, ed. by Bagenal, F., Dowling, T. E., & McKinnon, W. B. 2004, pp. 185–218
K. Zahnle, P. Schenk, H. Levison, L. Dones, Cratering rates in the outer Solar System. Icarus **163**(2),

263–289 (2003). doi:10.1016/S0019-1035(03)00048-4
P. Zarka, Fast radio imaging of Jupiter's magnetosphere at low-frequencies with LOFAR. Planet. Space Sci. **52**(15), 1455–1467 (2004). doi:10.1016/j.pss.2004.09.017